A Modeling Approach for Coefficient-Free Oscillometric Blood Pressure Estimation

by

Mohamad Forouzanfar

Thesis submitted to the
Faculty of Graduate and Postdoctoral Studies
in partial fulfillment of the requirements
for the Ph.D. degree in
Electrical and Computer Engineering

School of Electrical Engineering and Computer Science
Faculty of Engineering
University of Ottawa

Abstract

Oscillometry is the most common measurement method used in automatic blood pressure (BP) monitors. However, most of the oscillometric algorithms are without physiological and theoretical foundation, and rely on empirically derived coefficients for systolic and diastolic pressure evaluation which affects the reliability of the technique.

In this thesis, the oscillometric BP estimation problem is addressed using a comprehensive modeling approach, based on which coefficient-free estimation of BP becomes possible. A feature-based neural network approach is developed to find an implicit relationship between BP and the oscillometric waveform (OMW). The modeling approach is then extended by developing a mathematical model for the OMW as a function of the arterial blood pressure, cuff pressure, and cuff-arm-artery system parameters. Based on the developed model, the explicit relationship between the OMW and the systolic and diastolic pressures is found and a new coefficient-free oscillometric BP estimation method using the trust region reflective algorithm is proposed. In order to improve the reliability of BP estimates, the electrocardiogram signal is recorded simultaneously with the OMW, as another independent source of information. The electrocardiogram signal is used to identify the true oscillometric pulses and calculate the pulse transit time (PTT). By combining our developed model of oscillomtery with an existing model of the pulse wave velocity, a new mathematical model is derived for the PTT during the cuff deflation. The derived model is incorporated to study the PTT-cuff pressure dependence, based on which a new coefficient-free BP estimation method is proposed. In order to obtain accurate and robust estimates of BP, the proposed model-based BP estimation methods are fused by computing the weighted arithmetic mean of their estimates.

With fusion of the proposed methods, it is observed that the mean absolute error (MAE) in estimation of systolic and diastolic pressures is 4.40 and 3.00 mmHg, respectively, relative to the Food and Drug Administration-approved Omron monitor. In addition, the proposed feature-based neural network was compared with auscultatory measurements by trained observers giving MAE of 6.28 and 5.73 mmHg in estimation of systolic and diastolic pressures, respectively. The proposed models thus show promise toward developing robust BP estimation methods.

Acknowledgements

I would like to express my sincere gratitude to my advisors, Prof. Hilmi R. Dajani and Prof. Voicu Z. Groza, for their guidance and encouragement throughout this work. Without their patience, motivation, support, and immense knowledge, I would have never been able to finish my dissertation. I believe I was very lucky to have such great advisors during my PhD studies.

I would also like to thank Prof. Miodrag Bolic and our research group collaborators Dr. Izmail Batkin and Dr. Sreeraman Rajan for their advice, support, motivation, and valuable comments. Parts of the ideas behind this research grew out of my discussions with Dr. Izmail Batkin and Dr. Sreeraman Rajan.

My sincere thanks also go to the rest of my thesis committee including Prof. Domenico Grimaldi, Prof. Rafik A. Goubran, and Prof. Emil M. Petriu for their insightful comments and suggestions to improve my dissertation.

I wish to also thank all our research lab members including postdoctoral fellows: Dr. Saif Ahmad, Dr. Balakumar Balasingam, and Dr. Soojeong Lee, and graduate students: Mohamed Mabrouk, Silu Chen, Karen Soueidan, Majid Mafi, and Bahareh Taji, for their encouragement and support. I have to especially thank Dr. Saif Ahmad for designing our measurement prototype and collecting blood pressure data.

I would like to also acknowledge the service I received from the University of Ottawa's academic, administrative, and technical staff. Especially, I would like to thank the University of Ottawa's Science and Engineering Librarian Ms. Cynthia Bail for providing me with the necessary resources needed during my research work. My thanks also go to Prof. Wail Gueaieb for providing the LaTeX template used in writing my dissertation.

I would also like to thank the Ontario Ministry of Training, Colleges, and Universities, the Ontario Ministry of Economic Development and Innovation, the Natural Sciences and Engineering Research Council of Canada, the Ontario Centres of Excellence, and Biosign Technologies Inc. for their collaborative research support and funding. The blood pressure data used in parts of my research was provided by Biosign Technologies Inc.

Then last, but not the least, I would like to especially thank my family. Words cannot express how grateful I am to my family for all of the sacrifices that they have made on my behalf. Without their encouragement, love, and support I would have never achieved this success.

Contents

List of Tables

List of Figures

List of Abbreviations

ABP	Arterial Blood Pressure
ALA	Arterial Lumen Area
AMMI	Association for the Advancement of Medical Instrumentation
ANFIS	Adaptive Neuro Fuzzy Inference System
ANSI	American National Standards Institute
BFGS	Broyden–Fletcher–Goldfarb–Shanno
BHS	British Hypertension Society
BP	Blood Pressure
CG	Conjugate Gradient
DBP	Diastolic Blood Pressure
ECG	Electrocardiogram
ESH	European Society of Hypertension
FDA	Food and Drug Administration
FFNN	Feed–Forward Neural Network
FRU	Fletcher–Reeves Update
ISO	International Organization for Standardization
LM	Levenberg–Marquardt
MAE	Mean Absolute Error
MAP	Mean Arterial Pressure
ME	Mean Error
MF	Membership Function

mmHg	Millimeters of Mercury
NN	Neural Network
OMW	Oscillometric Waveform
OMWE	Oscillometric Waveform Envelope
OSS	One Step Secant
PBR	Powell–Beale Restarts
PEP	Pre–Ejection Period
PRU	Polak–Ribire Update
PTT	Pulse Transit Time
QN	Quasi Newton
RBP	Resilient Backpropagation
SBP	Systolic Blood Pressure
SCG	Scaled Conjugate Gradient
SD	Steepest Descend
SDE	Standard Deviation of Error
SD–VLR	Steepest Descent with Variable Learning Rate
SD–VLRM	Steepest Descent with Variable Learning Rate and Momentum

Chapter 1

Introduction

Blood pressure (BP) is one of the vital signs, which along with body temperature, heart rate, and respiratory rate carries significant information about the physiological state of a person [1]. BP is defined as the pressure applied by circulating blood on the walls of the blood vessels. In clinical use, the term "BP" usually refers to the arterial pressure measured at the brachial artery, the major artery in the upper arm [2]. In this thesis, we adopt the latter definition when referring to BP.

BP varies over each heartbeat from a minimum called diastolic pressure to a maximum called systolic pressure. Systolic blood pressure (SBP) occurs near the beginning of the cardiac cycle and indicates the maximum pressure exerted on the walls of the arteries after contraction of the heart. Diastolic blood pressure (DBP) occurs at the resting phase of the cardiac cycle and shows the minimum pressure in the arteries when the heart is relaxed. The average BP over a cardiac cycle is called mean arterial pressure (MAP). MAP is an indicator of the pressure at which blood is supplied to critical organs. Clinically, BP is reported in terms of SBP over DBP and is expressed in units of millimeters of mercury (mmHg), for example 120/80 mmHg [2].

1.1 Background

The most accurate method for measuring BP is the invasive arterial measurement. However, due to the difficulty and risk associated with invasive methods, the noninvasive auscultatory technique is widely used instead as the gold standard in the clinic [3]. In the auscultatory method, a cuff is placed by a trained examiner around the arm at the same height as the heart and is inflated until the artery is completely occluded. Then, the cuff is slowly deflated by the examiner while listening to the Korotkoff sounds with a stethoscope in order to identify the SBP and DBP values [2]. The auscultatory technique cannot be performed in noisy environments and requires expertise. Therefore, its usage is mostly limited to the doctor's office.

As an alternative, several automated techniques have been developed to determine the arterial BP. The most common of these techniques are Doppler ultrasound sphygmomanometry [4], oscillometry [5, 6], plethysmography [7], tonometry [8], and vascular unloading [9]. Among these techniques, oscillometry is the most popular one for estimation of SBP, DBP, and MAP as it can be relatively easily implemented in automated BP measurement devices. Unlike auscultatory technique, oscillometry can be repeatedly performed by patients at home and is able to operate in a noisy environment [2].

Oscillometry is performed similarly to the auscultatory technique but uses a pressure sensor to record the pressure oscillations within the cuff, instead of listening to Korotkoff sounds with a stethoscope. Over the deflation period, the recorded pressure waveform forms a signal known as the cuff deflation curve. A bandpass filter is utilized to extract the oscillometric pulses from the cuff deflation curve. Over the deflation period, the extracted oscillometric pulses form a signal known as the oscillometric waveform (OMW). The amplitude of these oscillations increases to a maximum and then decreases with further deflation. Different analysis algorithms are employed to estimate the SBP, DBP, and MAP from the OMW [10]. Oscillometry is the most common technique used in commercial electronic BP monitors and is the main focus of this thesis.

1.2 Motivation

High BP is a common chronic ailment that affects 1 in 5 Canadians and represents the primary risk factor for stroke and heart disease [11, 12]. A person's measured BP is an indicator of the state of his/her cardiovascular health, and is one of the most commonly measured physiological parameters. However, a recent editorial in the journal Hypertension of the American Heart Association asserts that, "few measurements in medicine are done as poorly and inconsistently as BP measurement. Methods used today in clinical practice and in clinical trials are little changed from the earliest days of measurement. Though there is a clear recognition of biological variability, we continue to make decisions based largely upon measurements taken at random times under poorly controlled condition" [13]. This observation supports the need to develop robust methods to accurately measure BP.

While there have been extensive studies on the theory of oscillometry [14–25], to the best of the author's knowledge, there has been no comprehensive study to find the fundamental relationship between the oscillometric waveform (OMW), the only signal obtained in oscillometry, and the SBP, DBP and MAP values. Most of the oscillometric algorithms rely on empirical coefficients for SBP and DBP evaluation that may differ in various patient populations, which affects the reliability of the technique [17, 26–28]. More information could be be obtained from the amplitude and time characteristics of the oscillometric pulses at different cuff pressures if a comprehensive mathematical model of oscillometry is developed. An accurate model of oscillometry can play an important role in the research and development of accurate BP monitoring devices and enables one to perform a thorough and systematic validation of commercially available BP monitors. A comprehensive oscillometry model provides a way to test BP estimation algorithms where the parameters of interest are not directly measurable. Accurate models also enable us to study and develop signal processing algorithms under different conditions without the need for access to real subjects, to improve algorithms quickly, and to reduce

product development time.

Moreover, oscillometry is solely based on recording and analyzing the pressure variations within the oscillometric cuff during the deflation period. It appears that the simultaneous measurement of other relevant physiological signals along with the oscillometric recordings, could provide additional useful information that may be incorporated to improve the accuracy and robustness of BP estimates. For example, measurement of the simultaneous electrocardiogram (ECG) signal could help us identify the true oscillometric pulses and enables us to measure the pulse transit time (PTT) which is highly correlated with BP [29].

It should be noted that there are number of commercially available oscillometric BP monitors that meet the current standards for automated BP devices [30–35]. However, the exact oscillometric algorithms used in these devices are not disclosed by the manufacturer limiting any further analysis, evaluation, and validation of these oscillometric algorithms. Moreover, the current standards for BP monitors are arguably too lax as the recommended mean error (ME) and standard deviation of error (SDE) for estimation of BP are within 5 mmHg and 8 mmHg, respectively [36, 37]. An editorial in the journal Hypertension states that "although some might argue that a 3-4 mmHg increase in BP is not clinically signicant, clinical trials and population studies remind us of the importance of these seemingly small changes" [13]. A recent 1 million-patient meta-analysis suggests that a 3-4 mmHg increase in systolic BP would translate into 20% stroke mortality and a 12% higher mortality from ischemic heart disease [38]. Therefore, even small errors in estimation of BP could have large consequences on health [39–41]. Also, the accuracy and reliability of the current BP devices for different patient populations such as patients with obesity, arterial stiffness, atrial fibrilation, etc., is questionable [42–44]. Hence, accurate estimation of SBP, DBP, and MAP from oscillometric recordings remains an ongoing challenge.

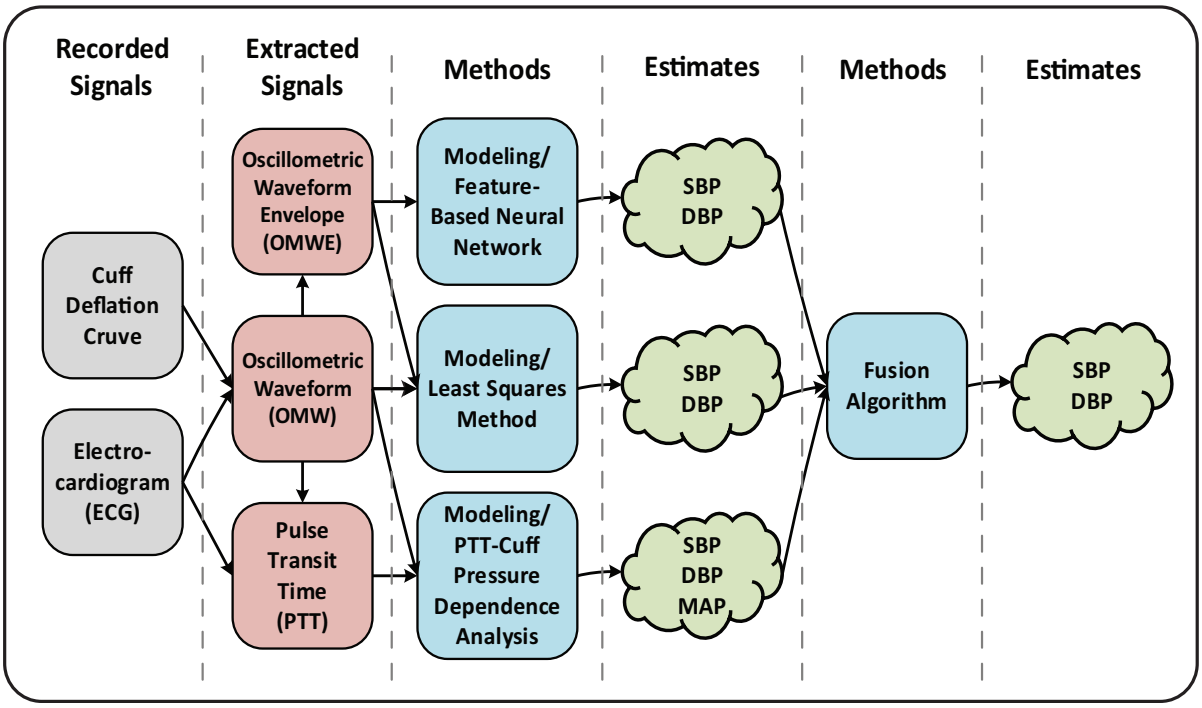

Figure 1.1: Block diagram representation of the proposed model-based oscillometric BP estimation methods.

1.3 Contributions

In this thesis, the problem of oscillometric BP estimation is addressed by incorporating a comprehensive modeling approach, based on which coefficient-free estimation of BP becomes possible. Figure 1.1 illustrates the block diagram representation of the proposed model-based BP estimation methods.

First, a feature-based neural network (NN) method is developed to find an implicit relationship between the SBP/DBP values and the oscillometric waveform envelope (OMWE). A New feature extraction technique is proposed to find an efficient representation of the OMWE samples, and several training algorithms are compared to find the best trained NN. In addition to the NN, the adaptive neuro-fuzzy inference system (ANFIS) is also utilized as an alternative to the NN for BP estimation from the extracted features. To the best of the author's knowledge, there is no research study that has derived features from the OMWE for estimation purposes. There is also no existing

work on comparing different NN training algorithms for BP estimation. This is also the first research study that applies the ANFIS to BP estimation. This research has been partly published in a refereed IEEE journal paper [45] and three refereed IEEE conference proceedings [46–48], and presented in the WiSense Seminar at the University of Ottawa.

Our modeling approach is then further extended by developing a comprehensive model that explicitly represents the relationship between the oscillometric recordings and intra-arterial blood pressure (ABP). The instantaneous ABP is mathematically modeled by considering different physiological parameters that contribute to the ABP total variability. These parameters include the amplitudes and phase angles of the cardiac and respiratory signals' fundamental frequency and higher harmonics. The cuff-arm-artery system is also modeled by incorporating the physical properties of the arterial wall, the arm, and the oscillometric cuff. These mathematical models are combined to obtain a mathematical model for the OMW. The envelope of the OMW (OMWE) is then explicitly modeled as a function of the SBP, DBP, and cuff-arm-artery system parameters. Based on our developed model, we propose a new coefficient-free oscillometric BP estimation method. The proposed method is based on minimizing the least squares error between our model and the OMWE using the trust region reflective algorithm. To the best of the author's knowledge, this is the first research study on developing a mathematical model for the OMW. Moreover, this is the first research study that proposes an explicit mathematical model for the OMWE as a function of SBP and DBP. The primary results of this part of the thesis have been presented as an invited plenary lecture at the IEEE International Symposium on Medical Measurements and Applications (MeMeA'12). Also, parts of this section have been accepted for publication in a refereed IEEE journal paper [49], published in two refereed IEEE conference proceedings [50, 51], and presented in a poster competition at the University of Ottawa.

OMW is usually the only signal obtained in oscillometry, and therefore it is the focus of all oscillometric algorithms to find the BP values [10]. In the last stage of this research,

the ECG signal is recorded simultaneously along with the OMW, as another independent source of information. The simultaneously recorded ECG signal is incorporated in the following ways: i) The ECG signal is used to identify the true oscillometric pulses in order to help reconstruct the OMW from cuff recordings which are usually contaminated with noise and artifacts; ii) Having the simultaneous ECG signal along with the OMW, measurement of pulse transit time (PTT), defined as the time taken by an arterial pulse to travel between the heart and a peripheral arterial site, becomes feasible. Our developed model of oscillometry is utilized to build a model of the PTT. A comprehensive theoretical explanation of the behaviour of PTT with respect to cuff pressure is provided. Based on the observed PTT-cuff pressure dependency, novel coefficient-free methods for estimation of SBP, DBP, and MAP are proposed. To the best of the author's knowledge, no previous work provided a theoretical explanation of the PTT-cuff pressure dependency along with employing a coefficient-free method for BP estimation from either the PTT-cuff pressure dependency or oscillometry. This research has been partly published in a refereed IEEE journal paper [52] and forms part of a pending patent [53]. Also, parts of this research have been submitted for publication in a journal paper which is currently under review.

Finally, the three proposed coefficient-free BP estimation methods are fused together to obtain more accurate and robust estimates of the BP. The proposed fusion algorithm is based on the weighted arithmetic mean of the three proposed methods' estimates. The primary results of this part of the thesis have been presented as an invited plenary lecture at the IEEE International Symposium on Applied Computational Intelligence and Informatics (SACI'13). Also, parts of this research have been accepted for publication in an IEEE conference paper [54].

1.4 Thesis Organization

This thesis is organized as follows. In Chapter 2, the related literature on the estimation of BP is reviewed. In Chapter 3, a new feature extraction technique from the OMWE

is proposed and a NN approach is developed for estimation of BP. In Chapter 4, a mathematical model for the OMW is derived by considering the cuff-arm-artery system, the OMWE is explicitly modeled as a function of SBP and DBP, and a coefficient-free BP estimation method using the trust region reflective algorithm is proposed. In Chapter 5, the PTT is mathematically modeled by considering the cuff-arm-artery system and blood flow dynamics, and a coefficient-free BP estimation method based on the PTT-cuff pressure dependency is proposed. In Chapter 6, the three proposed model-based BP estimation methods are compared, their particular applications are discussed, and a fusion algorithm is proposed to obtain more robust and accurate estimate of BP. In Chapter 7, the thesis is concluded and possible future directions are proposed.

Chapter 2

Literature Review

Methods of measuring BP are generally categorized into invasive and noninvasive methods. The most common invasive method of BP measurement is the intra-arterial measurement using a cannula [55]. A short, parallel-sided cannula composed of Teflon or polyurethane is passed into a non-end artery, such as the radial artery. The cannula is attached to a tubing system, which provides a constant infusion of saline. The pressure waveform is transmitted through the liquid within the infusion tubing to a diaphragm that moves in response to the pressure. A transducer then converts the movement to an electrical signal. The invasive method of BP measurement is usually restricted to a hospital setting and has the disadvantages of complexity, risk to the patient, and inconvenience.

As an alternative, several noninvasive BP estimation methods have been developed which are safer, quicker, and require less expertise. The noninvasive BP estimation techniques are either manual or automated. Palpation and auscultation are the two common manual methods of measuring BP. A sphygmomanometer composed of an inflatable cuff and a mercury manometer is used in both manual methods. The inflatable cuff is placed around the subject's upper arm at the same height as the heart. The cuff is inflated to supra-systolic pressure so that the artery is completely occluded. The cuff is then slowly released.

In the palpatory method, a trained examiner palpates the radial pulse at the subject's wrist. The pressure at which the pulse disappears during inflation and then subsequently reappears during deflation will be the SBP. Palpation is only used in emergency situations and cannot estimate the DBP and MAP. Moreover, the SBP estimates can have an error of up to 25% [55]. Recently, a palpation technique for DBP estimation has been introduced [56]. In this technique, the examiner puts his/her first three fingers lightly over the bend of the elbow at medial side of antecubital fossa. A pulsatile thrill can be palpated during the cuff deflation. The pressure at which this pulsatile thrill disappears is determined as the DBP.

In the auscultatory method, a trained examiner listens to the Korotkoff sounds with a stethoscope in order to identify the SBP and DBP values. The cuff pressure at which the first Korotkoff sound is heard is the SBP and the cuff pressure at which the sounds become muffled is the DBP. Since the auscultatory method requires a trained examiner to determine the SBP and DBP values, its usage is mostly limited to the hospital or doctor's office. Moreover, because of the anxiety of patients during visits to the doctor's office, the auscultatory readings can even be inaccurate [34].

The palpation and auscultatory methods use a mercury manometer for measuring the pressure which is now considered to be an environmental hazard, and therefore many countries in Europe and North America are in the process of eliminating the use of mercury sphygmomanometers and replacing them with automated BP monitors that do not use mercury [57, 58].

Several automated BP estimation techniques have been developed for continuous and home BP monitoring. These techniques can be broadly categorized into two types: i) the continuous recording techniques that provide the beat-to-beat arterial blood pressure (ABP) variations, and ii) the sampling techniques that only estimate SBP, DBP, and sometimes MAP in a short measurement period of less than a minute [18]. The remainder of this chapter is dedicated to the review of different automated BP estimation methods with a focus on oscillometry as the most popular automated method.

2.1 Continuous Methods

2.1.1 Pulse Sensing

The pulse sensing technique is based on noninvasive measurement of the ABP pulse waveform using either a volume or a pressure pulse sensor [18].

The volume pulse sensor measures the arterial volume changes that relate to the variations in ABP. Different transduction methods can be employed to measure the arterial volume such as resistive, capacitive, inductive, and optical. An example of such a technique is photoplethysmography where an infrared emitter and a photo-diode detector are used to measure the changes in infrared reflectance resulting from varying blood volume in the artery [59]. The disadvantage of this method is that the nonlinear and viscoelastic properties of the arterial wall makes it difficult to find the exact relationship between the measured volume and the corresponding ABP. Recently, artificial neural networks (NNs) have been employed to estimate BP from the photoplethysmogram (PPG) signal [60–62]. A NN is trained using features extracted from the PPG pulse as input, with reference BP readings as the corresponding network targets. The trained NN can be used to estimate the BP from any new PPG pulse that has not been provided during the training phase.

The pressure pulse sensor measures the transmitted arterial pressure at the skin surface. As the vascular nonlinear and viscoelastic properties do not affect this method, this technique provides superior waveform accuracy as compared to the volume sensors. However, this method is very sensitive to motion artifact [63]. Arterial tonometry is an example of pressure pulse method that is used at superficial arteries supported by a bone to obtain arterial pressure [8]. In this technique, a flat array of pressure sensors is pressed against the skin over the artery so that the arterial wall becomes flattened. At this position, the contact stress is equal in magnitude to the ABP.

Both volume and pressure sensors respond proportionally to the ABP, and therefore an important disadvantage of these methods is that they need be calibrated. Moreover, sensor positioning is a challenging task in the pulse sensing technique.

2.1.2 Vascular Unloading

In the vascular unloading technique, a small pressurized cuff is placed around the subject's finger. The pressure of the cuff is automatically adjusted so that the the blood volume under the cuff is always constant. To this end, a plethysmograph is utilized to measure the arterial blood volume underneath the cuff. The measured blood volume signal is used in a feedback controlled system to instantaneously adjust the cuff pressure. In this condition, the applied cuff pressure is always equal to the internal arterial pressure, and therefore a continuous measure for ABP is obtained. Since the arterial wall tension is zero at zero transmural pressure (arterial pressure minus external cuff pressure), this technique is known as "vascular unloading" [9].

One such commercial device is called the Finger Arterial Pressure System (FINAPRES) [64], that has shown good waveform agreement in comparison with the intra-ABP measurements [65]. However, mean pressure differences are expected as the device needs to be regularly calibrated. The technique is also prone to pulse wave reflection effects as the recording site is at the finger, and can be affected by skin temperature, vasoactive drugs, and anesthetics [18].

2.2 Sampling Methods

2.2.1 Automated Auscultatory

The auscultatory method can be automated by replacing the stethoscope with a microphone. Sound processing algorithms are then employed to estimate the SBP and the DBP. The automated auscultatory method is not reliable in noisy environments. Moreover, this method may not work for some patient conditions such as hypotension where the Korotkoff sounds may be muted [2].

2.2.2 Doppler Ultrasonic Sphygmomanometry

Doppler ultrasonic sphygmomanometry is similar to the auscultatory method but it uses a Doppler sensor instead of the stethoscope [4]. The opening and closing of the artery under the cuff generates Doppler-shift signals that are recorded and analyzed to estimate SBP and DBP. When the cuff pressure is above SBP or less than DBP, no Doppler-shift signal is detected. When the cuff pressure is between SBP and DBP, the ultrasonic sensor detects two Doppler-shift signals in each heartbeat corresponding to the opening and closing of the artery. In Doppler ultrasonic sphygmomanometry, SBP is estimated as the cuff pressure at which the the first Doppler-shift signal is detected. DBP is estimated as the cuff pressure at which the closing signal from one pulse coincides with the opening signal of the following pulse.

2.2.3 Oscillometry

Oscillometry is similar in principle to the auscultatory method, but uses a pressure sensor to record the small pressure oscillations within the cuff rather than listening to the Korotkoff sounds. An inflatable cuff, similar to the one used in the auscultatory method, is wrapped around the upper arm or wrist and is inflated to a supra-systolic pressure. The cuff is then slowly deflated to a sub-diastolic pressure while recording the pressure oscillations (also known as oscillometric pulses) within the cuff.

Figure 2.1 illustrates the oscillometry system physical setup. The main components of the oscillometry system are the artery, the cuff, and the arm. The inputs of the system are the applied cuff pressure and the intra-arterial blood pressure (ABP). As the cuff is inflated to a supra-systolic pressure, the cuff pressure is transmitted through the arm soft tissue to the arterial wall. During the inflation, arterial lumen area (ALA) decreases until it becomes flat and occluded. The cuff is then deflated gradually to a sub-diastolic pressure. During the deflation, ALA increases until it becomes completely open at very low cuff pressures.

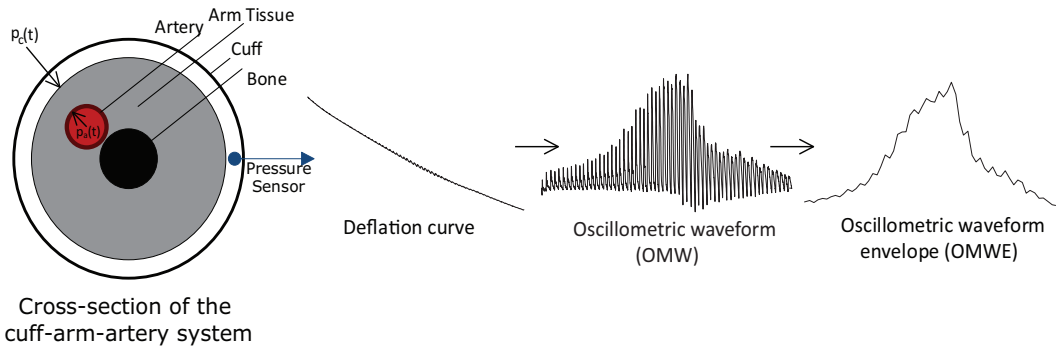

Figure 2.1: Oscillometry system physical setup. The arterial blood pressure and the cuff pressure have been shown by $p_a(t)$ and $p_c(t)$, respectively.

Over the deflation period, the recorded pressure waveform forms a signal known as the cuff deflation curve. A bandpass filter with a lower cutoff frequency of around 0.5 Hz and an upper cutoff frequency of around 20 Hz is utilized to extract the oscillometric pulses from the cuff deflation curve. Over the deflation period, the extracted oscillometric pulses form a signal known as the oscillometric waveform (OMW). The amplitude of the oscillometric pulses increases to a maximum and then decreases with further deflation. Since the oscillation amplitudes carry most of the BP information [14–17, 19, 20], the positive and negative peaks of the oscillations are detected. The oscillometric waveform envelope (OMWE) is then formed by subtracting the consecutive peaks and troughs of the OMW.

In oscillometry, MAP can be estimated with good accuracy as the cuff pressure at which the OMWE attains maximum amplitude [15]. A variety of analysis algorithms can be employed in order to estimate the SBP and DBP values [10, 66]:

1) *Maximum Amplitude Algorithm:* The most popular oscillometric algorithm is the maximum amplitude algorithms (MAA). The MAA approximates the MAP as the cuff pressure at which the OMWE attains a maximum, and then linearly relates the systolic and diastolic pressures to the mean pressure using empirically derived coefficients. These coefficients serve to determine the time points at which the cuff pressure coincides with the systolic and diastolic pressures, respectively [6]. The procedure of the MAA is shown

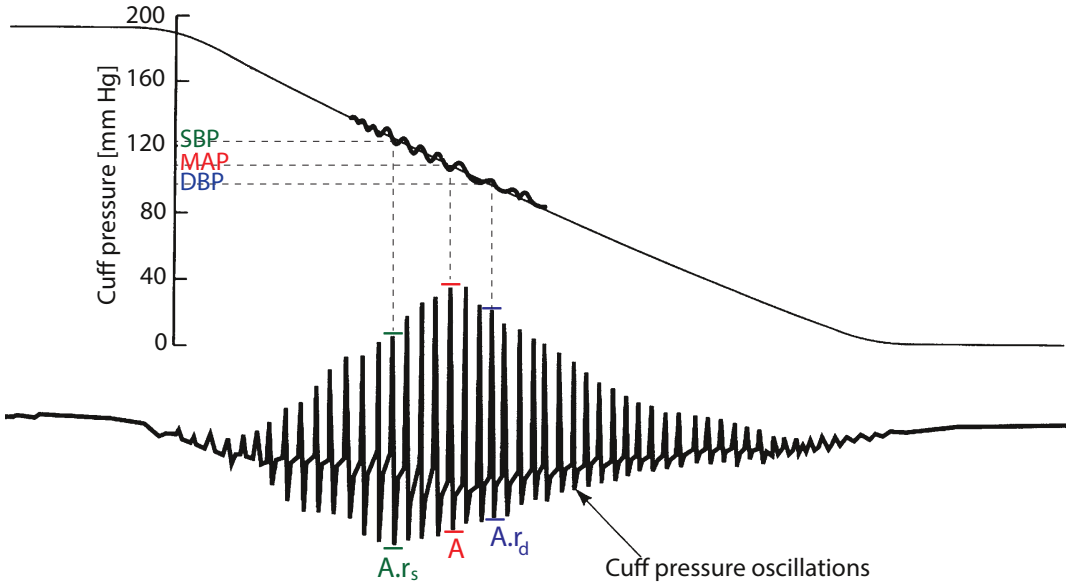

Figure 2.2: Procedure of the maximum amplitude algorithm (MAA). The cuff pressure oscillations are extracted using a band-pass filter. The cuff pressure at which the maximum amplitude oscillation occurs is determined as the MAP. The cuff pressure at which the amplitude of the oscillations reaches the systolic ratio r_s of the maximum amplitude A is determined as the SBP. The cuff pressure at which the amplitude of oscillations falls down the diastolic ratio r_d of the maximum amplitude A is determined as the DBP.

in Fig. 2.2.

The systolic coefficient r_s may range from 0.45 to 0.73 and the diastolic coefficient r_d may range from 0.69 to 0.83 in different devices [66]. In [15], it has been shown that the mean BP may be estimated accurately by MAA. However, due to the sensitivity of the method to variations in BP waveform, pulse pressure and arterial compliance, the systolic and diastolic pressures cannot be precisely determined. Moreover, it has been observed that the coefficients used in MAA should be changed as the parameters of the cardiovascular system vary between different health conditions, age groups, etc. [17, 26]. Recently, the Gaussian mixture regression technique was used to estimate the SBP and DBP coefficients [67]. Using a dataset of oscillometric BP measurements, several targeting clusters were built, each representing the measurements with similar SBP and DBP values. These targeting clusters were identified by a Gaussian mixture model. The

Gaussian mixture regression technique was then used to obtain the optimum SBP and DBP coefficients for each cluster.

2) *Linear Approximation Algorithm:* This algorithm is similar to the MAA, but approximates the OMWE by two lines of best fit; one for the systolic side and another for the diastolic side. The cuff pressure at which the two lines intersect is taken as the MAP. Similar to the MAA, empirically derived coefficients are then used to find the SBP and DBP values [68].

3) *Derivative Oscillometry:* The derivative oscillometry method is based on analyzing the slope of the OMWE. Drzewiecki et al. [17,18] found that the derivative of the OMWE plotted against the cuff pressure reaches a maximum at a cuff pressure equal to the DBP, and a minimum that occurs at a cuff pressure equal to the SBP. The advantage of derivative oscillometry is that it does not require any empirical coefficients. However, as the method is based on the derivative of the envelope, it is very sensitive to noise and artifacts such as movement and muscle contractions, and requires a good quality signal to perform well.

4) *Neural Network Method:* Recently, artificial neural networks (NNs) have been employed as a nonlinear tool to model the complex and nonlinear relationship between the OMWE and the BP [69–71]. Baker et al. [69] proposed a two-layer feed-forward NN (FFNN) with a steepest descent backpropagation training algorithm for estimation of BP from the superficial temporal artery. In a similar effort, Narus et al. [70] trained a three-layer FFNN using steepest descent backpropagation training with momentum for estimation of BP at the supraorbital artery. In [71], a two-layer FFNN was designed to estimate the BP from the upper arm and found to be superior to the MAA algorithm in terms of standard deviation of error (SDE). These methods are based on training a network using the OMWE as input, with intra-arterial measurements [69] or measurements made by a nurse [70, 71] as the corresponding network targets. Once the network has extracted information about the association between the input (OMWE) and target (measured BP), it can be used to estimate the BP from any unknown input pattern that

has not been provided during the training.

4) *Pulse Morphology Method:* This method is based on extracting particular features of the individual oscillometric pulses and studying their changes as a function of cuff pressure [72, 73]. In [74], a straight line was drawn between each two successive oscillometric pulse peak and trough. The area between this straight line and oscillometric pulse was then calculated and its changes were studied over the deflation period to estimate the MAP. In [75], quantitative measures such as augmentation index, reflection index, and stiffness index were extracted from individual oscillometric pulses and their changes were studied as a function of cuff pressure. It was found the extracted features attain a global maximum or minimum at a cuff pressure equal to MAP, while they exhibit local maxima or minima at cuff pressures equal to SBP and DBP. In [76], the statistical Wald t-test was used to detect the significant changes in the oscillometric pulse waveforms. The cuff pressures at which the first and last significant changes occurred in the oscillometric pulses were determined as the SBP and DBP values. The existing pulse morphology based methods are without physiological and theoretical basis and have not yet been adequately validated.

4) *Modeling:* It is of great importance to obtain a model of oscillometry to study, develop, and test different oscillometric algorithms. In the literature, several models for the oscillometric technique have been proposed. These studies can be classified into three categories: (i) the literature that build models to study and test the validity of empirical coefficients for estimation of SBP and DBP from the OMWE [14, 15, 17–21], and (ii) the literature that build models to develop new BP estimation methods [16, 24, 25].

In [14], a simple theoretical model of the cuff-arm-artery system was developed by analyzing an elastic vessel contained within an air compliance chamber. It was shown that the MAP can be accurately estimated as the cuff pressure at which the OMWE exhibits a maximum. A similar model was utilized in [15] to study the effect of different parameters on the cuff pressure oscillations. These parameters included the collapse behavior of the artery, the arterial volume-pressure relationship, the volume of the cuff,

and the arterial pressure waveform amplitude and shape. It was found that MAP can be accurately estimated from the peak of the OMWE. However, SBP and DBP cannot be accurately determined using fixed detection coefficients. In [16], a volume-pressure curve unique to each subject's artery was obtained by analyzing the individual oscillometric pulses. This curve along with the pre-estimates of the SBP and DBP were utilized to monitor the subject's BP in short periods of time without the need to apply cuff pressures much greater than the DBP. A more accurate description of the mechanics of the occlusive cuff and of brachial artery with details on arterial buckling was provided by Drzewiecki et al. [17]. Their model was found to represent the basic characteristics of oscillometry on actual blood vessel data. The effect of arterial pressure on the systolic and diastolic detection coefficients was evaluated using their model. It was found that the systolic and diastolic coefficients should be lowered at high SBP and low DBP values, respectively. In [19], a mathematical lumped parameter model of oscillometry was derived by incorporating the cuff compliance, pressure transmission from the cuff to the brachial artery through the arm soft tissue, and the biomechanics of the brachial artery. However, the estimation of BP still relied on empirical coefficients. In [21], the proposed model of oscillometry in [19] was further simplified by performing a global sensitivity analysis. The models of the cuff, arm, and artery were then replaced with simpler models with less number of parameters. In [22], a white box model was developed for oscillometric BP monitor by dividing the BP monitor system into two subsystems: the electromechanical subsystem that receives the electrical supply and outputs a torque to the crankshaft of the air pump, and the pneumatic subsystem that controls the cuff pressure. Subsequently, a black box model was derived for the oscillometric BP monitor that represents a single-input single-output relationship between the voltage supplied to the air pump and the cuff pressure. However, no method for estimation of BP was provided. In [24], a three-segment compliance model was developed to describe the volume changes of the artery recorded by a finger photoplethysmograph. A similar model was developed in [25] to describe the volume changes of the artery recorded by an oscillometric cuff. The vessel

compliance was first estimated using pre-estimates of the SBP and DBP obtained by an independent method. The compliance information was then used to estimate the subject's BP. Table 2.1 provides a comparison between different published model-based oscillometric BP estimation methods.

It has been assumed that the arm tissue is mostly incompressible, and therefore any change in the arterial volume results in a corresponding change in the cuff bladder volume [17,19,20,24,25]. Therefore, the oscillations of the cross-sectional area of the artery, also known as lumen area, are proportional to the oscillations observed on the recorded cuff pressure deflation curve [14–17]. In [17,19], the area oscillations were extracted from the simulated lumen area waveform using a high-pass filter with a cutoff frequency of 0.3-0.5 Hz, and were shown to be consistent with actual recorded oscillometric pulses.

While some of the above mentioned literature [15, 17, 19] studied the validity of the empirical coefficients used for estimation of SBP and DBP, none of them provided the fundamental relationship between the OMW and the SBP and DBP values.

2.2.4 Pulse Transit Time Analysis

A relatively new method that goes beyond oscillometry involves the estimation of BP from pulse transit time (PTT). PTT is defined as the time it takes by a pressure pulse to travel between the heart and a peripheral arterial site [29]. In practice, for ease of measurement, PTT is usually measured as the time interval between the ECG R-peaks and certain points on the arterial pulses recorded from a peripheral artery, as shown in Fig. 2.3. The reason to use the ECG R-peaks as the reference points for measuring the PTT is that the ECG R-peaks correspond approximately to the opening of the aortic valve.

It has been observed that there is a correlation between the PTT and BP that could be used to estimate BP [77, 78]. PTT-based methods can be broadly classified into two categories [79]: (i) PTT-BP correlation analysis, and (ii) PTT-cuff pressure dependence analysis.

Table 2.1: Comparison of different published model-based oscillometric blood pressure (BP) estimation methods.

Authors	Developed Models	Obtained Estimates	Drawbacks
Mauck et al. [14]	Simple model of the cuff-arm-artery system	MAP	No method for estimation of SBP and DBP was provided
Forster et al. [15]	Simple model of the cuff-arm-artery system	SBP, DBP, and MAP	The SBP and DBP estimation method relied on fixed coefficients.
Link et al. [16]	Model of the volume-pressure relationship of the artery	SBP, DBP, and MAP	Required pre-estimates of the SBP and DBP using another method.
Drzewiecki et al. [17, 18]	Model of the cuff-arm-artery system with details on arterial buckling	SBP, DBP, and MAP	Relied on empirical coefficients.
Ursino et al. [19, 20]	Mathematical lumped parameter model of the cuff-arm-artery system by incorporating the cuff, arm soft tissue, and the brachial artery effects.	SBP, DBP, and MAP	Relied on empirical coefficients.
James [21]	Simplified model of oscillometry proposed in [19, 20].	SBP, DBP, and MAP	Relied on empirical coefficients.
Pinheiro and Postolache [22]	White box and black box models for the oscillometric BP monitor by considering the electromechanical and pneumatic subsystems.	——	No method for estimation of SBP, DBP, and MAP was provided.
Sun et al. [23, 24]	Three-segment compliance model for the volume changes of the artery recorded by a photoplethysmograph.	SBP, DBP, and MAP	Required pre-estimates of the SBP and DBP using another method.
Babbs [25]	Three-segment compliance model for the volume changes of the artery recorded by an oscillometric cuff.	SBP, DBP, and MAP	Required pre-estimates of the SBP and DBP using another method.

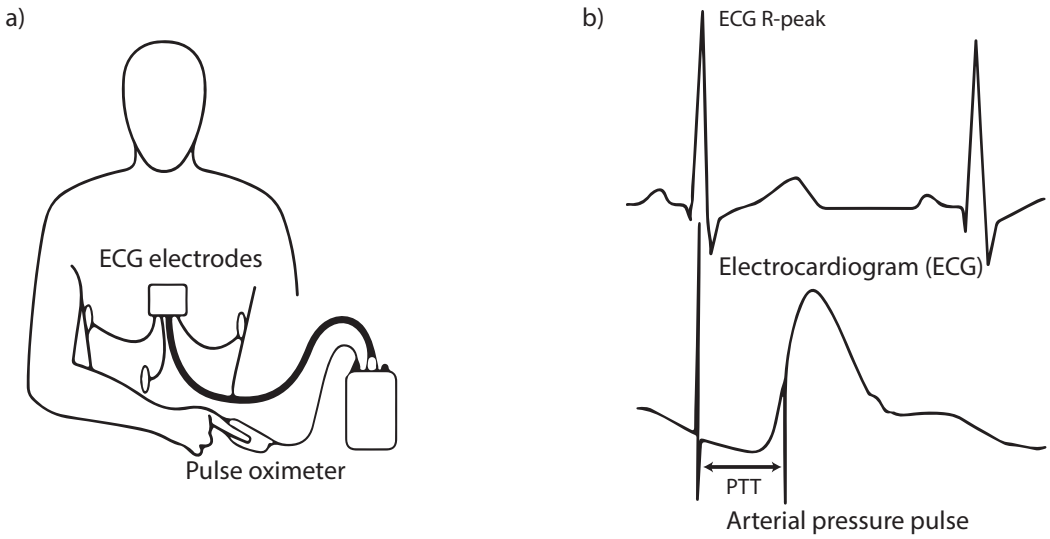

Figure 2.3: Pulse transit time (PTT) measurement principle. (a) Example of a PTT measurement system. ECG electrodes and oximetric photoplethysmography are used to obtain the ECG and the arterial blood pressure signals, respectively. (b) Schematic diagram showing the calculation of PTT as the time interval between the ECG R-peak (as the starting point reference) and the arterial pulse wave (as the end point).

PTT-BP Correlation Analysis

In the PTT-BP correlation method [80–90], a regression model is found between the BP and the PTT. PTT is estimated as the time interval between the ECG R-Peak and the arterial pulses measured at a peripheral artery. Another independent method is employed to measure the reference BP. A dataset of PTT and BP measurements is then collected based on which a regression model between the BP and the PTT is found. The main disadvantages of this method are the frequent need for calibration by a reference sphygmomanometer and the low accuracy because of the weak and inconsistent correlation between PTT and BP [91–93].

Table 2.2 provides a comparison between different published PTT-BP correlation analysis methods.

Table 2.2: Comparison of different published PTT-BP correlation analysis methods in terms of the proposed regression model and the obtained estimates.

Authors	Regression Model	Obtained Estimates
Chen et al. [80]	$BP = a + b \times \ln(PTT)$; where a and b are regression coefficients.	SBP and DBP
Meigas et al. [81], Yoon et al. [83], Sawada [89], Ma and Zhang [88]	$BP = a + b \times PTT$; where a and b are regression coefficients.	SBP and DBP
He et al. [90],	$BP = a + b \times PTT + c \times PTT^2 + d \times PTT^3$; where a, b, c, and d are regression coefficients.	SBP, DBP, and MAP
Kim et al. [82]	$BP = a \times A + b \times M + c \times I + d \times PTT +$ e; where a, b, c, d, and e are regression coefficients, and A, I, M, and D are particular features obtained from the arterial pulses.	SBP and DBP
Poon et al. [87]	$BP = a \times \ln(\frac{b}{PTT^2} - 1)$; where a and b are regression coefficients.	SBP and DBP
Gesche et al. [85]	$BP = a \times PTT \times e^{\frac{d}{PTT}} + \frac{b}{PTT^n} - c$; where a, b, c, d, and n are regression coefficients.	SBP
Cattivelli and Garudadri [86]	$BP = a \times PTT + b \times HR + c$; where a, b, and c are regression coefficients and HR is the heart rate.	SBP and DBP
Ha et al. [84]	$BP = f(PTT, age, sex, height, weight)$. Function f is not given.	SBP and DBP

PTT-Cuff Pressure Dependence Analysis

The PTT-cuff pressure dependence method uses an inflatable cuff to apply varying pressure to an artery and pressure sensors to measure the arterial pulses near the cuff. The PTT is then computed and analyzed as a function of applied cuff pressure in order the determine the BP. Geddes et al. [94] were the first who verified this principle on normal, hypertensive, and hypotensive dogs. An inflatable cuff was applied to the forelimb of anesthetised dogs and was inflated to a supra-systolic pressure. The cuff was then slowly released while measuring the BP invasively at the radial artery. PTT was measured as the time interval between the ECG R-peak and the beginning of the BP pulse upstroke.

It was found that SBP can be estimated as the cuff pressure at which the BP pulse appears at the radial artery. As the pulse appears at the radial artery, measurement of the PTT would be possible. It was observed that the PTT decreases as the cuff pressure decreases from SBP to DBP and then it remains constant for cuff pressures less than DBP. A similar approach was performed in [95] on humans to estimate the SBP and DBP. The results were validated against invasive estimates. In [96], the PTT-cuff pressure dependence method was compared with the oscillometric method. It was found that the PTT-based method is approximately as accurate as the oscillometric method, while it can also provide a measure of arterial stiffness. The results obtained in [95] and [96] were consistent with the one described earlier by Geddes et al. [94]. In [97] two piezoelectric sensors were placed proximally and distally under a brachial cuff. The PTT was measured as the time interval between the two recorded pulses. It was observed that the cuff pressure at which PTT attains its maximum value is close to the SBP and the cuff pressure at which the PTT attains a slope close to zero is close to DBP.

In [98], a wireless medical device was designed to continuously monitor the ECG, BP, and blood oxygen of a patient and deliver pertinent information to first responders. In [99], synchronized ECG signals were acquired for removing motion artifacts from oscillometric signals to increase the accuracy of BP measurements. However, these devices required pressure and ECG sensors auxiliary to the cuff, defeating the simplicity and straightforwardness of the oscillometric BP estimation method. Recently, our research group proposed an ergonomic integration of BP and ECG monitoring into a single device, providing a robust measurement of the PTT in oscillometry [79]. It was empirically found that the PTT measured as the time interval between the ECG R-Peaks and the maximum slope points of the oscillometric pulses exhibits a maximum at a cuff pressure close to MAP. Empirically derived coefficients were then used on the PTT-cuff pressure mapping to find SBP and DBP values. However, this work did not provide a theoretical grounding for this technique nor a coefficient-free approach to BP estimation.

2.3 Standards for Automated Blood Pressure Monitors

Several protocols have been introduced for evaluation/validation of the automated BP monitoring devices [37, 100–105]. The first protocol, the ANSI/AAMI SP10, was published by the American National Standards Institute (ANSI) and the Association for the Advancement of Medical Instrumentation (AAMI) in 1987 [100]. This protocol was updated in 1993 [101] and 2002 [102]. In 1990, the British Hypertension Society (BHS) published a protocol [103] which was updated in 1993 [104]. In 2009, the ANSI and the AAMI together with the International Organization for Standardization (ISO) introduced their latest standard for automated BP monitoring devices [37]. In these protocols, the noninvasive auscultatory or the invasive intra-arterial methods are considered as the reference.

In order to validate an automated BP monitor with auscultatory reference sphygmomanometer, both BHS and ANSI/AAMI/ISO protocols require a dataset of BP measurements obtained from a minimum of 85 subjects. At least three BP measurements should be performed on each subject for a total of 255 measurements. Two trained observers should make simultaneous BP readings on each subject using auscultatory technique with a double stethoscope. The observers' individual readings should be averaged to create the reference BP. Readings taken by the automated BP device and the trained observers can be either sequential or simultaneous. In the case of sequential measurement, there should be at least a one-minute delay between the automated BP device and the trained observers readings.

In order to validate an automated BP monitor with reference invasive BP monitoring equipment, the ANSI/AAMI/ISO protocol requires a dataset of at least 150 BP measurements obtained from a minimum of 15 subjects. No more than 10 valid BP measurements should be taken from each subject. Readings taken by the automated BP device and the reference invasive BP monitoring equipment should be sequential with at

least a one-minute delay. The BHS protocol does not recommend the use of invasive BP measurement as the reference.

The ANSI/AAMI/ISO protocol determines the accuracy of BP monitoring devices using two measures; the mean error (ME) and the standard deviation of error (SDE) obtained over all 255 measurements. This standard requires an absolute ME equal or less than 5 mmHg and an SDE equal or less than 8 mmHg.

The BHS protocol classifies the BP monitoring devices into grades A to D, where grade A shows the best accuracy. If 60, 85, and 95% of the readings have errors of less than 5, 10, and 15 mmHg, respectively, the BP monitor is graded in class A. If 50, 75, and 90% of the readings have errors of less than 5, 10, and 15 mmHg, respectively, the BP monitor is graded in class B. If 40, 65, and 85% of the readings have errors of less than 5, 10, and 15 mmHg, respectively, the BP monitor is graded in class C. Grade D is assigned to a device with worse accuracy than grade C.

The European Society of Hypertension (ESH) has also developed a protocol for evaluation of BP monitoring devices, called the international protocol [105]. However, the ANSI/AAMI/ISO protocol involves the most stringent requirements for evaluation/validation of BP monitors, and is the most popular and accepted standard.

The measures usually used in evaluating the automated BP monitors are the mean error (ME) and the standard deviation of error (SDE) obtained on a dataset of BP measurements [37]. ME shows the bias of the estimates, while SDE is a measure of error variability. A method with small ME can still be unreliable if it produces large values of SDE. In this thesis, we also compute the mean absolute error (MAE) that shows the overall accuracy in estimating the BP.

The true value of many quantities in the living body including BP are not exactly known unless an invasive approach, which is associated with potential adverse effects, is employed. Based on this problem, Bland and Altman [106, 107] developed a graphical statistical approach to assess the agreement between a newly developed measurement method and other established measurement methods rather than with the true quantity

being measured. "We cannot be certain that either method gives us an unequivocally correct measurement and we try to assess the degree of agreement between them. The standard method is sometimes known as the "gold standard", but this does not – or should not – imply that it is measured without error" [108]. Bland and Altman applied their assessment approach on BP data in [108, 109]. Suppose two BP devices are used to estimate the BP value. Each point on the Bland-Altman plot represents the difference between the two device estimates (y-axis) and their average (x-axis). The agreement between the devices is quantified by the bias (ME) and the limits of agreement (ME $\pm$ 1.96 $\times$ SDE) that are shown by horizontal lines on the plot. The Bland-Altman plot illustrates how the error between the two devices is distributed over the range of average values. In general, smaller bias and narrower limits of agreements show a better agreement between the two devices. In this thesis, Bland-Altman analysis is performed to study the agreement between our estimates and the reference readings.

Chapter 3

Modeling the Relationship Between Blood Pressure and Oscillometric Waveform Using Neural Networks [1]

Artificial neural networks (NNs) can be considered as a nonlinear statistical data modeling tool that can approximate almost any nonlinear relationship that may exist between inputs and outputs or find patterns in data. These computational models are characterized by their architecture, learning algorithm, and activation functions [110]. NNs do not require an explicit mathematical model and are thus suitable for physiological systems that defy modeling due to their nonlinear nature. NNs have been widely used in the

[1] Parts of this chapter have been published in:

1. M. Forouzanfar, H. R. Dajani, V. Z. Groza, M. Bolic, and S. Rajan, "Feature-based neural network approach for oscillometric blood pressure estimation," *IEEE Trans. Instrum. Meas.*, vol. 60, pp. 2786-2796, Aug. 2011.
2. ——, "Comparison of feed-forward neural network training algorithms for oscillometric blood pressure estimation," *in IEEE Int. Workshop on Soft Computing Applications (SOFA'10)*, (Arad, Romania), pp. 119-123, Jul. 2010.
3. ——, "Adaptive neuro-fuzzy inference system for oscillometric blood pressure estimation," *in IEEE Int. Workshop on Medical Measurements and Applications (MeMeA'10)*, (Ottawa, ON), pp. 125-129, May 2010.
4. ——, "Oscillometric blood pressure estimation using principal component analysis and neural networks," *in IEEE Toronto Int. Conf. Science and Technology for Humanity (TIC-STH'09)*, (Toronto, ON), pp. 981-986, Sep. 2009.

biomedical measurement and instrumentation area.

A possible solution to overcome the limitations of conventional oscillometric algorithms is the application of NNs. However, as mentioned in Chapter 2, only a few NN-based techniques have been proposed in the literature to address the oscillometric BP estimation problem [69–71].

In the existing literature, the raw oscillometric waveform envelope (OMWE) is evenly sampled at specific increments of cuff pressure and the resultant samples are fed to the NN as input. The slow rate of cuff deflation results in a smooth OMWE, if the artifacts that corrupt the envelope are disregarded. Therefore, the sampling rates that are used to capture the necessary information from the OMWE result in a large set of redundant correlated input data in the sense that each sample can be interpolated from its neighboring samples. There are several disadvantages in these algorithms. Firstly, the performance of NNs is dependent on the input data representation. An effective data representation can improve the learning and generalization capability of the network, while redundant input data, as is the case with the OMWE, would decrease the discrimination capability of the network and lead to degradation in the learning process. This results in a poorly generalizable network [111]. Secondly, a redundant input data would lead to a NN with a large number of input nodes. As the number of input nodes increases, the NN would require a larger number of hidden nodes in order to determine the exact input-output relationship [112]. Thirdly, as the number of NN weights is increased, a larger training dataset would be required. This is because the training of a NN involves an optimization process with degrees of freedom equal to the number of weights [113]. However, collecting a large oscillometric waveform (OMW) dataset would be very expensive and time consuming. As a result, a NN with a smaller number of input nodes is preferred. This can be achieved if the entire signal can be represented by a reduced set of either samples or parameters that capture the essential features of the signal. Finally, the research on estimation of BP using NNs has been limited to the use of standard feed-forward neural networks (FFNNs) without the use of appropriate training algorithms. The existing

literature uses steepest descent [69], or steepest descent with momentum [70] algorithms with a fixed learning rate to train the NN. The steepest descent algorithm has several disadvantages such as slow learning, requiring a good training dataset, getting stuck in local minima, and providing little or no robustness to noise [110]. These disadvantages can be circumvented by using more advanced training algorithms.

In this chapter, an effective NN approach for BP estimation is developed which is novel in the following ways: (a) Instead of directly applying the raw OMWE to the NN [69–71], we propose a feature extraction technique that derives a small set of features that forms an effective representation of the entire OMWE. The idea is to model the OMWE by an analytic expression with a small set of parameters. This is performed by fitting the OMWE with the sum of two Gaussian functions. The optimum parameters of the Gaussian functions are found by minimizing the least squares error between the model and the actual signal using the trust region reflective algorithm [114]. These parameters are taken as the features for the NN. To the best of our knowledge, there is no previous published research work that has derived features from the OMWE for prediction purposes. (b) The performance of ten different training algorithms belonging to three classes: steepest descent (with variable learning rate, with variable learning rate and momentum, resilient backpropagation), quasi-Newton (Broyden-Fletcher-Goldfarb-Shanno, one step secant, Levenberg-Marquardt) and conjugate gradient (Fletcher-Reeves update, Polak-Ribire update, Powell-Beale restart, scaled conjugate gradient) are evaluated in the estimation of SBP and DBP. (c) In addition to the NN, a hybrid neuro-fuzzy technique that combines the advantages of both NN and fuzzy logic is utilized for estimation of BP from OMWE. This technique is called adaptive neuro-fuzzy inference system (ANFIS). It employs a NN approach to the design of a fuzzy inference system [115]. Learning and adaptation of the NNs makes this fuzzy system more systematic and less reliant on the knowledge of experts. It has been shown that under proper conditions, ANFIS can be used as a universal approximator [116]. Therefore, it is particularly suited for solving function approximation problems such as our case where we want to find an

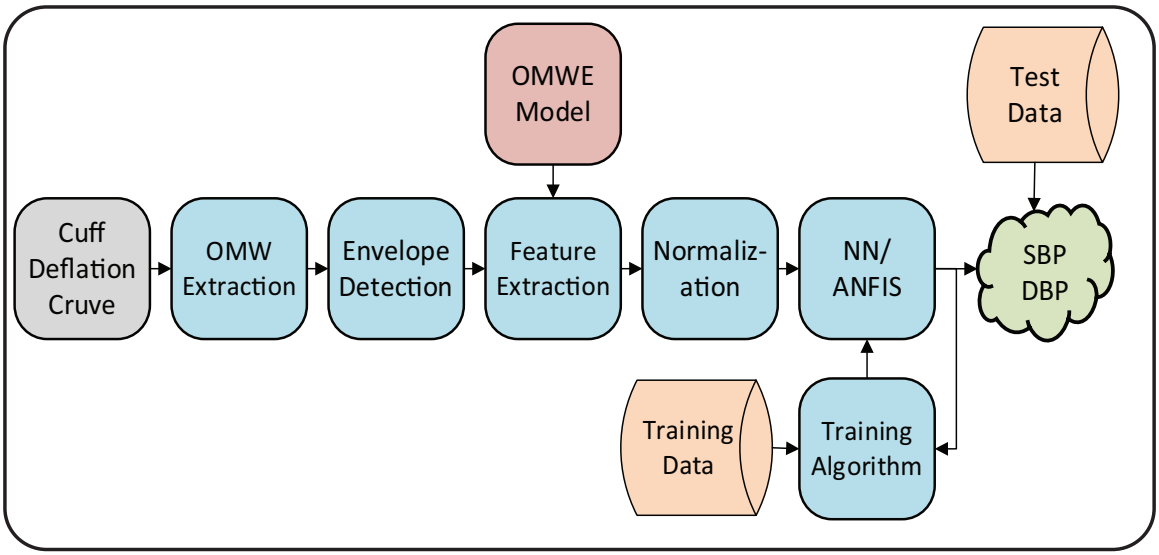

Figure 3.1: Block diagram of the proposed feature-based neural network approach.

implicit relationship between BP and OMWE.

The block diagram representation of the proposed feature-based neural network approach is shown in Fig. 3.1.

The proposed methods are tested on a dataset of wrist oscillometric measurements collected from 85 subjects and the results are compared with the conventional MAA and published NN-based methods. The results are compared in terms of mean error (ME), mean absolute error (MAE), and standard deviation of error (SDE).

The remainder of this chapter is organized as follows. In Section 3.1, the necessary steps to form the OMWE are explained. In Section 3.2, the proposed feature extraction technique is presented. In Section 3.3, the structure of the NNs used for BP estimation and the different training algorithms used to train the NNs are introduced. In Section 3.4, the structure of the ANFIS used for BP estimation is described. In Section 3.5, the experimental results are provided, and in Section 3.6 the chapter is concluded.

3.1 Oscillometric Waveform Envelope Detection

In the oscillometric method, an occluding cuff is placed around the upper arm or wrist and is deflated from a suprasystolic to a subdiastolic pressure. A pressure sensor embedded in the cuff records the pressure variations within the cuff, as shown in Fig. 3.2(a). A bandpass filter with a lower cutoff frequency of 0.5 Hz and an upper cutoff frequency of 20 Hz is utilized to extract the OMW from the recorded cuff deflation curve, as shown in Fig. 3.2(b). In order to be able to analyze the behaviour of oscillometric pulses at different cuff pressures, all the recorded/extracted signals are plotted as a function of cuff pressure.

As the OMWE contains information about the BP [17], in the next step, the peaks and troughs of the oscillometric pulses are detected. A zero crossing algorithm for peak detection borrowed from existing ECG methods is used in this study [117]. In the zero crossing method, the mean is first subtracted from the original signal. The resultant signal is then used to find where zero crossings occur. Each downward zero crossing should follow an upward zero crossing and vice versa. In between two consecutive crossings should lie a peak. The maximum value in the group of points that lies between the upward and downward zero crossing is the identified peak. The minimum value in the group of points that lies between two consecutive peaks is identified as a trough. Figure 3.2(b) shows the peaks and troughs of the OMW in upward and downward triangles, respectively. Afterwards, the consecutive peaks and troughs are subtracted, interpolated, and then plotted as a function of the cuff pressure, as illustrated in Fig. 3.3. For more details on extraction of OMW and detection of its peaks and troughs, the reader is referred to [10, 66].

3.2 Feature Extraction

In the existing literature [69–71], the raw OMWE, after applying noise reduction algorithms, is evenly sampled at specific increments of cuff pressure and directly fed to two

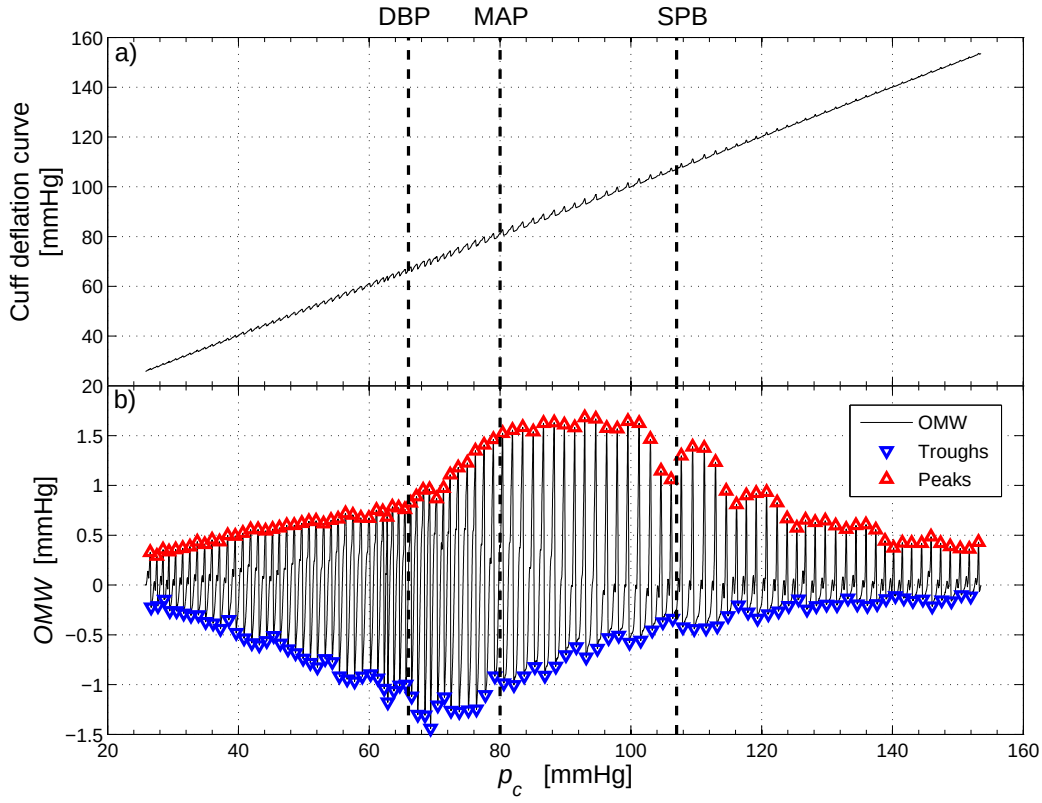

Figure 3.2: Examples of (a) the cuff deflation curve recorded by a pressure transducer embedded in the cuff, and (b) the oscillometric waveform (OMW) extracted from the cuff deflation curve. The detected peaks and troughs are shown by upward and downward triangles, respectively, on the OMW. The waveforms are plotted as a function of cuff pressure p_c. The vertical dashed lines from left to right show the points at which cuff pressure is equal to DBP, MAP, and SBP, respectively.

separate NNs to estimate the SBP and DBP. The sampling step is usually chosen between 3 to 4 mmHg resulting in tens of highly correlated samples per each OMWE [69, 70]. For example, in [69], the OMWE was sampled at 4 mmHg increments of cuff pressure resulting in 40 samples per each OMWE. A complex network with 40 input nodes was then designed to estimate BP and the optimum number of hidden nodes was found to be 63. Instead of using the raw OMWE, through appropriate data preprocessing and representation, a compressed representation of the input data in the form of features can be achieved. Such a concise representation of the input data aids in fast training of neu-

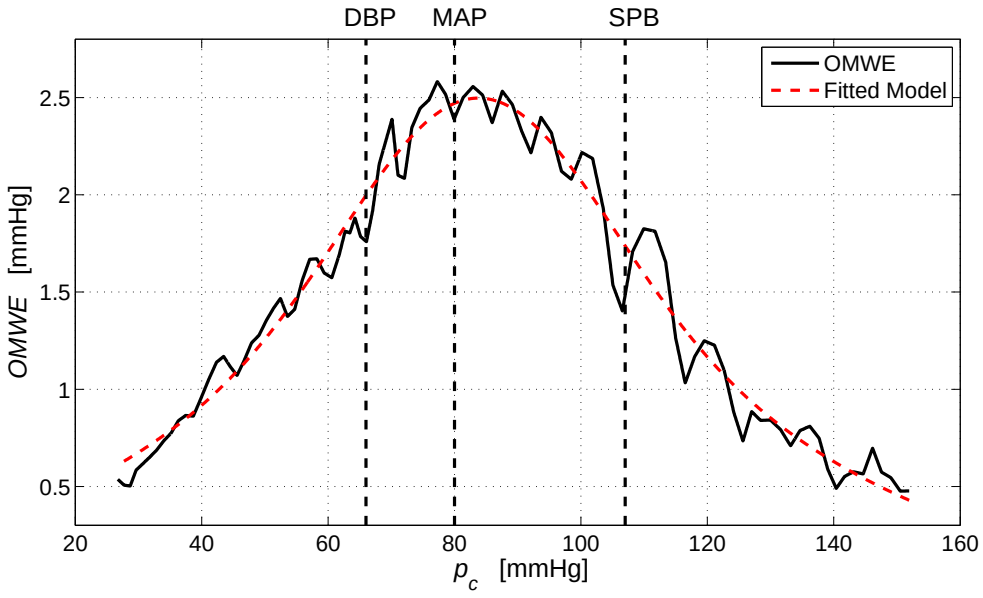

Figure 3.3: Example of the oscillometric waveform envelope (OMWE) plotted as a function of cuff pressure p_c. The red dashed curve represents a fit to the OMWE with the sum of two Gaussian functions. The vertical dashed lines from left to right show the points at which cuff pressure is equal to DBP, MAP, and SBP, respectively.

ral networks, a better generalized network due to higher discrimination capability [111], a smaller network with fewer hidden nodes [112] and hence lesser storage requirement, and a smaller training data set [111, 113].

3.2.1 Modeling the Oscillometric Waveform Envelope

Our proposed feature extraction technique is based on modeling the OMWE by an analytic expression that is completely characterized by a small set of parameters. These parameters are then treated as inputs to the NN instead of the entire set of OMWE samples. In the existing literature, several curve fitting algorithms have been employed in order to obtain a smoothed envelope from the extracted peak-to-trough values of the OMW [118–120]. Hersh et al. [118] proposed that the OMWE has the shape of a Gaussian function. They used the Gauss-Marquardt algorithm to fit the Gaussian function to the OMWE. In [119], a Lorentzian function was expanded to a power series and employed

in a regression algorithm in order to reconstruct the relationship between OMWE and cuff pressure. In order to improve the precision and accuracy of curve fitting, in [120], the sum of two Gaussian functions was proposed to model the OMWE and the results were compared against the polynomial fits. It was found that the sum of two Gaussian functions results in the best fit in terms of sum of squared error. Inspired by this research, we utilized the sum of two Gaussian functions to mathematically model the OMWE. The parameters of the Gaussian curve best fitted to the OMWE were then considered as features for the NN.

The proposed model is described as a sum of two Gaussian functions with different spreads and amplitudes but with the same center, as follows [120]:

$$f(x) = A_1 e^{\frac{-(x-\mu)^2}{2\sigma_1^2}} + A_2 e^{\frac{-(x-\mu)^2}{2\sigma_2^2}} \tag{3.1}$$

where A_1 and A_2 are the amplitudes and σ_1 and σ_2 are the spreads of the two Gaussian functions, respectively. The center of the Gaussian functions is represented by μ. It is worthwhile to mention that several Gaussian models were investigated to find out the suitable model of OMWE for BP estimation. The investigated models were i) a single Gaussian function, ii) sum of two Gaussian functions with same centers, iii) sum of two Gaussian functions with different centers, iv) sum of three Gaussian functions with same centers, and v) sum of three Gaussian functions with different centers. Of the models, the sum of two Gaussian functions with same centers was found to be the best model for estimation of BP in terms of MAE and SDE. More details are provided in Section 3.5.3.

The optimum parameters of the proposed model are found by fitting the model to the OMWE using the least squares method:

$$\{\hat{A}_1, \hat{A}_2, \hat{\sigma}_1, \hat{\sigma}_2, \hat{\mu}\} = \arg \underbrace{\min}_{A_1, A_2, \sigma_1, \sigma_2, \mu} \sum_{p_c} \big(f(p_c) - OMWE(p_c)\big)^2 \tag{3.2}$$

where p_c represents the cuff pressure that varies from a suprasystolic to a subdiastolic

pressure. The estimated parameters are shown on the left hand side of the equation. To solve the above curve-fitting problem, we employ the trust region reflective algorithm explained in Section 4.5.1.

An important factor in any optimization problem is the initialization of the parameters. Using a fixed set of initialization rules helps the method to be completely automated. Here, the initial parameters are found as follows. A 10th order lowpass FIR filter with cut-off frequency of 0.01 is first applied to the OMWE to be fitted. Then, the location of the maximum point is found which is taken as the initial guess for the center of the Gaussian functions. The maximum amplitude of the OMWE is taken as the initial guess for the amplitudes A_1 and A_2. On each side of the maximum point of the OMWE, the point which corresponds to half of the maximum is found and its width is computed. The widths corresponding to the left and right of the OMWE are taken as the initial guesses for the spreads σ_1 and σ_2, respectively. These initializations are performed to reduce the amount of time needed for the optimization to converge.

Figure 3.3 illustrates an example of such curve-fitting. It is observed that in addition to the advantages explained early in this section, such curve fitting can also reduce general artifacts and interferences by smoothing the OMWE. The five parameters ($\hat{A}_1$, $\hat{A}_2$, $\hat{\sigma}_1$, $\hat{\sigma}_2$, $\hat{\mu}$) of the curve best fitted to the OMWE are then taken as the inputs to the NN. This feature extraction technique gives us an efficient representation of the raw OMWE that comprises tens of samples.

3.2.2 Normalization

Before applying the input data to the NN, it is often useful to scale them so that they always fall within a specified range. This helps the NNs train faster, reduces the chances of getting stuck in local minima and avoids saturation of the network [121]. Here we

scale each of the extracted features to the interval $[-1, 1]$ using the following formula:

$$Y = 2\left(\frac{X - X_{min}}{X_{max} - X_{min}}\right) - 1 \tag{3.3}$$

where X and Y represent the extracted feature before and after scaling, and X_{min} and X_{max} denote the minimum and maximum value of that particular feature.

3.3 Artificial Neural Network

3.3.1 Artificial Neural Network Architecture

The Feed-Forward Neural Network (FFNN) architecture is selected in this study. It consists of one or more nonlinear hidden layers along with a linear output layer. The hidden layers' activation functions are sigmoidal functions that empower the network to learn the complex and nonlinear relationship between the inputs and the targets, while the linear output layer makes it possible to have outputs of any range. In this architecture, a unidirectional weight connection exists between each two successive layers. It has been proved that a two-layer FFNN with sigmoidal functions in the hidden layer, and a linear output layer can potentially approximate any function with finite number of discontinuities, provided a sufficient number of neurons exists in the hidden layer [122].

In our application, two separate two-layer FFNNs with one output neuron were designed: one to estimate the SBP and the other to estimate the DBP. The hyperbolic tangent sigmoid transfer function was used in the hidden layer and a linear transfer function in the output. The network weights were initialized using the Nguyen-Widrow method [123]. The Nguyen-Widrow method initializes the weights of a layer in order to distribute the active regions of the layers' neurons approximately evenly over the input space. This method has been tested on different training problems and found to achieve significant improvements in learning speed compared to several other initialization techniques [123, 124]. The networks were first trained using the extracted features as the

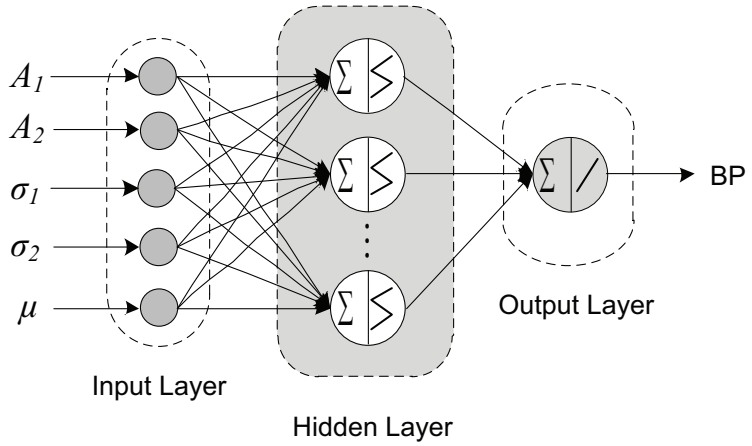

Figure 3.4: Structure of the proposed feature-based feed-forward neural network (FFNN).

input, with averaged auscultatory measurements made by two nurses as the corresponding target. Once the networks extracted information on the association between the input (extracted features) and target (measured BP), they can be used to estimate the BP from any new input pattern that has not been provided during training.

Figure 3.4 shows the structure of the proposed FFNN with input features extracted using the the Gaussian function approximation.

3.3.2 Training Algorithms

Training is the process of determining the optimal weights of the NN. This is done by defining a performance function and then minimizing it with respect to the weights. The minimization is performed by calculating the gradient using a technique called backpropagation which can be done in batch or incremental styles [110]. Here, the training was performed in batch style and the performance function was set to the mean square error between the network's output and the desired target. The NNs were trained using different training algorithms belonging to three backpropagation classes described as follows.

Steepest Descent (SD)

Existing NN-based BP estimation methods use the steepest descent backpropagation learning algorithm [69, 70]. The steepest descent algorithm is derived based on the first-order Taylor series expansion of the performance function. In this algorithm, the update is done in the negative gradient direction. An iteration of this algorithm can be written as follows [110]:

$$\Delta \mathbf{w}_i = -\mu_i \mathbf{g}_i \tag{3.4}$$

where $\Delta \mathbf{w}_i$ is the vector of weights changes, $\mathbf{g}_i$ is the vector of gradients and μ_i is the learning rate that determines the size of the weight update.

For the FFNNs with sigmoidal activation functions, the gradient can be of very small magnitude even though the weights are far from their optimum values. This is due to the slope of sigmoidal functions that approaches zero as the input magnitude increases. This causes several disadvantages such as slow learning and getting stuck in local minima for FFNNs when using steepest descent learning algorithm [125]. Heuristic modifications can be applied to improve the performance of steepest descent algorithm.

1) *Steepest Descent with Variable Learning Rate (SD-VLR):* The performance of the NN is very sensitive to the initial choice of learning rate, especially when the rate is fixed during the whole learning process. A solution to overcome the sensitivity issue is the use of a variable (adaptive) learning rate. In the variable learning technique, the step size is chosen as large as possible while keeping learning stable. In each iteration, if the new error is greater than the old one by a predefined ratio (here set to 1.04), the new parameters (weights) are discarded and the learning rate is decreased (here by multiplying by 0.7). Otherwise, the new parameters are kept. If the new error is less than the old error, the learning rate is increased (here by multiplying by 1.05). The initial value of learning rate was set to 0.01.

2) *Steepest Descent with Variable Learning Rate and Momentum (SD-VLRM):* In

order to reduce the sensitivity of the network to fast changes of the error surface, a fraction of the previous weight change (called momentum term) can be added to the gradient decreasing term, as follows [110]:

$$\Delta \mathbf{w}_i = -\mu_i \mathbf{g}_i + \rho \Delta \mathbf{w}_{i-1} \tag{3.5}$$

where ρ ($0 \leq \rho \leq 1$) is the momentum parameter. The momentum parameter ρ was set to 0.9 in our application.

3) *Resilient Backpropagation (RBP):* As mentioned above, the magnitude of the gradient for NNs with sigmoidal activation functions can be very small even though the weights are far from their optimum values. A solution to this problem is to use only the direction of the gradient to update the weights, while the amount of the update is determined by another update factor (here initially set to 0.07). When the gradient has the same sign for two successive iterations, the update factor is increased by a ratio (here set to 1.05). The update factor is decreased (here by multiplying by 0.8) when the gradient changes sign from the previous iteration. When the derivative is zero, the update value is not changed [125].

Quasi Newton (QN)

Newton's method is based on the second-order Taylor series expansion. The iterative procedure of Newton's algorithm is obtained as [110]:

$$\Delta \mathbf{w}_i = -\mathbf{A}_i^{-1} \mathbf{g}_i \tag{3.6}$$

where $\mathbf{A}_i$ is the Hessian matrix of the performance function at iteration i. Computation of the Hessian matrix in each iteration is computationally expensive for FFNNs. To solve this problem, some algorithms have been proposed which are based on Newton's method but do not compute the second derivatives at each step.

1) *Broyden–Fletcher–Goldfarb–Shanno (BFGS):* In the BFGS algorithm, the inverse

of Hessian matrix is updated as a function of successive gradients of the performance function. The method is fully described in [126].

2) *One Step Secant (OSS):* This algorithm is same as BFGS, but based on the assumption that in each iteration the preceding Hessian was the identity matrix [127]. Therefore, the OSS method does not need to store the large Hessian matrix.

3) *Levenberg–Marquardt (LM):* The LM method assumes that the performance function has a quadratic form in a region around the current search point, called trusted region. Based on this assumption, the Hessian matrix is approximated by the Jacobian matrix and the weight update is obtained as [128]:

$$\Delta \mathbf{w}_i = -\left[\mathbf{J}^T\mathbf{J} + \lambda \mathbf{I}\right]^{-1} \mathbf{J}^T \mathbf{e} \tag{3.7}$$

where $\mathbf{J}$ is the Jacobian matrix containing the first derivatives of the errors with respect to weights, $\mathbf{e}$ is a vector of network errors, and λ is a constant (here set to 0.001). When the performance function decreases, this parameter is multiplied by a factor (here set to 0.1) and when the performance function increases it is multiplied by another factor (here set to 10). Same as the SD algorithms, in most of the QN algorithms, the step size is adjusted at each iteration. A search is performed along the new search direction to determine the step size that minimizes the performance function along that line. Here, we used the backtracking search method in all the QN algorithms [126].

Conjugate Gradient (CG)

The SD algorithm produces rapid function decrease along the negative of the gradient. Newton's method is more accurate and much faster in convergence but it needs the computation and storage of Hessian matrix which may be impractical. The CG algorithm searches along the conjugate directions, which provides generally more robust convergence than the SD while it does not need the Hessian matrix. The new search direction $\mathbf{p}_i$ is determined as a combination of the new SD direction $\mathbf{g}_i$ with the previous search

direction $\mathbf{p}_{i-1}$ [110]:

$$\mathbf{p}_i = -\mathbf{g}_i + \beta_i \mathbf{p}_{i-1} \tag{3.8}$$

where β_i is a constant that can be computed by various methods:

1) *Fletcher–Reeves Update (FRU):* This method updates β_i as the norm squared of the current gradient vector divided by the norm squared of the previous gradient vector [129]:

$$\beta_i = \frac{\mathbf{g}_i^T \mathbf{g}_i}{\mathbf{g}_{i-1}^T \mathbf{g}_{i-1}} \tag{3.9}$$

2) *Polak–Ribire Update (PRU):* This method updates β_i as the dot product of the previous change in the gradient vector with the current gradient vector divided by the norm squared of the previous gradient vector [129]:

$$\beta_i = \frac{\Delta \mathbf{g}_{i-1}^T \mathbf{g}_i}{\mathbf{g}_{i-1}^T \mathbf{g}_{i-1}} \tag{3.10}$$

3) *Powell-Beale Restarts (PBR):* In all CG algorithms the search direction is periodically reset to the negative direction of the gradient. This is done usually when the number of iterations reaches the number of network parameters. In PBR approach, orthogonality between the current and the previous gradient vectors is checked at each iteration. If there is not enough orthogonality left, then the search direction is reset. The orthogonality is considered inadequate if the following inequality is true [130]:

$$\left| \mathbf{g}_{i-1}^T \mathbf{g}_{i-1} \right| \geq 0.2 ||\mathbf{g}_i||^2 \tag{3.11}$$

where $||\cdot||$ is the norm operator.

4) *Scaled Conjugate Gradient (SCG):* The CG algorithms introduced so far are based on a line search in each iteration which is computationally expensive. To overcome this

shortcoming, the SCG method combines the trust region approach (same as LM) with CG algorithm. For more details, the reader is referred to [131].

Same as the SD and QN algorithms, in most of the CG algorithms, the step size is adjusted at each iteration. Here, the Charalambous search method [132] was utilized to adjust the step size in all the CG algorithms except the SCG.

3.4 Adaptive Neuro-Fuzzy Inference System

A fuzzy inference system is a system that uses fuzzy set theory to map a set of inputs to desired outputs. A Fuzzy inference system consists of three conceptual components: a rule base that contains the set of fuzzy rules, a database that defines the membership functions used in the fuzzy rules, and a reasoning mechanism that performs the inference procedure (derives the output from the rules and inputs). The main problem with the fuzzy inference system is that there is no systematic procedure to define its parameters.

Adaptive Neuro-Fuzzy Inference System (ANFIS) is a newly developed class of hybrid intelligent systems that combine the main features of the NN with those of the fuzzy systems [115]. ANFIS can be viewed as a mapping of a fuzzy system into a NN structure where each module of the fuzzy system is interpreted as a particular layer of the NN. The parameters of the fuzzy system are adaptively optimized by incorporating NN learning concepts. It has been mathematically proved that ANFIS is a universal approximator [116]. Therefore, it can approximate any arbitrary nonlinear function such as the relationship between BP and OMWE.

Different ANFIS models have been developed in the literature [133–136]. The main difference between these models is the inferencing procedure used to obtain the system output. In this thesis, a five-input first-order Sugeno fuzzy model [135, 136] is used for the ANFIS. Each input is fuzzified using N membership functions (MFs) leading to the total number of $M = N^5$ rules. Figure 3.5 shows the structure of the proposed ANFIS with input features extracted using the Gaussian function approximation.

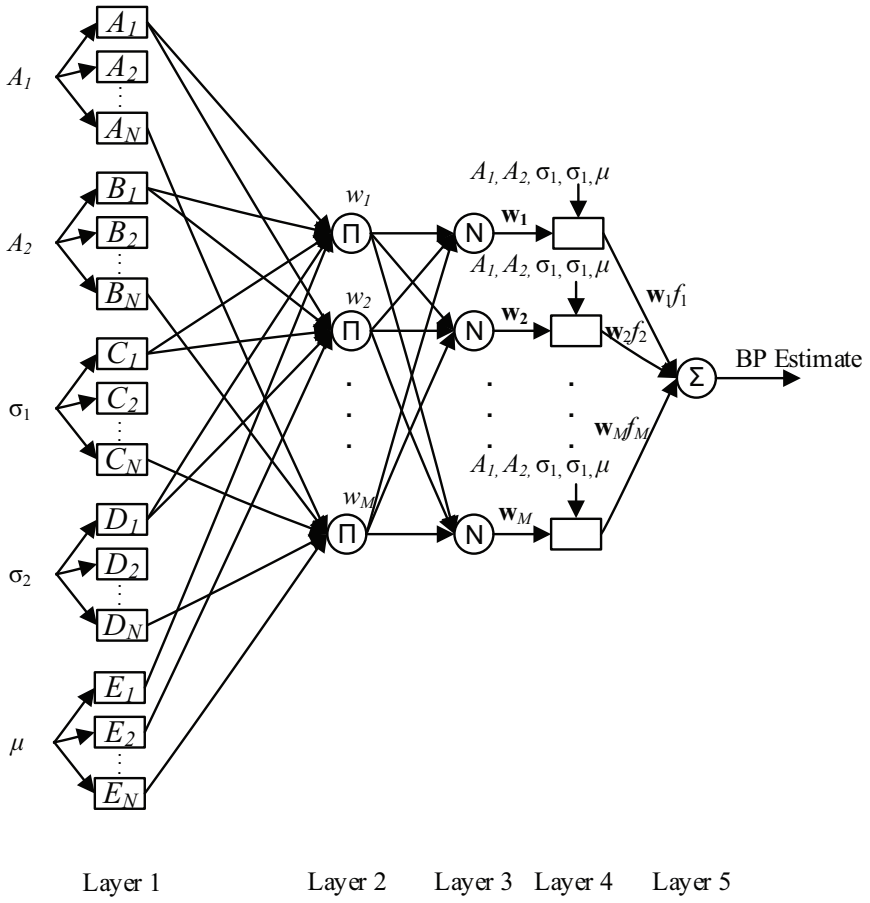

Figure 3.5: Structure of the proposed feature-based adaptive neuro-fuzzy inference system (ANFIS). The connections are only shown for rules 1, 2, and M.

A five-input first-order Sugeno fuzzy model has the following rule-based structure:

$$\text{if } I_1 \text{ is } A \text{ and } I_2 \text{ is } B \text{ and } I_3 \text{ is } C \text{ and } I_4 \text{ is } D \text{ and } I_5 \text{ is } E \text{ then,} \qquad (3.12)$$
$$f = pI_1 + qI_2 + rI_3 + sI_4 + tI_5 + u$$

where I_1, I_2, ..., I_5 represent the inputs, A, B, C, D and E are fuzzy sets for the input, $\{p, q, r, s, t, u\}$ is the consequent parameter set, and f is the rule output. For the ANFIS employed in this study, the nodes in Layer 1 (premise parameters) were all symmetric gaussian MFs which have a flexible parameterization. For example, for the fuzzy set A,

the symmetric gaussian MF takes the form:

$$\mu_A(I_1) = e^{\frac{-(I_1 - c)^2}{2\sigma^2}} \tag{3.13}$$

where parameters c and σ determine the center and spread of the gaussian function.

The next layer (Layer 2) multiplies the inputs from the nodes in Layer 1 and generates the firing strength of the rules. The output of this layer is given by:

$$w_i = \mu_A(I_1) \times \mu_B(I_2) \times \mu_C(I_3) \times \mu_D(I_4) \times \mu_E(I_5) \tag{3.14}$$

where w_i is the firing strength of rule i.

The output of this layer is then fed to Layer 3 to normalize the firing strengths of the fuzzy rules. For the jth node in this layer, the output is given by:

$$\mathbf{w}_j = \frac{w_j}{\sum_{i=1}^{M} w_i} \tag{3.15}$$

The nodes of the next layer (Layer 4) multiply the normalized firing strengths $\mathbf{w}_i$ by the rule outputs f_i:

$$\text{output}_i = \mathbf{w}_i f_i \tag{3.16}$$

The output of this layer is passed to the final layer (Layer 5), which generates a crisp output value by computing the weighted average of all the rule outputs:

$$\text{Overal output} = \sum_{i=1}^{M} \mathbf{w}_i f_i \tag{3.17}$$

The ANFIS is first trained using the extracted features as the input, with averaged auscultatory measurements made by two nurses as the the corresponding network targets. The backpropagation gradient descent learning method [115] is adopted to identify

parameters in the ANFIS. Once the network has extracted information about the association between the input (OMWE features) and target (measured BP), it can be used to estimate the BP from any unknown input that has not been provided during the training.

3.5 Experimental Results

Our proposed method was tested on an oscillometric waveform dataset provided by Biosign Technologies Inc. The dataset was acquired from 85 subjects using an automated wrist BP monitor (UFIT TEN-10) in accord with the recommendations of the ANSI/AMMI/ISO standard [37]. The dataset is fully described in Appendix A.1.

3.5.1 Train and Test Strategy

The challenge is to design a neural network that can attain an acceptable estimation error when presented with new inputs. Employing a large representative training dataset, with input-output mappings of the relationship to be approximated, results in a network that is more likely to generalize to new inputs. The network should then be trained until the necessary input-output relationships are found without overfitting the training dataset. To this end, the early-stopping technique is utilized [124, 128]. In the early stopping technique, the dataset is divided into three sets, called training, validation and testing such that the training data is as large as possible and the validation data is a fair representative of all points in the training set. The network is trained with the training data and the error obtained with the validation data is checked at every iteration. When the validation error increases for a specified number of successive iterations (here set to 50), the network's parameters that lead to the best validation performance are saved. Then, the network's performance is assessed using the test data. The error obtained on the test data, called generalization error, is used as a measure to evaluate the network performance when new data that was not provided during the training is presented. In our study, one subject (with five measurements) was selected for the test, which led to

the largest possible set of data for training and validation. The rest of the subjects were randomly divided into training (80%–336 measurements) and validation (20%–84 measurements) [137]. This process was then repeated such that each subject in the dataset was used once for the test. Despite the advantage of having the largest possible training data set, a drawback of this testing strategy is the computational cost, because of the large number of training iterations.

3.5.2 Comparison of NN Training Algorithms

Different NN training algorithms were compared in terms of BP estimation error and training performance. Two metrics were chosen to compute the estimation error: i) mean absolute error (MAE) and ii) standard deviation of error (SDE). The training performance of the NNs was compared in terms of i) training time and ii) number of training iterations to reach the optimal weights. The NNs were designed with the same settings as described in Section 3.3.

The BP estimation errors in terms of MAE and SDE for the FFNN using different training algorithms are shown in Table 3.1. The NN training performance in terms of training time and number of training iterations to reach the optimal weights are listed in Table 3.2. These values were averaged over the 85 runs of the algorithms. The results were obtained on a Pentium IV 2.8 GHz processor with 2.0 GB of RAM.

It is observed that among the SD training algorithms, the SD-VLR has the largest estimation error with the worst training performance. The SD-VLRM significantly improves the training performance while the estimation error is only slightly improved. The best result in terms of both estimation error and training performance is obtained using RBP. Among the QN training algorithms, the BFGS and OSS obtain the least estimation errors. However, the BFGS is the worst in training performance with the longest training time and the maximum number of iterations. The BFGS training time is even longer than SD-VLR, but it needs a smaller number of training iterations. This is due to the fact that QN algorithms make advantage of the second-order Taylor series

Table 3.1: Comparison of different neural network (NN) training algorithms in terms of estimation error (MAE and SDE)

		Steepest Descent (SD)			Quasi-Newton (QN)			Conjugate Gradient (CG)			
		SD-VLR	SD-VLRM	RBP	BFGS	OSS	LM	FRU	PRU	PBR	SCG
SBP	MAE [mmHg]	7.19	7.00	**6.90**	6.91	6.98	7.76	7.28	7.04	7.26	7.02
	SDE [mmHg]	10.71	10.10	**9.90**	10.24	10.21	10.81	10.61	10.43	10.56	10.36
DBP	MAE [mmHg]	6.44	6.29	**5.83**	6.32	6.02	6.54	5.95	5.88	5.91	6.24
	SDE [mmHg]	8.17	8.40	**7.34**	8.03	7.58	8.38	7.59	7.50	7.64	7.96

expansion of the performance function which makes the training faster in terms of the number of iterations. However, since each iteration is computationally more expensive than that of the SD algorithms, the whole training time is longer. The training time has been significantly improved in the OSS algorithm with estimation errors similar to BFGS algorithm. The best training performance is achieved using the LM algorithm but with the cost of slight increase in estimation errors. The LM is the second fastest algorithm after the RBP, with the least number of training iterations among all the training algorithms. Among the CG training algorithms, the FRU, PRU, and PBR have very similar results both in estimation error and in training performance. They are faster than the SD-VLR, BFGS and OSS algorithms but not as fast as the advanced SD (SD-VLRM, RBP) and QN (LM) methods. The CG based algorithms have estimation errors that are almost the same as the other algorithms. The training performance is improved in SCG by employing the trust region approach while achieving comparable estimation errors to the other CG algorithms. Comparing all the ten different training algorithms together, it is found that the estimation errors are very close while the training performances significantly differ. However, the best estimation errors and fastest training are obtained using the RBP algorithm.

Table 3.2: Comparison of different neural network (NN) training algorithms in terms of training performance (training time and number of iterations to reach the optimal weights).

		Steepest Descent (SD)			Quasi-Newton (QN)			Conjugate Gradient (CG)			
		SD-VLR	SD-VLRM	RBP	BFGS	OSS	LM	FRU	PRU	PBR	SCG
SBP	Avg. no. iterations	597	273	194	379	137	**110**	132	129	124	140
	Avg. train time [sec]	15.16	6.65	**5.53**	28.60	9.61	6.85	8.84	8.93	8.78	8.32
DBP	Avg. no. iterations	689	351	163	264	163	**107**	136	140	133	150
	Avg. train time [sec]	17.82	8.52	**4.82**	20.68	11.30	6.68	8.97	9.65	9.23	8.90

3.5.3 Gaussian Model Selection

As mentioned in Section 3.2.1, in the existing literature [69–71], it has been proposed that the OMWE has the shape of a Gaussian function. We investigated five Gaussian models to determine the appropriate model for OMWE to be utilized for BP estimation. The investigated models were i) a single Gaussian function, ii) sum of two Gaussian functions with same centers, iii) sum of two Gaussian functions with different centers, iv) sum of three Gaussian functions with same centers, and v) sum of three Gaussian functions with different centers. For each model, the amplitude(s), center(s), and spread(s) were considered as inputs to the FFNN. The FFNNs were designed with the same settings as described in Section 3.3.1. The RBP learning algorithm, as described in Section 3.3.2, was used to train the networks. The number of hidden nodes was set to 10. The BP estimation results obtained on the test set are listed in Table 3.3. It is observed that the BP estimation results are improved in terms of MAE and SDE by presenting the features extracted using the sum of two Gaussian functions with same centers instead of one Gaussian function. This improvement is due to fact that the sum of two Gaussian functions provides a better fit to the OMWE compared to a single Gaussian function. However, by further increasing the complexity of our model, estimation results are not improved anymore. We conjecture that a more complex model may approximate in addition to the envelope, the fine structure variations and artifacts that do not contribute to

Table 3.3: Comparison of different Gaussian models in estimation of blood pressure (BP) from oscillometric waveform envelope (OMWE)

		1 Gaussian function	2 Gaussian functions		3 Gaussian functions	
			Same centers	Different centers	Same centers	Different centers
SBP	MAE [mmHg]	6.96	**6.76**	11.38	7.24	11.07
	SDE [mmHg]	9.21	**8.89**	14.49	9.66	14.17
DBP	MAE [mmHg]	6.74	**5.98**	7.67	6.39	7.92
	SDE [mmHg]	8.82	**7.90**	10.14	8.41	10.13

the pressure estimates. Using different centers for the Gaussian models further degrades the BP estimation results. Moreover, as discussed earlier, by using more complex models, the number of inputs to the NN increases and the learning performance degrades.

3.5.4 Evaluated Methods

To evaluate performance on the test data, the following methods were implemented:

- **Method 1:** FFNN with the raw OMWE as the input. The OMWE was evenly sampled at 3 mmHg increments of the cuff pressure (other sampling rates were also tested; however, the best BP estimation results were achieved with 3 mmHg increments). This led to a redundant set of 48 samples per each OMWE that were considered as inputs to the network.

- **Method 2:** FFNN with feature extraction using Gaussian function approximation. The sum of two Gaussian functions was used to model the OMWE. The model parameters which are two amplitudes A_1, A_2, two spreads σ_1, σ_2, and a center μ were considered as inputs to the network (See Section 3.2.1).

- **Method 3:** ANFIS with feature extraction using Gaussian function approximation. The sum of two Gaussian functions was used to model the OMWE. The

model parameters which are two amplitudes A_1, A_2, two spreads σ_1, σ_2, and a center μ were considered as inputs to the ANFIS.

- **Method 4:** Conventional MAA which is the most commonly used oscillometric method for estimating the BP in noninvasive electronic BP devices [17]. Systolic and diastolic coefficients that led to the least estimation error were chosen for this study.

All the NN-based methods were designed with the same settings as described in Section 3.3.1. The RBP learning algorithm, as described in Section 3.3.2, was used to train the NNs. The ANFIS was designed with the same settings as described in Section 3.4. It should be noted that since the number of rules in ANFIS exponentially increases with the number of inputs and makes the ANFIS very complex (see Section 3.5.5 and Table 3.7), we only implemented the featured-based ANFIS.

In order to compare the results, ME, MAE, and SDE between the estimated BP and the averaged nurse measurements are computed over the whole dataset.

3.5.5 Results and Discussion

As mentioned in Section 3.3, two separate two-layer FFNNs were designed to estimate SBP and DBP. The hyperbolic tangent sigmoid transfer function was used in the hidden layer and linear transfer function in the output, making the networks capable of approximating any complex input-output mapping. The number of hidden neurons was a free parameter and needed to be chosen judiciously.

An important factor in the design of a generalizable NN is the proper choice of number of hidden neurons. A smaller number of hidden neurons will increase the training and generalization errors due to underfitting. On the other hand, using too many neurons will decrease the training error but increase the generalization error due to overfitting. There are guiding principles for determining the upper and lower bounds for the number of hidden neurons [137–141], but it is not possible to exactly determine the best number of

hidden neurons without computing the generalization error for each structure [112, 137]. Therefore, we iterated the training and testing process with different number of hidden neurons.

Figures 3.6 and 3.7 illustrate the performance of the FFNN in the estimation of SBP and DBP, with raw OMWE as input, as a function of number of hidden neurons (1, 2, 4, 8, 16, and 32). The performance is reported in terms of MAE and SDE obtained on the test set. The same performance curves for the FFNN with feature extraction using the Gaussian function approximation are shown in Figs. 3.8 and 3.9. It is observed that the networks with a larger number of hidden neurons exhibit overfitting. On the other hand, networks with a smaller number of hidden neurons appear to underfit the training data due to lack of power to capture the exact input-output relationship. However, there exists an optimum point where the networks reach the best generalization performance, as shown in the figures. The network structures with the best generalization performance were saved and compared. For estimation of SBP and DBP from raw OMWE, the networks with 4 hidden neurons achieved the best results. For estimation of SBP and DBP from extracted features using the Gaussian function approximation, the networks with 2 and 4 hidden neurons obtained the best performance, respectively. For the ANFIS with feature extraction using the Gaussian function approximation, the training and testing process were iterated with different numbers of membership functions. It was found that networks with two membership functions per input achieve the best results in estimation of both SBP and DBP [45, 47].

Table 3.4 lists the ME, MAE, and SDE values of the four different methods used for the estimation of SBP while Table 3.5 lists the values for estimation of DBP.

Comparing the proposed feature-based FFNN with the conventional MAA, it is found that the SBP and DBP estimation errors have been reduced by 3.28 mmHg and 3.91 mmHg in terms of ME, by 1.9 mmHg and 1.88 mmHg in terms of MAE, and by 3.45 mmHg and 1.75 in terms of SDE, respectively. The feature-based ANFIS has also achieved improved performance compared to the MAA; the SBP and DBP errors are

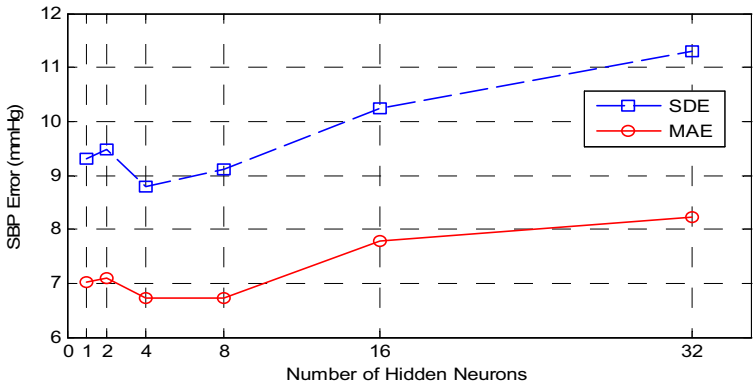

Figure 3.6: Performance of FFNN (with raw OMWE as input) in estimation of SBP as a function of number of hidden neurons. The performane is reported in terms of MAE and SDE obtained on the test set.

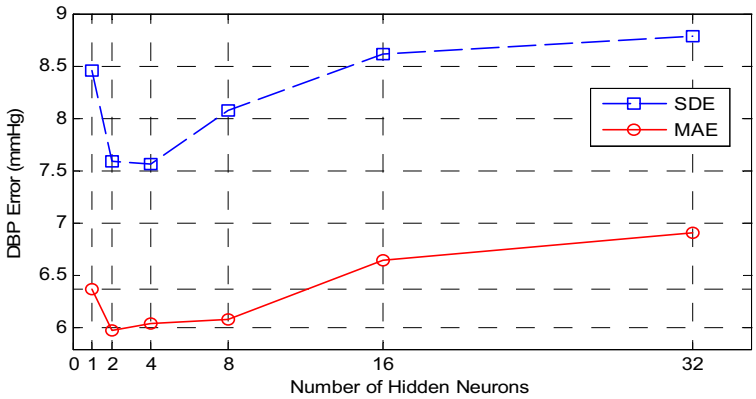

Figure 3.7: Performance of FFNN (with raw OMWE as input) in estimation of DBP as a function of number of hidden neurons. The performane is reported in terms of MAE and SDE obtained on the test set.

improved by 1.81 mmHg and 2.59 mmHg in terms of ME, by 1.2 mmHg and 1.44 mmHg in terms of MAE, and by 3.01 mmHg and 1.02 in terms of SDE, respectively. Comparing the proposed feature-based FFNN with the FFNN with raw OMWE as input, it is found that the SBP and DBP estimation errors have been reduced by 0.44 mmHg and 0.30 mmHg in terms of MAE and by 0.22 mmHg and 0.23 in terms of SDE, respectively, while

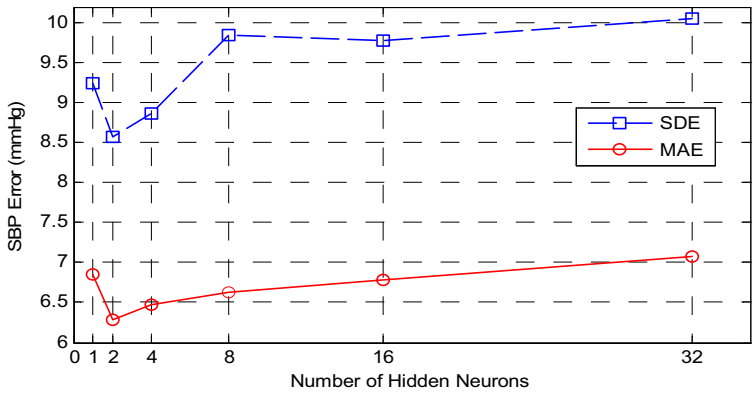

Figure 3.8: Performance of feature-based FFNN in estimation of SBP as a function of number of hidden neurons. The performance is reported in terms of MAE and SDE obtained on the test set.

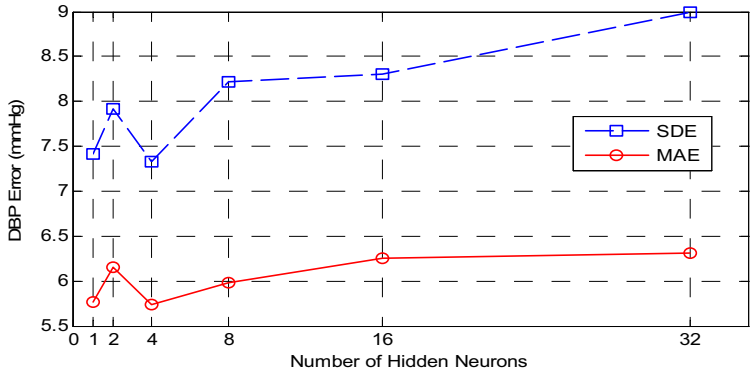

Figure 3.9: Performance of feature-based FFNN in estimation of DBP as a function of number of hidden neurons. The performance is reported in terms of MAE and SDE obtained on the test set.

the ME for both methods is close to zero. The feature-based FFNN has also achieved superior performance compared to the feature-based ANFIS. As mentioned earlier, the ANFIS was not implemented using the raw OMWE as input due to the high complexity of the corresponding network.

The improvement of the proposed feature-based methods is attributed to the result

Table 3.4: Comparison of different methods in estimation of systolic blood pressure (SBP) on a dataset of 425 recordings from 85 subjects. The averaged nurse measurements were used as the reference.

SBP	MAA	FFNN (raw input)	Feature-based FFNN	Feature-based ANFIS
ME (mmHg)	3.46	-0.03	-0.18	1.65
MAE (mmHg)	8.18	6.72	6.28	6.98
SDE (mmHg)	12.03	8.80	8.58	9.02

Table 3.5: Comparison of different methods in estimation of diastolic blood pressure (DBP) on a dataset of 425 recordings from 85 subjects. The averaged nurse measurements were used as the reference.

DBP	MAA	FFNN (raw input)	Feature-based FFNN	Feature-based ANFIS
ME (mmHg)	-3.91	0.14	0.00	1.39
MAE (mmHg)	7.61	6.03	5.73	6.17
SDE (mmHg)	9.08	7.56	7.33	8.06

of i) capturing the nonlinear and complex relationship that likely exists between the OMWE and BP, and ii) effective data representation obtained by performing feature extraction before applying the OMWE to the NNs. In addition to the improvement of ME, MAE and SDE in estimation of BP, the proposed feature-based FFNN uses a smaller NN compared to the FFNN with raw OMWE as input.

As mentioned earlier, by using features instead of the whole OMWE as input to the NNs, the number of inputs is significantly decreased, which reduces the number of the first layer's connections. Moreover, as is observed in Fig. 3.8, the FFNN designed for estimation of SBP achieves the best performance with a smaller number of hidden neurons. As the number of inputs and hidden neurons decreases, the resultant NN

has fewer weights. For example, by reducing the number of inputs from 48 to 5 and the number of hidden neurons from 4 to 2, as is the case for the FFNNs designed for estimation of SBP, the number of the first layer weights decreases from $48 \times 4 = 192$ to $5 \times 2 = 10$, and the number of the second layer weights reduces from 4 to 2. Table 3.6 compares the complexity of the FFNN with raw OMWE as input versus the feature-based FFNN. It is observed that the proposed feature-based FFNN achieves significant improvements in terms of computational complexity, making it an efficient oscillometric method for BP estimation.

The feature-based ANFIS has also achieved lower complexity compared to the ANFIS using the raw OMWE as input, making it possible to be efficiently implemented. Table 3.7 compares the complexity of the ANFIS with raw OMWE as input versus the feature-based ANFIS. As can be observed, by reducing the number of inputs from 48 to 5, the number of membership functions is reduced from $48 \times 2 = 96$ to $5 \times 2 = 10$, and the number of rules is decreased from 2^{48} to 2^5. Since each symmetric Gaussian membership function has two parameters, the number of premise parameters would be reduced from $2 \times 96 = 192$ to $2 \times 10 = 20$, and the number of consequent parameters decreases from $(48 + 1) \times 2^{48}$ to $(5 + 1) \times 2^5$.

The number of rules in ANFIS exponentially increases with the number of inputs which makes the ANFIS very complex compared to the NN. The complexity of the ANFIS may lead to overfitting of the network to the training data and, as a results, higher estimation errors on the test data. This can be observed in tables 3.4 and 3.5 where the BP estimates using ANFIS are slightly higher than those obtained using NN.

3.6 Conclusion

Estimation of systolic and diastolic pressures from the oscillometric waveform is a challenging task in noninvasive electronic BP monitoring devices. Since the conventional oscillometric algorithms cannot model and extract the complex and nonlinear relation-

Table 3.6: Comparison of the FFNN with raw input, with the feature-based FFNN in terms of complexity.

Complexity of FFNNs		#inputs	#hidden neurons	#1st layer's weights	#2nd layer's weights	Total #weights
Feature-based	SPB	**5**	**2**	**10**	**2**	**12**
	DBP	**5**	**4**	**20**	**4**	**24**
With raw input	SBP	48	4	192	4	196
	DBP	48	**4**	192	**4**	196

Table 3.7: Comparison of the ANFIS with raw input, with the feature-based ANFIS in terms of complexity.

Complexity of ANFISs		#inputs	#Membership Functions	#Rules	#Premise parameters	#Consequent parameters
Feature-based	SPB	**5**	**10**	2^5	**20**	$\mathbf{6}\times 2^5$
	DBP	**5**	**10**	2^5	**20**	$\mathbf{6}\times 2^5$
With raw input	SBP	48	96	2^{48}	192	49×2^{48}
	DBP	48	96	2^{48}	192	49×2^{48}

ship that may exist between BP and OMW, NNs have been proposed as a possible alternative. However, the research on this topic has been limited to simple architectures that directly estimate the BP from raw OMWE. Our proposed method established a new feature extraction technique from the OMWE that resulted in better NN BP estimators that were superior with respect to training, generalization and computation when compared with the existing NN-based techniques. It should be noted that even though the proposed feature-based method was designed and tested on the wrist oscillometric measurements, it can be easily extended to BP estimation from oscillometric measurements obtained from other locations such as the upper arm (see Chapter 6).

It should be noted that our dataset consisted of reference and oscillometric measurements that were made one minute apart. This lack of simultaneity of the oscillometric and reference measurements contributes to the error in our estimation due to the intrinsic physiological variability over time. It has been demonstrated that the arterial BP can vary by up to 20 mmHg within around 10 seconds, in normal healthy humans [41].

Therefore, future work can look at simultaneously recorded test and reference data.

Even though the obtained results were promising, the proposed feature-based NN method has a black box structure that implicitly models the relationship between the BP and the OMWE. Once the network recognizes a given input pattern (OMWE features), it predicts an output pattern (BP value) corresponding to the given input. However, it is very difficult to explicitly describe the meaning of weights at the nodes of the NN. Moreover, the proposed feature-based NN method can only perform well in various patient populations if the training dataset contains a uniform distribution of all those populations. In the next chapter, we will drive a new physiological-based mathematical model that explicitly represents the relationship between the OMWE and the SBP and DBP. The proposed model will be used to estimate the SBP and DBP from the oscillometric BP recordings without the need for any training dataset.

Chapter 4

Mathematical Modeling of the Oscillometric Waveform and Coefficient-Free Estimation of Blood Pressure [1]

In Chapter 3, the relationship between the SBP and DBP values and the oscillometric waveform envelope (OMWE) was implicitly modeled using the NNs. However, no explicit relationship between the SBP and DBP values and the oscillometric waveform (OMW) was provided. OMW is usually the only signal obtained in oscillometry, and therefore it is the focus of all oscillometric algorithms for finding the BP values [10]. Hence, it is of great importance to obtain a model of the OMW to study, develop, and test the

[1] Parts of this chapter have been published in:

1. M. Forouzanfar, H. R. Dajani, V. Z. Groza, M. Bolic, S. Rajan, and I. Batkin "Ratio-independent blood pressure estimation by modeling the oscillometric waveform envelope," *IEEE Trans. Instrum. Meas.*, in press.
2. M. Forouzanfar, B. Balasingam, H. R. Dajani, V. Groza, M. Bolic, S. Rajan, and E. M. Petriu, "Mathematical modeling and parameter estimation of blood pressure oscillometric waveform," *in IEEE Int. Symp. Medical Measurement and Applications (MeMeA'12)*, (Budapest, Hungary), pp. 208-213, May 2012.
3. B. Balasingam, M. Forouzanfar, M. Bolic, H. R. Dajani, V. Z. Groza, and S. Rajan, "Arterial blood pressure parameter estimation and tracking using particle filters," *in IEEE Int. Workshop Medical Measurements and Applications (MeMeA'11)*, (Bari, Italy), pp. 473-476, Sep. 2011.

oscillometric algorithms [142–145].

In Chapter 2, several existing models of oscillometry were reviewed. While there have been extensive studies on the theory of oscillometry [14, 15, 17, 19, 24, 25], to the best of the author's knowledge, no mathematical model of the OMW has been derived. A precise mathematical model can represent and quantify a wealth of information that is contained in the OMW including the SBP, DBP, and MAP values.

In this chapter, (a) a physiologically-based mathematical model for the OMW is developed by incorporating the existing models of the arterial blood pressure (ABP) pulse waveform and the cuff-arm-artery system; (b) this model is then utilized to obtain an explicit mathematical model of the OMWE as a function of SBP and DBP; (c) we propose a new coefficient-free oscillometric BP estimation method based on minimizing the least squares error between our model and the OMWE using the trust region reflective algorithm [114]; and (d) we conduct initial cross-validation of our theoretical findings by estimating BP from 150 actual oscillometric recordings obtained from ten healthy subjects.

The block diagram representation of the proposed model-based oscillometric BP estimation method is shown in Fig. 4.1.

The remainder of this chapter is organized as follows. In Sections 4.1 and 4.2, the ABP and the cuff-arm-artery system models are introduced, respectively. In Section 4.3, a mathematical model for the OMW as a function of the ABP, cuff pressure, and the cuff-arm-artery system parameters is proposed. In Section 4.4, an explicit mathematical model for the OMWE as a function of SBP and DBP is derived. In Section 4.5, a new coefficient-free oscillometric BP estimation method using the trust region reflective algorithm is proposed. In Section 4.6, the experimental results are provided and in Section 4.7 the chapter is concluded.

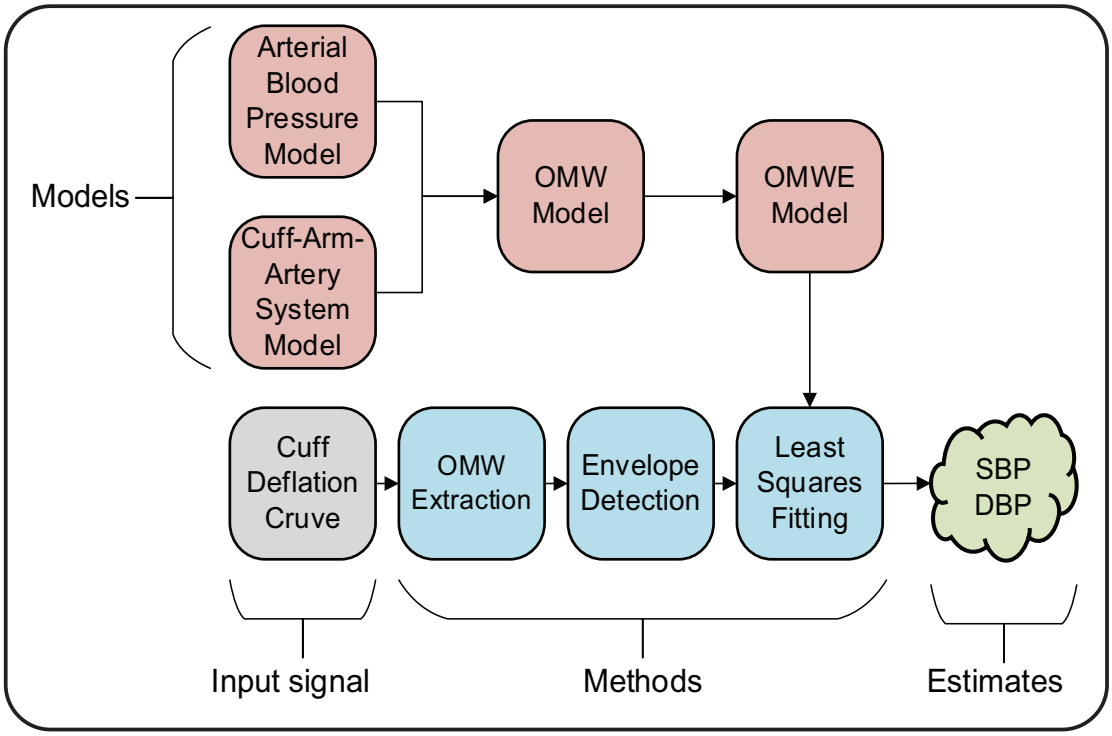

Figure 4.1: Block diagram of the proposed coefficient-free blood pressure (BP) estimation method by modeling the oscillometric waveform.

4.1 Arterial Blood Pressure Pulse Waveform Model

In [50, 146–149], the periodic cardiovascular signals such as the ABP pulse were mathematically modeled using the fourier series representation. The ABP pulse was modeled as a sum of harmonically related sinusoids modulated by respiration. Each sinusoidal function represented a cardiovascular component and was characterized by three parameters: amplitude, frequency, and phase. Alternatively, in [150, 151], an equivalent parametrization was proposed by replacing the amplitudes and phases with sine and cosine components, represented as follows [151, 152]:

$$p_a(t) = \mu(t) + r(t) + c(t) + v(t) \tag{4.1}$$

where t is the time index, $\mu(t)$ represents the low frequency ABP pulse trend including its mean, $r(t)$ is the additive quasi-periodic respiratory signal, $c(t)$ is the quasi-periodic cardiac signal that is modulated by respiration, and $v(t)$ is the white noise signal that accounts for the high frequency variation that is not described by the other components.

These components can be modeled as follows:

$$c(t) = \sum_{i=1}^{N_c} m_i(t)\left[\alpha_{1,i}(t)\cos(i\theta_c(t)) + \alpha_{2,i}(t)\sin(i\theta_c(t))\right] \tag{4.2}$$

$$r(t) = \sum_{j=1}^{N_r} \beta_{1,j}(t)\cos(j\theta_r(t)) + \beta_{2,j}(t)\sin(j\theta_r(t)) \tag{4.3}$$

$$m_i(t) = 1 + \sum_{k=1}^{N_r} \gamma_{1,i,k}(t)\cos(k\theta_r(t)) + \gamma_{2,i,k}(t)\sin(k\theta_r(t)) \tag{4.4}$$

$$\theta_c(t) = 2\pi f_c(t) \tag{4.5}$$

$$\theta_r(t) = 2\pi f_r(t) \tag{4.6}$$

where N_c and N_r are the number of cardiac and respiratory harmonics. $f_c(t)$ and $f_r(t)$ represent the instantaneous cardiac and respiratory frequencies, respectively. $\alpha_{1,i}(t)$ and $\alpha_{2,i}(t)$ are the amplitudes of the ith harmonic sinusoidal components of the cardiac signal. $\beta_{1,j}(t)$ and $\beta_{2,j}(t)$ are the amplitudes of the jth harmonic sinusoidal components of the respiratory signal. $m_i(t)$ is a quasi-periodic signal due to respiration that causes the amplitude modulation of the ith harmonic of the cardiac signal. $\gamma_{1,i,k}$ and $\gamma_{2,i,k}$ are the amplitudes of the kth harmonic sinusoidal components of $m_i(t)$.

In the aforementioned model, each cardiac harmonic is separately amplitude-modulated by the respiratory modulation signal. This accounts for the asymmetry typically observed between the upper and lower envelopes of the ABP pulse waveform [150].

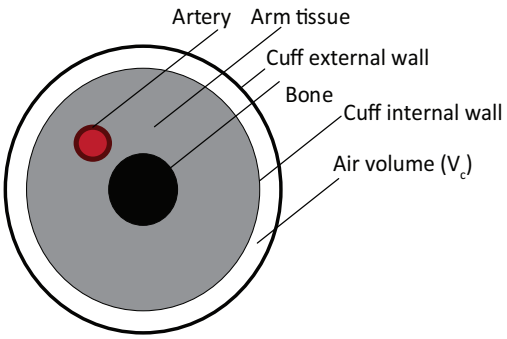

Figure 4.2: Cross-sectional representation of the cuff-arm-artery system.

4.2 Cuff-Arm-Artery System Model

The cross-section of the cuff-arm-artery system is illustrated in Fig. 4.2. When the cuff is not placed on the arm, the ABP is the only pressure that is exerted on the arterial wall. Since the ABP is always greater than zero, the brachial artery in this situation is always stretched and distended. When the oscillometric cuff is placed around the arm, the arterial wall confronts another pressure in the opposite direction of the ABP. To study the arterial vessel behavior in this condition, the transmural pressure, defined as the difference in pressure between the two sides of the arterial wall, should be considered. The transmural pressure p_t is defined as follows [17]:

$$p_t(t) = p_a(t) - p_c(t) \tag{4.7}$$

where $p_c(t)$ is the cuff pressure. Depending on the cuff pressure value, the transmural pressure can vary from negative to positive values.

In oscillometry, the cuff is inflated to a supra-systolic pressure SSP and then slowly released to a sub-diastolic pressure. Assuming that the deflation is performed linearly over time, the cuff pressure can be modeled as follows:

$$p_c(t) = SSP - rt \tag{4.8}$$

where r is the deflation rate which is kept constant between 1 to 4 mmHg/sec [79]. It should be noted that if the deflation deviates from linearity, the cuff pressure model can be readily adjusted.

4.2.1 Model of the Cuff and the Arm

The mechanics of the occlusive arm cuff have been analyzed in several previous studies [14, 15, 17, 19]. The cuff is usually characterized by its internal and external wall and the enclosed air. The cuff volume is defined as the volume difference between the outer and inner cuff layers, as follows: .

$$V_c(t) = V_e(t) - V_i(t) \tag{4.9}$$

where V_i is the inside volume in contact with arm and V_e is the external sheath volume.

The cuff volume V_c is related to the cuff pressure p_c and the pumped volume into the cuff V_p according to Boyle's law, as follows:

$$\left(p_c(t) + p_A\right) V_c(t) = p_A \left(V_{c0} + V_p(t)\right) \tag{4.10}$$

where p_A is the atmospheric pressure, V_{c0} is the initial air volume in the cuff at p_A, and V_p is the volume of air pumped into the cuff. p_c is referenced to zero when cuff pressure equals p_A.

The cuff pressure p_c is determined according to the following nonlinear relationship:

$$p_c(t) = E_c \left[(V_e(t)/V_{e0})^{1/n} - 1 \right]^n \tag{4.11}$$

where E_c is the maximum cuff elastance, V_{e0} is the zero stretch volume of the bladder, and n is a constant of nonlinearity.

The arterial lumen area (ALA) A is linked to the cuff through the following equation:

$$V_i(t) = V_{i0} + A(t)L_c \tag{4.12}$$

where V_{i0} is the arm volume for a collapsed brachial artery and L_c is the cuff bladder width.

4.2.2 Model of the Artery

The study of the arterial mechanics at different transmural pressures is of critical importance in modeling oscillometry [18]. There have been several research studies on modeling the arterial pressure-area relationship [14–17, 19]. It has been found that when the transmural pressure is positive, the arterial wall is stretched and distended and the arterial lumen area (ALA) exhibits a circular shape. In contrast, with negative transmural pressures, the arterial wall is bent and collapsed. During collapse, the ALA changes its shape from circular to elliptical until it becomes flat and occluded.

In [17], a description of the mechanics of the occlusive cuff and of brachial artery with details on arterial buckling was provided. The combination of nonlinear geometric collapse and elastic distention of an artery was modeled with a single equation as follows:

$$A(t) = c_4 \frac{\ln(c_1 p_t(t) + c_2)}{1 + e^{-c_3 p_t(t)}} \tag{4.13}$$

where A represents the ALA, and c_1, c_2, c_3, and c_4 are subject-dependent constants that account for different cuff-arm-artery system characteristics.

Figure 4.3 illustrates examples of the arterial BP and ALA obtained by equations (4.1)-(4.6) and (4.13), respectively, as a function of cuff pressure. Two harmonics of the cardiac signal were considered to be adequate as they carry most of the signal power [17]. The cuff was assumed to be linearly deflated from a supra-systolic pressure (here 140 mmHg) to a sub-diastolic pressure (here 40 mmHg) using a deflation rate of 3 mmHg/sec.

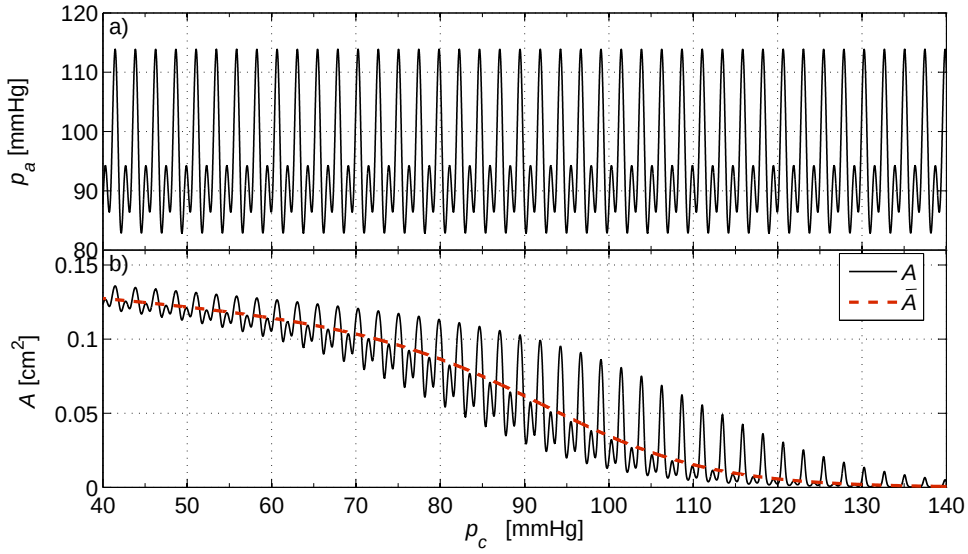

Figure 4.3: Examples of (a) the arterial blood pressure p_a and (b) the arterial lumen area A. The slow-varying component of the arterial lumen area $\bar{A}$ is shown by a red dashed line. The waveforms have been plotted as a function of cuff pressure p_c.

The time sampling period T_s was set to 1 msec. Typical values of the cardiovascular parameters in human artery were used in this simulation [17]; where $c_1 = 0.03$ mmHg^{-1}, $c_2 = 3.3$, $c_3 = 0.1$ mmHg^{-1}, $c_4 = 0.08$ cm^2, $f_c = 80$ beats/min, $\alpha_{1,1} = 0$ mmHg, $\alpha_{2,1} = 10$ mmHg, $\alpha_{1,2} = -8.4$ mmHg, $\alpha_{2,2} = 3.5$ mmHg, $\mu = 95$ mmHg, $SBP = 114$ mmHg, and $DBP = 82$ mmHg. It should be noted that the used cardiovascular parameters are only for the purpose of demonstration and can vary between different subjects. It should be also noted that the respiration effect was not considered in this simulation, as the main goal was to show the main properties of the ALA model.

4.3 Oscillometric Waveform Model

Over the duration of the cuff deflation, the recorded cuff pressure oscillations form a signal known as the oscillometric waveform (OMW) that may be viewed mathematically as a function of cuff pressure [15]. It has been shown that the oscillometric pulses are proportional to the arterial lumen area (ALA) oscillations during the cuff deflation

[17, 19]. Therefore, a model of the arterial lumen area oscillations as a function of cuff pressure can equivalently represent the OMW. In [17,19], the oscillations of the simulated ALA were extracted using a high-pass filter with cut-off frequency of 0.3 Hz [17] – 0.5 Hz [19]. The extracted ALA oscillations were then analyzed and compared with the OMW extracted from the actual recorded cuff pressure. It was found that the two waveforms match very closely. However, no mathematical model was proposed for the OMW.

According to equations (4.7) and (4.13), the ALA is composed of two main components: the slow-varying component due to the deflating cuff pressure (represented as $\bar{A}(t)$ hereafter) and the oscillations due to the quasi-periodic nature of the arterial pressure (represented as $\tilde{A}(t)$ hereafter). The slow-varying component of the ALA $\bar{A}_c(t)$ is modeled and subtracted from the whole ALA $A(t)$ model given in equation (4.13) to obtain a model of the ALA oscillations, as follows:

$$\tilde{A}(t) = A(t) - \bar{A}(t) \tag{4.14}$$

The slow-varying component of the ALA $\bar{A}$ can be obtained by fixing the arterial pressure $p_a(t)$ in (4.13) to its mean μ, as follows:

$$\bar{A}(t) = c_4 \frac{\ln(c_1(\mu - p_c(t)) + c_2)}{1 + e^{-c_3(\mu - p_c(t))}} \tag{4.15}$$

where $p_c(t)$ is the cuff pressure. The slow-varying component of the ALA is shown by a red dashed line in Fig. 4.3(b).

Since the oscillometric pulses are proportional to the ALA oscillations during the cuff deflation [17, 19], according to (4.14), the OMW can be modeled as follows:

$$OMW(t) = \eta \left(A(t) - \bar{A}(t) \right) \tag{4.16}$$

where η is a scaling factor.

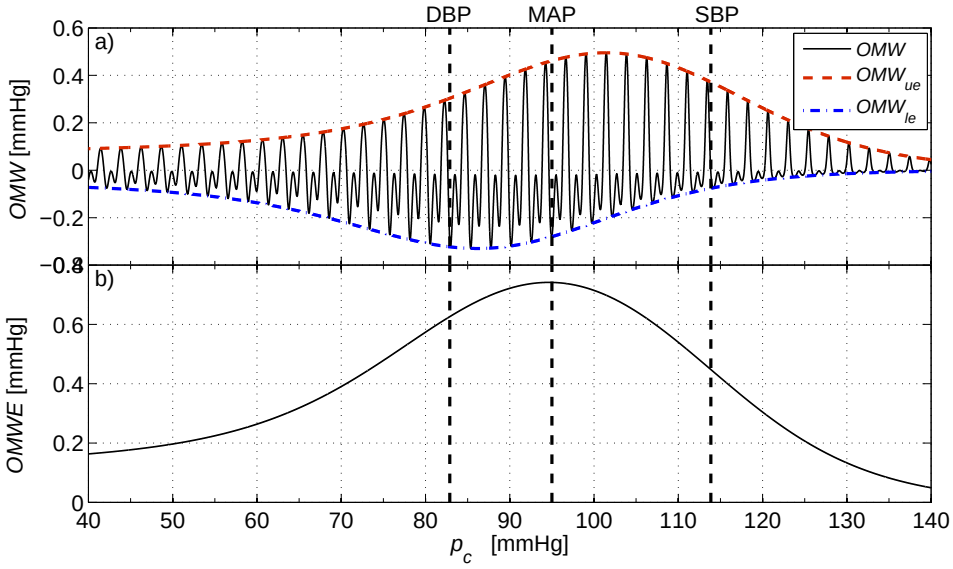

Figure 4.4: Examples of the simulated (a) oscillometric waveform OMW and (b) oscillometric waveform envelope $OMWE$ obtained by equations (4.17) and (4.20), respectively. The upper and lower envelopes of the oscillometric waveform are shown in red dashed and blue dashdot curves, respectively. The vertical dashed lines from left to right show the points at which cuff pressure p_c is equal to DBP, MAP, and SBP, respectively.

By substitution of equations (4.13) and (4.15) into (4.16), the OMW model is obtained as follows:

$$OMW(t) = c_4' \frac{\ln(c_1(p_a(t) - p_c(t)) + c_2)}{1 + e^{-c_3(p_a(t) - p_c(t))}} - c_4' \frac{\ln(c_1(\mu - p_c(t)) + c_2)}{1 + e^{-c_3(\mu - p_c(t))}} \tag{4.17}$$

It should be noted that the derived OMW model in equation (4.17) is a function of the arterial pressure p_a, the cuff pressure p_c, and four cuff-arm-artery system parameters c_1, c_2, c_3, and c_4'.

Figure 4.4(a) illustrates an example of the the OMW obtained by equation (4.17) as a function of cuff pressure. The same parameter values used in the simulation of Fig. 4.3 were used in the simulation of Fig. 4.4. The scaling parameter η was set to 10 mmHg/cm^2.

As mentioned earlier, the cuff pressure deflation rate is usually between 1-4 mmHg/sec. On the other hand, the arterial pressure changes from DBP to SBP within a heartbeat

which has a duration of about 0.6-1.2 second in healthy adults during rest [2]. Therefore, the variation of cuff pressure is smaller than the variations of the arterial pressure in each heartbeat (see Fig. 4.3(a)). As a result, the cuff pressure $p_c(t)$ can be assumed constant in each heartbeat. Based on the above discussion and according to equation (4.17), it can be concluded that the peaks of the OMW occur when arterial pressure is maximum, i.e. when $p_a(t) = SBP$. The troughs of the OMW occur when the arterial pressure is minimum, i.e. when $p_a(t) = DBP$. Also, the OMW crosses zero when the arterial pressure is equal to MAP, i.e., $p_a(t) = \mu$. This equivalence between the time points at which the arterial pressure is equal to SBP, DBP, and MAP and the time points at which the OMW is maximum, minimum, and zero, respectively, can be observed in Figs. 4.3 and 4.4.

4.4 Oscillometric Waveform Envelope Model

The amplitudes of the oscillometric pulses form the oscillometric waveform envelope (OMWE) and may be viewed mathematically as a function of cuff pressure [15]. Therefore, a model of the amplitude of the oscillometric pulses as a function of cuff pressure can equivalently represent the OMWE. The amplitude of the oscillometric pulses during the cuff deflation can be modeled as the difference between the upper and lower envelopes of the OMW, as shown in Fig. 4.4. According to equations (4.7)-(4.13), the peaks of the oscillometric pulses occur when the arterial pressure $p_a(t)$ is maximum, i.e., at $p_a(t) = SBP$. Therefore, the OMW upper envelope OMW_{ue} can be modeled as:

$$OMW_{ue}(t) = c_4' \frac{\ln(c_1(SBP - p_c(t)) + c_2)}{1 + e^{-c_3(SBP - p_c(t))}} - c_4' \frac{\ln(c_1(\mu - p_c(t)) + c_2)}{1 + e^{-c_3(\mu - p_c(t))}} \tag{4.18}$$

Likewise, the troughs of the oscillometric pulses occur when the arterial pressure $p_a(t)$ is minimum, i.e., at $p_a(t) = DBP$. Therefore, according to equations (4.7)-(4.13), the

OMW lower envelope OMW_{le} can be modeled as:

$$OMW_{le}(t) = c_4' \frac{\ln(c_1(DBP - p_c(t)) + c_2)}{1 + e^{-c_3(DBP - p_c(t))}} - c_4' \frac{\ln(c_1(\mu - p_c(t)) + c_2)}{1 + e^{-c_3(\mu - p_c(t))}} \tag{4.19}$$

Now, the OMWE can be modeled as the difference between the upper and lower envelopes of the OMW, as follows:

$$OMWE(t) = \frac{c_4' \ln(c_1(SBP - p_c(t)) + c_2)}{1 + e^{-c_3(SBP - p_c(t))}} - \frac{c_4' \ln(c_1(DBP - p_c(t)) + c_2)}{1 + e^{-c_3(DBP - p_c(t))}} \tag{4.20}$$

Note that the OMWE model in equation (4.20) consists of six unknown parameters including the cuff-arm-artery system parameters c_1, c_2, c_3, and c_4' and the desirable BP parameters SBP and DBP.

Figure 4.4(b) shows the OMWE obtained through Eq. (4.20). As is expected [14–19], it is obvious that the OMWE has a maximum close to the point at which the cuff pressure is equal to MAP.

4.5 Coefficient-Free Blood Pressure Estimation

In order to find the SBP and DBP values, the proposed model in equation (4.20) is fitted to the measured OMWE. The optimum parameters of the model are found using the least squares method, as follows:

$$\{\hat{SBP}, \hat{DBP}, \hat{c_1}, \hat{c_2}, \hat{c_3}, \hat{c_4'}\} = \arg \underbrace{\min}_{SBP, DBP, c_1, c_2, c_3, c_4'} \int_t \Big(OMWE(t) - \widetilde{OMWE}(t) \Big)^2 dt \tag{4.21}$$

where $\widetilde{OMWE}(t)$ represents the measured OMWE. The estimated parameters are shown on the left-hand side of the equation. The aforementioned optimization problem is solved using the trust region reflective algorithm [114].

4.5.1 Trust Region Reflective Algorithm

Line search algorithms are the conventional methods for optimization. In each iteration of a line search algorithm, a search direction is computed. It is then decided how far to move along that direction to find a better point.

Trust region algorithms are a class of relatively new line search algorithms. In a trust region algorithm, the search direction is found by solving a subproblem that approximates the original optimization in only a trusted region near the current iterate. The trust region is adjusted in each iteration based on the previous iteration performance. Compared to the conventional line search algorithms, trust region algorithms are more reliable and robust, they can be applied to ill-conditioned problems, they have very strong convergence properties, and they can handle bound constraints [153].

The trust region reflective algorithm [114] is adopted to solve the optimization problem in equation (4.21). The trust region reflective algorithm can be described as follows.

Consider an optimization problem where function $f(x)$, which takes vector arguments and returns scalars, is to be minimized. At each optimization iteration, the goal is to find a point $x + s$ in n-space where the function $f(x)$ has a lower value than the current point x. The trust region reflective algorithm approximates f with a simpler function q which reasonably reflects the behaviour of function f in a neighborhood N around point x, called the trust region N. Function q is defined as the quadratic approximation of function f using the first two terms of the Taylor series, as follows:

$$q(s) = g^T s + \frac{1}{2} s^T H s \tag{4.22}$$

where g is the gradient of f at the current point x and H is the Hessian matrix.

Since minimizing equation (4.22) can be computationally expensive, the optimization problem is restricted to a two-dimensional subspace S. The two-dimensional subspace S is determined as the linear space spanned by s_1, the vector in the direction of the

gradient, and s_2, an approximate Newton direction obtained as the solution to:

$$Hs_2 = -g \tag{4.23}$$

The trial step s is obtained by minimizing equation (4.22). If $f(x+s) < f(x)$, then the current point x is updated to $x+s$. Otherwise, the current point remains unchanged and the trust region is shrunk and the trial step computation is repeated. For more details on the trust region reflective algoritm, the reader is referred to [114].

4.6 Experimental Results

As an initial validation of our proposed method, it was tested on real-world data collected by our research group [79]. This dataset comprised 150 oscillometric BP recordings acquired with a prototype designed in our research laboratory. Analogous Food and Drug Administration (FDA)-approved Omron HEM-790IT monitor readings were used as the reference. The dataset is fully described in Appendix A.2.

The oscillometric waveform (OMW) was obtained from the recorded cuff pressure signal using a 2^{nd} order band-pass digital Butterworth filter with lower cutoff frequency of 0.5 Hz and upper cutoff frequency of 20 Hz. A local maxima detection technique [10] was applied to detect the peaks and troughs of the OMW. The oscillometric waveform envelope (OMWE) was formed by subtracting the consecutive peaks and troughs of the OMW. Examples of the measured OMW and OMWE are shown in Fig. 4.5.

The optimum model parameters including SBP and DBP were obtained as the solution to the optimization problem in equation (4.21) which was implemented in discrete time. Typical values of the cardiovascular parameters in human artery were used as initial values for the trust-region-reflective algorithm [17]; where $c_1 = 0.03$ mmHg^{-1}, $c_2 = 3.3$, $c_3 = 0.1$ mmHg^{-1}, $c_4 = 0.08$ cm^2, $SBP = 114$ mmHg, and $DBP = 82$ mmHg.

Examples of the OMWE and the fitted model are shown in the solid grey and dashed

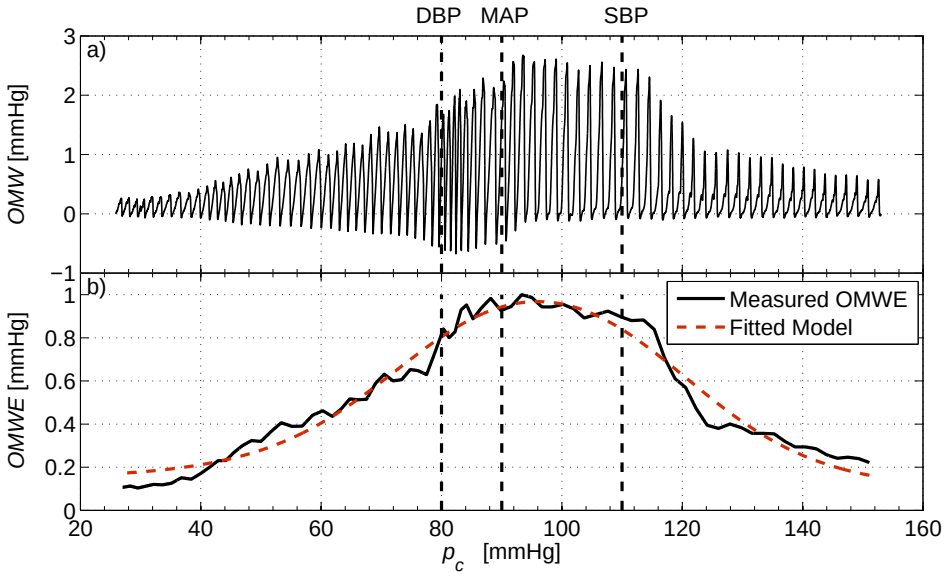

Figure 4.5: Examples of the measured (a) oscillometric waveform OMW and (b) oscillometric waveform envelope $OMWE$. The dashed red curve represents the fitted model proposed in equation (4.20). The vertical dashed lines from left to right show the points at which cuff pressure p_c is equal to DBP, MAP, and SBP, respectively.

Table 4.1: Mean error (ME), mean absolute error (MAE), and standard deviation of error (SDE) of the coefficient-free BP estimates based on the proposed oscillometric waveform model on the dataset of 150 recordings.

	SBP	DBP
ME [mmHg]	0.04	-1.75
MAE [mmHg]	4.60	4.53
SDE [mmHg]	5.84	5.97

black curves, respectively, in Fig. 4.5 (b).

The performance of the proposed method was evaluated in terms of mean error (ME), mean absolute error (MAE), and standard deviation of error (SDE) on the dataset of 150 recordings. It was found that the ME, MAE, and SDE in estimation of SBP are 0.04, 4.60, and 5.84 mmHg, respectively. It was also found that the ME, MAE, and SDE in estimation of DBP are -1.75, 4.53, and 5.97 mmHg, respectively. The results are summarized in Table 4.1.

In order to analyze the agreement between our proposed method and the FDA-

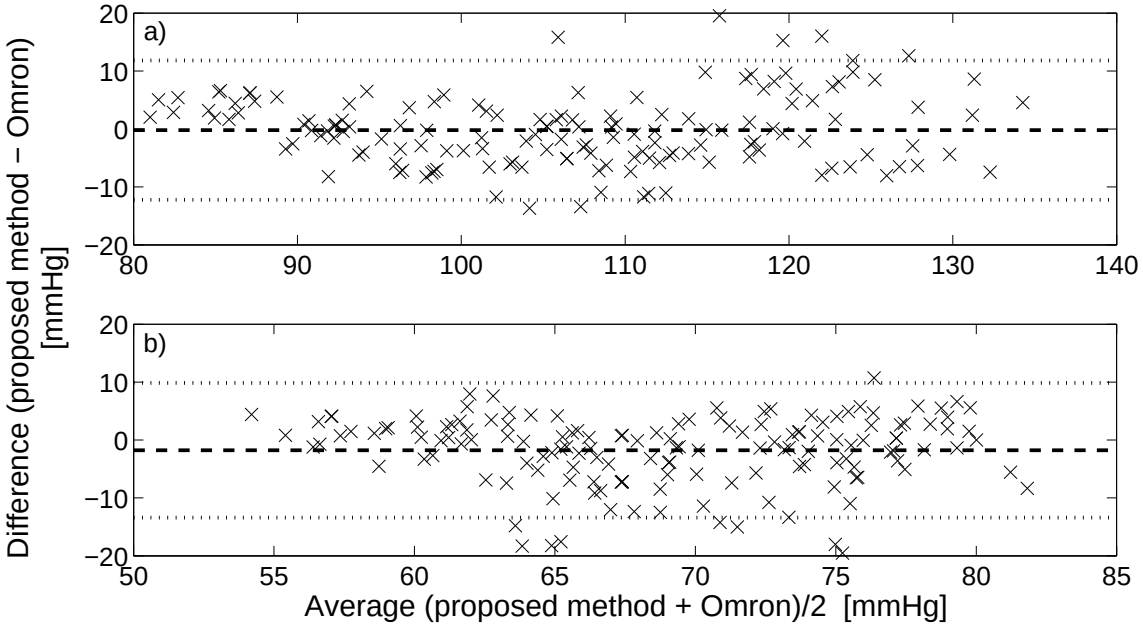

Figure 4.6: Bland-Altman plot of the (a) SBP and (b) DBP estimates for our proposed model-based method versus Omron monitor. The horizontal dotted lines show the limits of agreement, while the horizontal dashed line shows the bias.

approved Omron monitor, Bland-Altman analysis was performed [106, 107]. Figure 4.6 shows the Bland-Altman plot of the SBP and DBP estimates for our proposed method versus the Omron monitor. The x-axis of the plots shows the average of our proposed method and the Omron monitor, while the y-axis shows the difference between the two methods. The bias (ME) and the limits of agreement (ME $\pm$ 1.96 $\times$ SDE) are shown in dashed and dotted lines, respectively. It is observed that our method slightly overestimates the SBP and DBP at pressures approximately under 90 mmHg and 60 mmHg, respectively, compared to the Omron monitor. There is also a slight increase in variability of SBP estimates at pressures approximately above 120 mmHg. However, in total, the errors are almost evenly distributed over the measured pressure range. That is, the BP estimates made by our proposed method are in close agreement with those made by the Omron device.

4.7 Conclusion

The main contributions of this chapter were the development of a new mathematical model for the OMWE as a function of the SBP and DBP, and the formulation of a novel coefficient-free method for estimating BP. The successful cross-validation with empirical data confirmed the accuracy of the proposed theoretical model and BP estimation method. Future work will involve undertaking clinical testing on a larger number of healthy subjects as well as patients, where the method will be compared against auscultatory measurements by trained observers.

Unlike existing models of oscillometry, our proposed model provides an explicit relationship between the OMWE and the SBP and DBP. Therefore, our proposed model can be used to develop accurate BP estimation algorithms and study the effect of different cuff-arm-artery system parameters on the accuracy of BP estimates. Since our proposed model is a function of parameters characterizing the arterial collapse and distension, it can also be used to estimate arterial stiffness in oscillometry. Moreover, the proposed model can be used to remove noise and unwanted artifacts from the OMWE.

It should be noted that the optimization problem in equation (4.21) may converge towards local minima due to the number of unknown parameters. Therefore, it is expected that the BP estimation results would improve if the number of unknown parameters is reduced. One possibility that we are currently investigating is to estimate the cuff-arm-artery system parameters (c_1, c_2, c_3, and c_4') and the BP parameters (SBP and DBP), separately, using multiple measurements from a subject.

We also assumed that the SBP and DBP do not change during a measurement which is usually shorter than 30 s. Future work will focus on models that incorporate the time variability of the SBP and DBP during the measurement period. The extended Kalman filter can then be used to estimate the SBP and DBP values that correspond to any heartbeat, in contrast to the conventional oscillometric method that estimates the SBP and DBP values at two random instants in time over the deflation period. Moreover, by

incorporating the time variability of the model parameters, the proposed model can be used to estimate, track, and predict the BP variability over time.

Chapter 5

Mathematical Modeling of the Pulse Transit Time and Coefficient-Free Estimation of Blood Pressure [1]

Since most of the oscillometric methods are solely based on changes in oscillometric pulse amplitudes, they fail to provide accurate estimation in several conditions such as atrial fibrillation, obesity, and atherosclerosis, where pulse amplitudes may be weak or erratic [154–158].

Previous studies have tried to overcome the above mentioned problem by employing an alternative time-based method for automatic BP estimation [95–97, 159]. These studies investigated the dependence of pulse transit time (PTT) on cuff pressure for BP estimation, where PTT is the time delay between ECG R-peaks and arterial pulses.

[1] Parts of this chapter have been published in:

1. M. Forouzanfar, S. Ahmad, I. Batkin, H. R. Dajani, V. Z. Groza, and M. Bolic, "Coefficient-free blood pressure estimation based on pulse transit time-cuff pressure dependence," *IEEE Trans. Biomed. Eng.*, vol. 60, pp.1814-1824, Jul. 2013.
2. I. Batkin, S. Ahmad, M. Bolic, V. Z. Groza, H. R. Dajani, and M. Forouzanfar, "Apparatus and method for electrocardiogram-assisted blood pressure measurement," US, UK, and Canadian Non-Provisional Patent Application, No. US 20120283583 A1, May 2012.
3. M. Forouzanfar, S. Ahmad, I. Batkin, H. R. Dajani, V.Z. Groza, and M. Bolic, "Model-based mean arterial pressure estimation using simultaneous electrocardiogram and oscillometric blood pressure measurements," submitted to *Ann. Biomed. Eng.*.

However, these techniques were not suitably developed; for example, they required pressure/ECG sensors auxiliary to the cuff. Problems like these defeated the simplicity and straightforwardness of the oscillometric BP estimation method. In a recent article, our research group proposed an ergonomic integration of the PTT-cuff pressure method with the oscillometric method for accurate BP measurement [79]. However, that work still relied on using empirical coefficients on the PTT-cuff pressure mapping for SBP and DBP estimation. Moreover, the focus of that work was on the validation of the method/algorithms and not on developing a theoretical foundation of the analysis. To the best of our knowledge, no previous work (including our research group's - [79]) provided a theoretical explanation of the PTT-cuff pressure method along with employing a non-parametric (coefficient-free) method for SBP/DBP estimation from either the PTT-cuff pressure dependency or oscillometry.

In Chapter 4, a mathematical model of oscillometry was derived to describe the interaction between the cuff and the artery. In this chapter, this model is utilized to build a model for the PTT based on which the coefcient-free estimation of BP is proposed. We will (a) develop a theoretical framework for the PTT-cuff pressure BP estimation method, which is an extension of previous modeling work done on oscillometry alone [14–19]; (b) show that with the developed model, SBP, DBP, and MAP can be determined directly from maxima of PTT-cuff pressure mappings without empirical coefficients when PTT is measured from ECG R-peak to the oscillometric pulse peak, trough, and zero-crossing, respectively; and (c) cross-validate the theoretical findings of (b) by estimating BP from 150 actual ECG and oscillometric recordings obtained from ten healthy subjects using our prototype [79] and comparing it with analogous BP estimates made by the Food and Drug Administration (FDA)-approved Omron monitor (HEM-790IT).

The block diagram representation of the proposed model-based oscillometric BP estimation method is shown in Fig. 5.1.

The remainder of this chapter is organized as follows. In Section 5.1, our simultaneous ECG and oscillometric BP measurement system is introduced. In Section 5.2, the

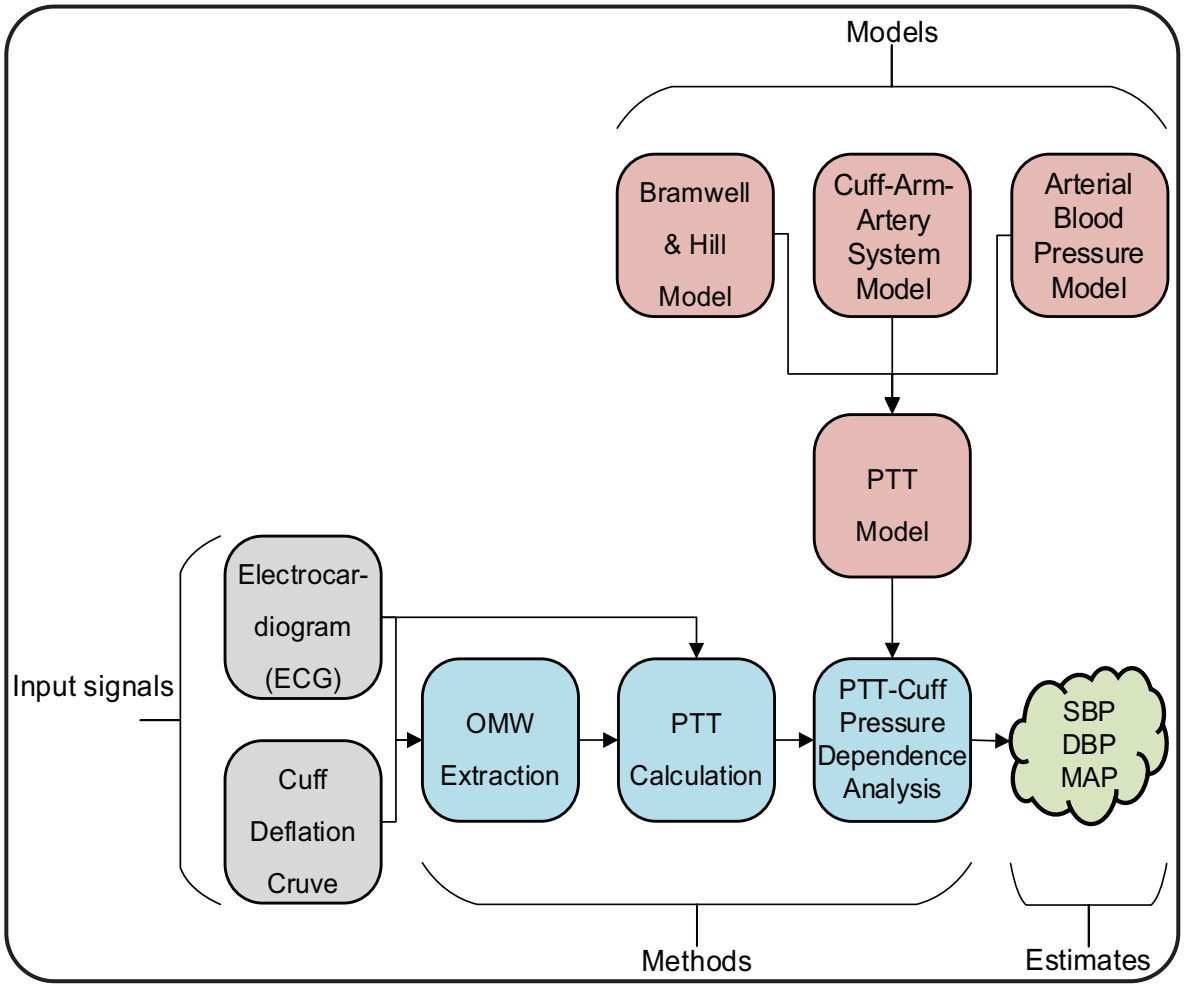

Figure 5.1: Block diagram of the proposed coefficient-free blood pressure (BP) estimation method using pulse transit time (PTT).

oscillometry model proposed in Chapter 4 is utilized to build a model for the PTT, based on which the coefficient-free estimation of SBP, DBP, and MAP is proposed. In Section 5.3, the experimental determination of PTT in oscillometry is described. In Section 5.4, an alternative PTT-based method is proposed for estimation of MAP. In Section 5.5, the experimental results are provided and in Section 5.6 the chapter is concluded.

5.1 Measurement System

In order to measure the PTT, defined as the time taken by an arterial pulse to travel between the heart and the brachial artery, oscillometric BP and the ECG signals should be recorded simultaneously [29]. In [98], a wireless medical device was designed to continuously monitor the ECG, BP, and blood oxygen of a patient and deliver pertinent information to first responders. In [99], synchronized ECG signals were acquired for removing motion artifacts from oscillometric signals to increase the accuracy of BP measurements. However, these devices required pressure and ECG sensors auxiliary to the cuff, defeating the simplicity and straightforwardness of the oscillometric BP estimation method.

In this study, the oscillometric BP and the ECG signals were acquired simultaneously using a prototype designed in our research laboratory [79], as shown in Fig. 5.2. Our measurement system consists of eight main components; a) a brachial cuff with a flexible dry ECG electrode, b) a wrist band with a flexible dry ECG electrode, c) a manual air pump with a screw-controlled pressure-release valve, d) a mini direct-current (DC) automatic air pump, e) an analog pressure transducer, f) an analog ECG amplifier, g) the National Instruments^{TM} C Series 9239 data acquisition module, and h) the National Instruments^{TM} LabVIEW system design software.

The brachial BP cuff is placed around the subject's upper left arm and controlled by an automatic 6 volt DC mini air pump. The pump operates with a push-button mounted on the prototype. Once the push-button is pressed, it turns the pump on and the brachial cuff is gradually inflated and then deflated to conduct the oscillometric measurement. A screw-controlled manual pressure release valve is connected in-line with the brachial cuff. The screw on the valve can be rotated manually to control the deflation rate of the cuff.

Dry flexible ECG electrodes are embedded both inside the brachial cuff that is wrapped around the subject's arm and inside a wristband that the subject wears on the other hand's wrist. The two ECG leads, one from the brachial cuff and one from the

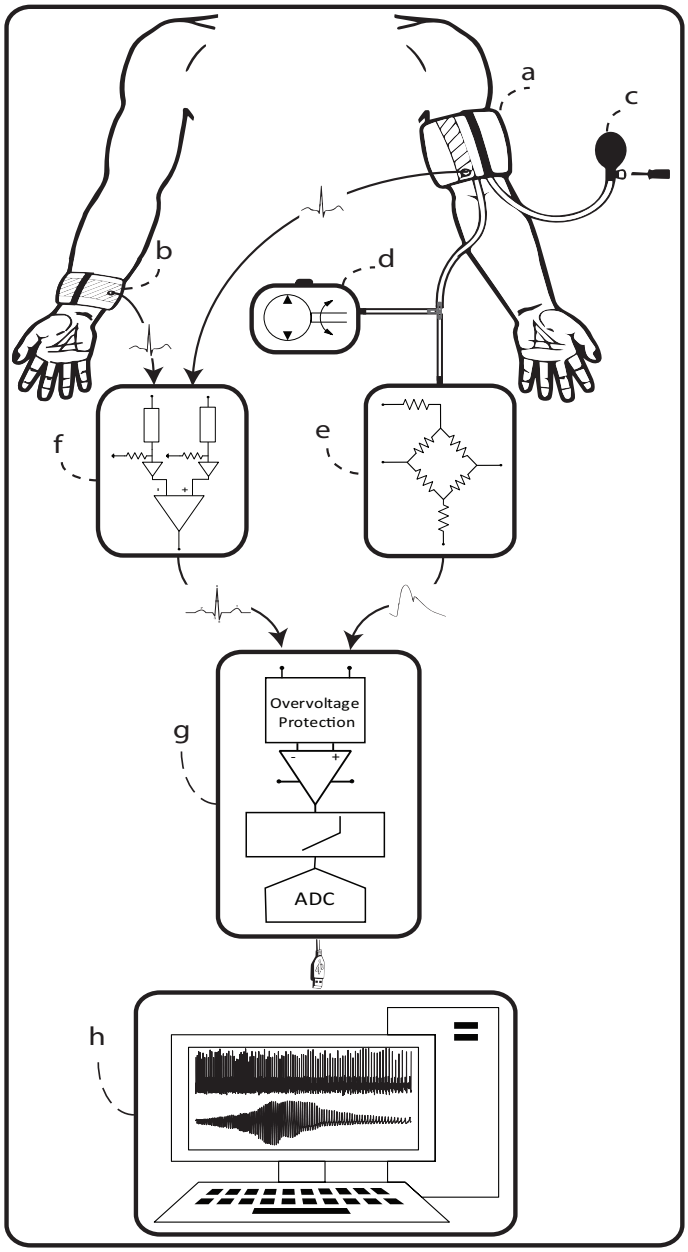

Figure 5.2: Functional block diagram of our pulse transit time (PTT) measurement system. (a) Brachial cuff with conductive fabric. (b) Wrist band with conductive fabric. (c) Manual air pump and screw-controlled pressure-release valve. (d) Automatic DC mini air pump. (e) Vernier pressure transducer. (f) ECG amplifier. (g) National Instruments^{TM} C Series 9239 data acquisition module. (h) Personal computer with National Instruments^{TM} LabVIEW system design software.

wristband, form the input to the ECG amplifier. This is equivalent to an ECG lead 1 configuration. The ECG amplifier has an input impedance of 20 Mohm and a voltage gain of 1000. The ECG amplifier includes circuitry for stabilizing the supply voltage and for signal conditioning.

A Vernier pressure transducer is connected to the brachial cuff through an air hose to convert the cuff pressure oscillations into an analog voltage signal. The Vernier pressure transducer operates on a DC supply voltage of five volts.

The analog voltage outputs from the ECG amplifier and the Vernier pressure transducer are fed to two of the four simultaneously-sampled analog input channels of the National Instruments^{TM} C Series 9239 module mounted on a CompactDAQ data acquisition board. The National Instruments^{TM} module operates on a DC supply voltage of 10 volts. These analog signals are conditioned, buffered, and then sampled at a frequency of 1.613 kHz by a 24-bit delta-sigma analog-to-digital converter. The quantized signals are transmitted to a personal computer via a universal serial bus cable.

National Instruments^{TM} LabVIEW system design software is used for data acquisition of the ECG and the oscillometric BP signals. A customized LabVIEW user interface is developed that displays the acquired ECG and oscillometric BP signals in real-time. Signal processing and statistical analysis are performed offline using Matlab.

This configuration provides an ergonomic integration of ECG and oscillometric BP monitoring that enables the robust measurement of the PTT.

5.2 Pulse Transit Time Model

In this section, we prove analytically how the pulse transit time (PTT) measured at certain points of the arterial pulses can be employed to estimate the SBP, DBP, and MAP. These theoretical findings will be then validated in Section 5.5 on real oscillometric measurements.

In oscillometry, the cuff affects the propagation of the BP pulse wave locally in the

brachial artery under the cuff, while the propagation of the BP pulse wave from the heart to the brachial artery is not affected. Therefore, the PTT is modeled with two components: the time it takes for the BP pulse wave to arrive from the heart to the brachial artery under the cuff $\tau_a(t)$ and the time it takes for the BP pulse wave to travel in the brachial artery underneath the cuff $\tau_c(t)$ [79, 160]:

$$\tau(t) = \tau_a(t) + \tau_c(t) \tag{5.1}$$

where $\tau_a(t) = L_a/\nu_a(t)$ and $\tau_c(t) = L_c/\nu_c(t)$. L_a and L_c are the length of the arterial segments between the heart and the arm and underneath the cuff, respectively, and $\nu_a(t)$ and $\nu_c(t)$ are the average pulse wave velocities (PWV) over L_a and L_c, respectively. As our goal is to analyze the changes in PTT as a function of applied cuff pressure, we do not take into account the pre-ejection period (PEP) in our model. Since PEP can be treated as a constant at rest and is not sensitive to cuff pressure variations, this is a reasonable assumption [160].

Using the Bramwell and Hill equation [2], $\nu_c(t)$ and $\nu_0(t)$ can be written, respectively, as follows:

$$\nu_c(t) = \sqrt{\frac{A_c(t)}{\rho}} \times \sqrt{\frac{\partial\left(p_a(t) - p_c(t)\right)}{\partial A_c(t)}} \tag{5.2}$$

$$\nu_a(t) = \sqrt{\frac{A_a(t)}{\rho}} \times \sqrt{\frac{\partial p_a(t)}{\partial A_a(t)}} \tag{5.3}$$

where ρ is the blood density, $p_a(t)$ and $p_c(t)$ represent the ABP and cuff pressure as defined in equations (4.1) and (4.8), respectively. $A_c(t)$ and $A_a(t)$ are the average ALAs along the arterial segments underneath the cuff and between the heart and the arm, respectively. By the end of this Section, it will be shown that our proposed BP estimation method is independent of ρ, L_a, and L_c.

According to equations (5.2) and (5.3), equation (5.1) can be re-written as follows:

$$\tau(t) = L_a\sqrt{\frac{\rho}{A_a(t)}\frac{\partial A_a(t)}{\partial p_a(t)}} + L_c\sqrt{\frac{\rho}{A_c(t)}\frac{\partial A_c(t)}{\partial p_t(t)}} \tag{5.4}$$

where the PTT $\tau(t)$ is a function of four variable terms: $A_a(t)$, $A_c(t)$, $\partial A_c(t)/\partial p_t(t)$, and $\partial A_a(t)/\partial p_a(t)$.

In [161, 162], the arterial pressure-area relationship at positive transmural pressures was modeled by an exponential curve. A similar model was adopted in [15] to model the arterial pressure-area relationship at negative transmural pressures. The combination of the two models, results in the following two-segment model for the arterial pressure-area relationship [24]:

$$A(t) = \begin{cases} A_0 e^{ap_t(t)} & \text{for } p_t(t) \leq 0 \\ A_m + (A_0 - A_m)e^{-bp_t(t)} & \text{for } p_t(t) \geq 0 \end{cases} \tag{5.5}$$

where $A(t)$ represents the ALA, a and b are compliance indices that relate to the arterial stiffness, A_0 represents the ALA at zero transmural pressure, and A_m is the fully expanded ALA. All the model parameters a, b, A_0, and A_m are always positive. The following relationship is held between the model parameters:

$$a = b\left(\frac{A_m}{A_0} - 1\right) \tag{5.6}$$

Recently, Lan et al. [163–165] developed and validated clinically a 3D finite element upper arm model to study the effect of arm soft tissue, muscle, brachial artery and humerus mechanical properties on oscillometric measurements. They showed that the pressure transmission from the external surface of the arm to the tissue surrounding the brachial artery varies at different longitudinal locations even if the external pressure is uniformly applied along the arm. They defined a pressure transmission ratio as the pressure at the external brachial artery surface divided by the pressure on the arm surface

and found that this ratio degrades by up to 70% from the center to the edge of the cuff. This means that the ALA increases from center to the edge of the cuff, and when the artery is closed at the center it can remain open underneath the rest of the cuff. Since the measured cuff pressure in oscillometry is a reflection of the entire arterial area change under the cuff rather than one section, equation (5.5) should be modified accordingly to represent the average ALA under the cuff. This is done by adding a small constant A_{cst} to equation (5.5), as follows:

$$\begin{aligned} A_c(t) &= A(t) + A_{cst} \\ &= \begin{cases} A_{cst} + A_0 e^{a p_t(t)} & \text{for } p_t(t) \leq 0 \\ (A_{cst} + A_m) + (A_0 - A_m) e^{-b p_t(t)} & \text{for } p_t(t) \geq 0 \end{cases} \end{aligned} \tag{5.7}$$

where $A_c(t)$ represents the average ALA under the oscillometric cuff. The ALA model in (5.7) is different from (5.5) only in the constant A_{cst} that represents the average non-zero ALA over the whole cuff bladder width when the arterial area at the center of the cuff is zero. The necessity of the constant A_{cst} in the ALA model will be verified in Section 5.5 on estimated PTTs from actual recordings. Nevertheless, we will show by the end of this section that our proposed BP estimation method is independent of the ALA parameters including the constant A_{cst}.

According to equation (5.5), $A_a(t)$ can be written as follows:

$$A_a(t) = A'_m + (A'_0 - A'_m) e^{-b' p_a(t)} \tag{5.8}$$

where the prime is used to distinguish between the ALA model parameters of the arterial segment between the heart and the arm from those of the arterial segment underneath the cuff. Since there is no cuff over the arterial branch from the heart to the arm, $p_t(t)$ is always greater than zero for this section of the artery. Therefore, the second term in equation (5.5) was used to derive equation (5.8).

$\partial A_a(t)/\partial p_a(t)$ is obtained by taking the derivative of equation (5.8), as follows:

$$\frac{\partial A_a(t)}{\partial p_a(t)} = (A'_m - A'_0)b'e^{-b'p_a(t)} \tag{5.9}$$

Finally, $\partial A_c(t)/\partial p_t(t)$ is obtained by taking the derivative of equation (5.7), as follows:

$$\frac{\partial A_c(t)}{\partial p_t(t)} = \begin{cases} aA_0e^{ap_t(t)} & \text{for } p_t(t) \leq 0 \\ (A_m - A_0)be^{-bp_t(t)} & \text{for } p_t(t) \geq 0 \end{cases} \tag{5.10}$$

Now, by substituting equations (5.7)-(5.10) into (5.4), we obtain:

$$\tau(t) = \tau_a(t) + \begin{cases} \tau_{c1}(t) & \text{for } p_t(t) \leq 0 \\ \tau_{c2}(t) & \text{for } p_t(t) \geq 0 \end{cases} \tag{5.11}$$

where

$$\tau_a(t) = L_a\sqrt{\rho b'\left(\frac{1}{1 - \frac{A'_m - A'_0}{A'_m}e^{-b'p_a(t)}} - 1\right)} \tag{5.12}$$

$$\tau_{c1}(t) = L_c\sqrt{\rho a\left(1 - \frac{1}{1 + \frac{A_0}{A_{cst}}e^{ap_t(t)}}\right)} \tag{5.13}$$

$$\tau_{c2}(t) = L_c\sqrt{\rho b\left(\frac{1}{1 - \frac{A_m - A_0}{A_m + A_{cst}}e^{-bp_t(t)}} - 1\right)} \tag{5.14}$$

The second term on the right side of equation (5.11) represents $\tau_c(t)$.

Figure 5.3(a) shows the simulated PTT during cuff deflation period with $L_a = 70$ cm, $L_c = 10$ cm, $\rho = 1060$ kg/m^3 [166], $a = 0.09$ mmHg^{-1}, $b = 0.03$ mmHg^{-1}, $A_0 = 0.1$

cm^2, and $A_{max} = 0.4\ cm^2$ [23]. The rest of the parameters were the same as the ones used to simulate Fig. 4.3. It should be noted that the used cardiovascular parameters are only for the purpose of demonstration and can vary between different subjects. The observed oscillations of the PTT are due to the changes in arterial pressure during each heartbeat. The gradual change in the amplitude and shape of the PTT oscillations is due to the change in cuff pressure.

From equations (5.13)-(5.14), it is observed that $\tau_{c1}(t)$ and $\tau_{c2}(t)$ are functions of $p_t(t) = p_a(t) - p_c(t)$. Since parameter a is always positive, $\tau_{c1}(t)$ is monotonically increasing as the transmural pressure increases. On the other hand, since parameter b is always positive, $\tau_{c2}(t)$ is monotonically decreasing as the transmural pressure increases. This bring us to the conclusion that $\tau_c(t)$ has a maximum at $p_t(t) = 0$, or in other words, when $p_c(t) = p_a(t)$.

From equation (5.12) it can be observed that $\tau_a(t)$ is only a function of the arterial pressure $p_a(t)$. Therefore, $\tau_a(t)$ oscillates during each heartbeat as $p_a(t)$ changes. However, $\tau_a(t)$ would be constant if the arterial pressure $p_a(t)$ in equation (5.12) is replaced by a fixed value such as SBP, DBP, and MAP. In other words: $\tau_a(t)|_{p_a(t)=SBP}$, $\tau_a(t)|_{p_a(t)=DBP}$, and $\tau_a(t)|_{p_a(t)=MAP}$ are all constants. It should be noted that the arterial elastic properties may change along the arterial branch from the heart to the arm, and therefore $\tau_a(t)$ model parameters could change at different locations of the arterial branch. In our PTT model, $\tau_a(t)$ parameters were assumed to be constant and equal to their average value over the corresponding arterial segment. Also, notice that as we are studying the changes in PTT with respect to the changes in cuff pressure applied to the subject's arm, $\tau_a(t)$ is treated as a constant with respect to the cuff pressure changes.

If the PTT associated with the points at which arterial pressure equals to SBP, DBP, and MAP, is represented as $\tau_s(t)$, $\tau_d(t)$, and $\tau_m(t)$, respectively, then from the above discussion it can be concluded that:

$$\tau_s(t) \text{ has a maximum at } p_c(t) = SBP \tag{5.15}$$

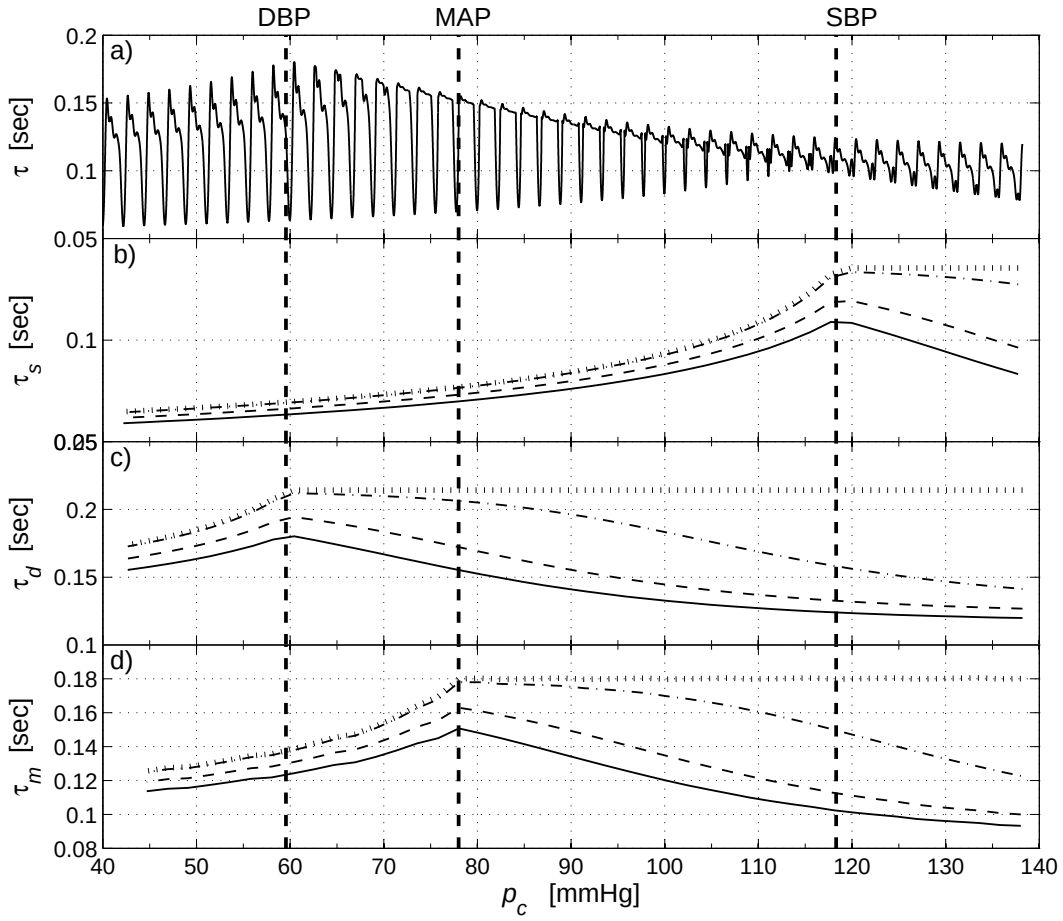

Figure 5.3: Simulated pulse transit time (PTT) as a function of cuff pressure. (a) Simulated PTT. (b-d) Simulated PTT computed at the points at which the arterial pressure is equal to SBP, DBP, and MAP, respectively. The PTT has been depicted for $A_{cst} = 0\%$, $A_{cst} = 1\%$, $A_{cst} = 10\%$, and $A_{cst} = 20\%$ of the maximum arterial lumen area (ALA) in dotted, dashdot, dashed, and solid lines, respectively. All the waveforms are plotted as a function of cuff pressure p_c. The vertical dashed lines from left to right show the points at which cuff pressure is equal to DBP, MAP, and SBP, respectively.

$$\tau_d(t) \text{ has a maximum at } p_c(t) = DBP \tag{5.16}$$

$$\tau_m(t) \text{ has a maximum at } p_c(t) = MAP \tag{5.17}$$

where

$$\tau_s(t) = \tau(t)\big|_{p_a(t)=SBP} \tag{5.18}$$

$$\tau_d(t) = \tau(t)\big|_{p_a(t)=DBP} \tag{5.19}$$

$$\tau_m(t) = \tau(t)\big|_{p_a(t)=MAP} \tag{5.20}$$

Therefore, the estimation of the SBP, DBP, and MAP can be performed by finding the cuff pressures at which $\tau_s(t)$, $\tau_d(t)$, and $\tau_m(t)$ have a maximum, respectively, as illustrated in Figs. 5.3(b-d). The same parameter values used in the simulation of Fig. 5.3(a) were used for the rest of the parameters in the simulation of Fig. 5.3. The SBP, DBP, and MAP values were determined as the maximum, minimum, and arithmetic mean of the arterial pressure in a cardiac cycle, respectively. The important point is that $\tau_s(t)$, $\tau_d(t)$, and $\tau_m(t)$ always exhibit a maximum independent of the model parameter values at cuff pressure equal to SBP, DBP, and MAP, respectively. The only exception is when the constant A_{cst} is equal to zero. In this case, $\tau_s(t)$, $\tau_d(t)$, and $\tau_m(t)$ will exhibit a flat maximum starting at the point at which the cuff pressure equals to SBP, DBP, and MAP, respectively. In such a case, the BP values can be determined as the cuff pressure at which the slope of PTT becomes zero. However, as explained earlier, the constant A_{cst} is always greater than zero since the arterial branch under the cuff is never occluded completely across its length at typical cuff pressure values. The non-zero value of the constant A_{cst} was verified on the PTT curves obtained on real measurements, as will be shown in Section 5.5. $\tau_s(t)$, $\tau_d(t)$, and $\tau_m(t)$ are plotted for $A_{cst} = 0\%$, $A_{cst} = 1\%$, $A_{cst} = 10\%$, and $A_{cst} = 20\%$ of the maximum ALA in Figs. 5.3(b-d), respectively. It should be pointed out that the PEP could alter Figs. 5.3(a-d) by shifting them upward by a small constant. However, PEP does not alter the shape of the PTT curves and location

of their maxima as it can be assumed to be constant at rest during the measurement interval [160]. Therefore, our proposed method is independent of the PEP.

5.3 Experimental Determination of Pulse Transit Time

In this section, we demonstrate how to experimentally measure the PTT from the simultaneous ECG and oscillometric recordings and how the experimental measured PTT is related to the theory developed in the previous section.

A prototype designed in our research laboratory was used to record the simultaneous oscillometric BP and ECG signals [79]. PTT was estimated as the time interval between the ECG R-peaks and certain points of the oscillometric pulses, i.e, the peaks, troughs, and zeros. As it was shown in Chapter 4, there is an equivalence between the time points at which the arterial pressure is equal to SBP, DBP, and MAP and the time points at which the OMW is maximum, minimum, and zero, respectively. In other words, the peaks of the OMW occur when arterial pressure is maximum, i.e. when $p_a(t) = SBP$. The troughs of the OMW occur when the arterial pressure is minimum, i.e. when $p_a(t) = DBP$. Also, the OMW crosses zero when the arterial pressure is equal to MAP, i.e., $p_a(t) = \mu$.

For the purpose of better illustration, this process is shown on a simulated pulse in Fig. 5.4. The corresponding arterial pressures at the aorta and the brachial artery are shown in Fig. 5.4(a) by dashed and solid lines, respectively. The aortic pressure waveform is obtained as the time-shifted version of the brachial artery pressure waveform defined in equation (4.1). The amount of time shift was determined according to equations (5.11)-(5.14). The time interval between the ECG R-peak (shown by the bold vertical dashed line) and the aortic pulse peak was set to 30 ms. These values were arbitrarily chosen for the purpose of illustration only. The theoretical PTTs associated with the points at which the arterial pressure equals to SBP, DBP, and MAP are shown in Fig. 5.4(a) as τ_s, τ_d, and τ_m, respectively. In theory, these PTTs can be computed through

equations (5.18-5.20), respectively. However, in experiment, the PTT is estimated as the time interval between the ECG R-peaks and the oscillometric peaks, troughs, and zeros, as shown Fig. 5.4(b). The estimated PTTs are shown as τ_p, τ_t, and τ_z, respectively. As it can be observed from Fig. 5.4, there are time differences between the estimated and the theoretical PTTs that have been shown as T_s, T_d, and T_m. T_s, T_d, and T_m are the time intervals between the ECG R-peak and the time points at which the aortic pulse is equal to SBP, DBP, and MAP, respectively. It is obvious that these time intervals are independent of the cuff pressure that is applied to the brachial artery because they relate to the aortic pulse. Therefore, they are assumed to be constant during the deflation period. As a result, equations (5.15)-(5.17), can be re-written for $\tau_p(t)$, $\tau_t(t)$, and $\tau_z(t)$, as follows:

$$\tau_p(t) \text{ has a maximum at } p_c(t) = SBP \tag{5.21}$$

$$\tau_t(t) \text{ has a maximum at } p_c(t) = DBP \tag{5.22}$$

$$\tau_z(t) \text{ has a maximum at } p_c(t) = MAP \tag{5.23}$$

where

$$\tau_p(t) = \tau_s(t) + T_s \tag{5.24}$$

$$\tau_t(t) = \tau_d(t) - T_d \tag{5.25}$$

$$\tau_z(t) = \tau_m(t) - T_m \tag{5.26}$$

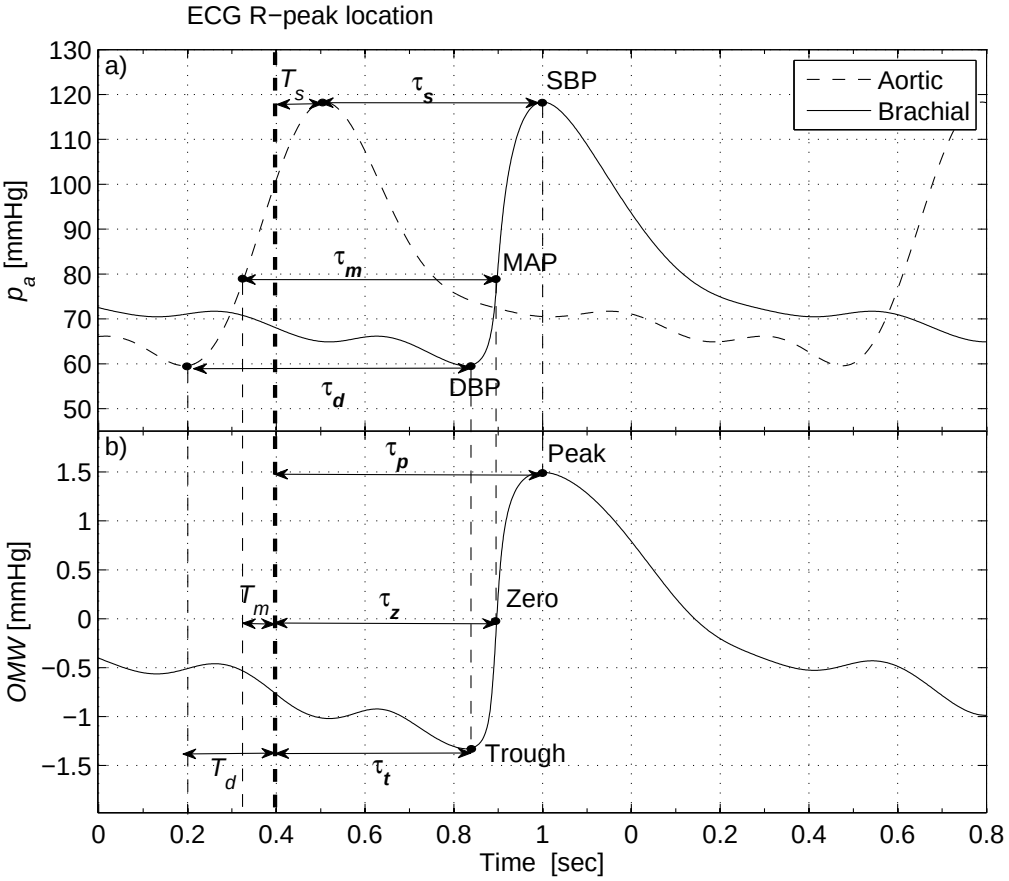

Figure 5.4: Experimental determination of pulse transit time (PTT) shown on simulated pulses for a better illustration. (a) Simulated arterial pressure waveforms in the aorta and the brachial artery. (b) Simulated oscillometric waveform (OMW). $\tau_s(t)$, $\tau_d(t)$, and $\tau_m(t)$ represent the theoretical PTTs that can be computed through equations (5.18)-(5.20), respectively. $\tau_p(t)$, $\tau_z(t)$, and $\tau_t(t)$ are the experimentally measured PTTs according to equations (5.24)-(5.26), respectively. The bold vertical dashed line shows the ECG R-peak location in both figures.

Equations (5.21-5.23) provide the means to estimate SBP, DBP, and MAP, respectively, independent of any parameters.

5.4 Estimation of Mean Arterial Pressure from Maximum Slope Pulse Transit Time

While determining the location of peaks and troughs of the oscillometric pulses is trivial, finding the correct location of the OMW zero-crossings is challenging as it is very sensitive to the filtering technique used to extract the oscillometric pulses from the cuff deflation curve. This makes the proposed PTT-based MAP estimation technique somewhat unreliable.

In [79], it was empirically found that the PTT measured as the time interval between the ECG R-Peaks and the maximum slope points of the oscillometric pulses exhibits a maximum at a cuff pressure close to MAP. However, since the focus of that work was on developing hardware, software, and algorithms for ECG-assisted BP estimation, no theoretical foundation of the PTT analysis was developed. Moreover, the sensitivity of the MAP estimates to cardiovascular system parameters was not studied. The advantage of using the oscillometric maximum slope points instead of the zero-crossings in computation of PTT is that the maximum slope points can be detected more accurately, directly from the cuff deflation curve using a simple differential operator.

In this section, we derive a new mathematical model for the PTT computed as the time interval between the ECG R-peaks and the maximum slope points on the oscillometric pulses. Based on the developed model, we show that the MAP can be approximated as the cuff pressure at which the computed PTT attains a maximum. We will then study the sensitivity of the MAP estimates to changes in various cardiovascular parameters including the ABP pulse and the arterial lumen area parameters

5.4.1 Maximum Slope Pulse Transit Time Model

Equation (5.4) represents the general PTT model for any point on the arterial pressure pulse. Therefore, in order to find the PTT model corresponding to the maximum slope points of the oscillometric pulses, the general arterial pressure model $p_a(t)$ in equation

(5.4)) should be replaced by the arterial pressure values (represented by $p_{am}(t)$ hereafter) at which the oscillometric pulses exhibit the maximum slope. It has been shown that the oscillometric pulses are proportional to the oscillations of the ALA segment underneath the cuff [17]. Therefore, the arterial pressure values $p_{am}(t)$ corresponding to the the maximum slope points of the oscillometric pulses can be found as the solution to $\partial^2 A_c(t)/\partial t^2 = 0$ which can be formulated as follows:

$$p_{am}(t) = \begin{cases} P_{a1} & \text{for } p_c(t) \leq P_{a1} \\ p_c(t) & \text{for } P_{a1} < p_c(t) \leq P_{a2} \\ P_{a2} & \text{for } p_c(t) > P_{a2} \end{cases} \tag{5.27}$$

where P_{a1} and P_{a2} are obtained as the solution to the following equations, respectively:

$$-b\left(\partial p_a(t)/\partial t\right)^2 + \partial^2 p_a(t)/\partial t^2 = 0 \tag{5.28}$$

$$a\left(\partial p_a(t)/\partial t\right)^2 + \partial^2 p_a(t)/\partial t^2 = 0 \tag{5.29}$$

with $p_a(t)$ given in equation (4.1).

Now, by substitution of equations (5.7)-(5.10) and (5.27) in equation (5.4) and simplification, the PTT computed from maximum slope points on the oscillometric pulses, $\tau_{ms}(t)$, is obtained as follows:

$$\tau_{ms}(t) = \tau_{msa}(t) + \tau_{msc}(t) \tag{5.30}$$

where

$$\tau_{msa}(t) = \begin{cases} T_a(P_{a1}) & \text{for } p_c(t) \leq P_{a1} \\ T_a(p_c(t)) & \text{for } P_{a1} < p_c(t) \leq P_{a2} \\ T_a(P_{a2}) & \text{for } p_c(t) > P_{a2} \end{cases} \tag{5.31}$$

$$\tau_{msc}(t) = \begin{cases} T_{c1}(P_{a1} - p_c(t)) & \text{for } p_c(t) \leq P_{a1} \\ T_{c1}(0) & \text{for } P_{a1} < p_c(t) \leq P_{a2} \\ T_{c2}(P_{a2} - p_c(t)) & \text{for } p_c(t) > P_{a2} \end{cases} \tag{5.32}$$

$$T_a(x) = L_a \sqrt{\rho b' \left(\frac{1}{1 - \frac{A'_m - A'_0}{A'_m} e^{-b'x}} - 1 \right)} \tag{5.33}$$

$$T_{c1}(x) = L_c \sqrt{\rho a \left(1 - \frac{1}{1 + \frac{A_0}{A_c} e^{ax}} \right)} \tag{5.34}$$

$$T_{c2}(x) = L_c \sqrt{\rho b \left(\frac{1}{1 - \frac{A_m - A_0}{A_m + A_c} e^{-bx}} - 1 \right)} \tag{5.35}$$

From equations (5.31) and (5.33) it is observed that $\tau_{msa}(t)$ has a flat maximum for cuff pressures less than P_{a1}, as shown in Fig. 5.5(a). From equations (5.32), (5.34) and (5.35) it is observed that $\tau_{msc}(t)$ exhibits a flat maximum for cuff pressures between P_{a1} and P_{a2}, as shown in Fig. 5.5(b). Therefore, according to equation (5.30), $\tau_{ms}(t)$ attains a maximum at cuff pressure equal to P_{a1}, as is shown in Fig. 5.5(c). From Fig. 5.5, it is

observed that $\tau_{ms}(t)$ maximum occurs at a cuff pressure very close to MAP (2.30 mmHg difference). Therefore, MAP can be approximated as the cuff pressure at which $\tau_{ms}(t)$ attains a maximum, or in other words at cuff pressure equal to P_{a1}.

For the simulation of Fig. 5.5, a simplified model of the ABP pulse proposed in [17] was adopted. The ABP pulse model is given by:

$$p_a(t) = MAP + \alpha_1 \cos(2\pi f_c t) + \alpha_2 \cos(4\pi f_c t + \phi) \tag{5.36}$$

where two harmonics of the cardiac signal were considered to be adequate as they carry most of the signal power [17]. In this model, f_c is the cardiac rate, α_1 and α_2 represent the amplitude of the first and second harmonics of the cardiac signal, respectively, and ϕ is the phase difference between the the two harmonics. Typical values of the cardiovascular parameters in human artery were used in this simulation [17, 23]; where $a = 0.09$ mmHg^{-1}, $b = 0.03$ mmHg^{-1}, $A_0 = 0.1$ cm^2, $A_m = 0.4$ cm^2, $MAP = 95$ mmHg, $f_c = 75$ beats/min, $\alpha_{1,1} = 0$ mmHg, $\alpha_{2,1} = 10$ mmHg, $\alpha_{1,2} = -8.39$ mmHg, $\alpha_{2,2} = 3.28$ mmHg.

According to equations (5.28) and (5.36), P_{a1} is a function of arterial compliance index b and the ABP pulse parameters α_1, α_2, and ϕ. As a result, MAP estimation results could be affected as these parameters vary between different health conditions, age groups, etc. A parametric sensitivity analysis was performed to reveal the accuracy of MAP estimation results as parameters b, α_1, α_2, and ϕ change by $\pm 50\%$ around their typical values in human brachial artery with α_2 set to 0.7 of α_1 [17, 23]. It was observed that the MAP estimation error gradually increases as the cardiovascular parameter values increase from their typical values. However, the absolute error was always less than 5 mmHg, which meets the international standard requirement for automatic noninvasive BP devices [37]. Therefore, the cuff pressure at which $\tau_{ms}(t)$ attains a maximum could be used as an accurate approximation of the MAP.

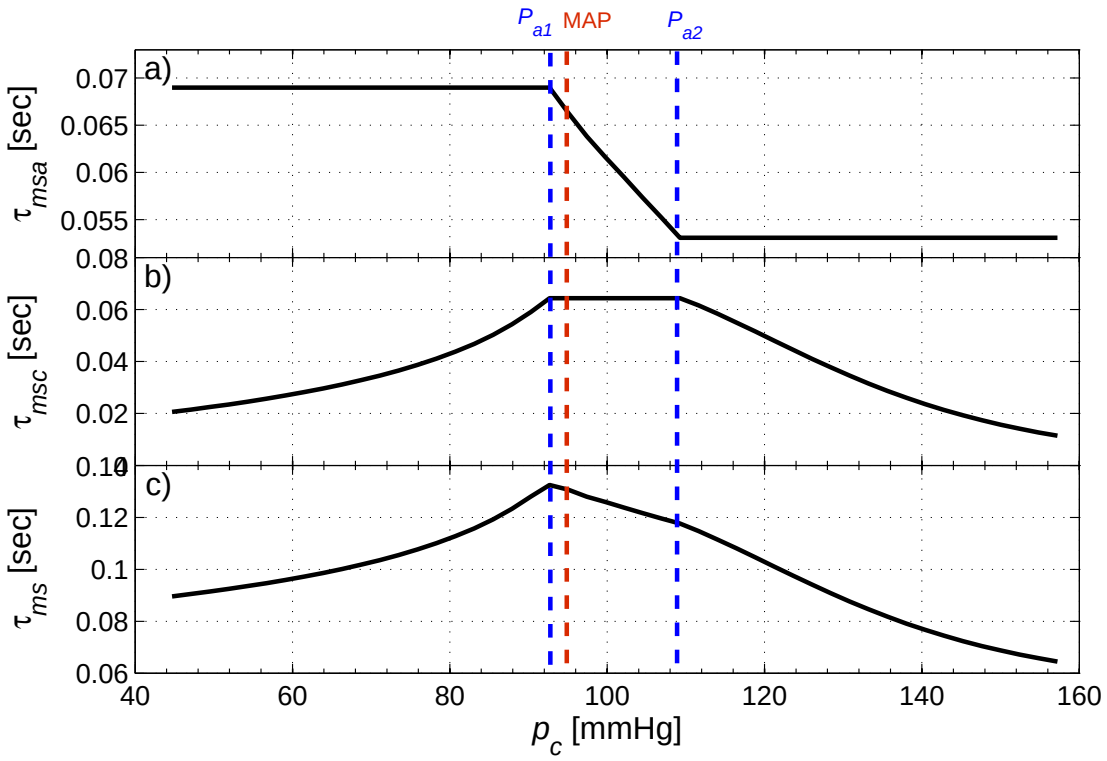

Figure 5.5: Simulated PTT computed from maximum slope points on the oscillometric pulses. (a) The PTT from the heart to the brachial artery (τ_{msa}), (b) the PTT along the brachial artery underneath the cuff (τ_{msc}), and (c) the total PTT (τ_{ms}). The vertical dashed lines from left to right show the points at which cuff pressure is equal to P_{a1}, MAP, and P_{a2}, respectively.

5.5 Experimental Results

As an initial validation of our proposed method, it was tested on real-world data collected by our research group [79]. This dataset comprised 150 simultaneous oscillometric BP and ECG recordings acquired with a prototype designed in our research laboratory [79]. The dataset is fully described in Appendix A.2.

5.5.1 Oscillometric Waveform Detection

As explained in Section 5.3, our proposed BP estimation method is based on measuring the time interval between the ECG R-peaks and the peaks, troughs, and zeros of the

OMW. Therefore, detection of the correct location of peaks, troughs and zeros of the OMW is of great importance.

Detecting the Peaks, Troughs, and Maximum Slope Points

In order to find the peaks, troughs, and maximum slope points of the OMW, an ECG-based detrending approach was utilized [79]. The R-peaks of the ECG signal were first found using the MIT/PhysioNET MATLAB QRS onset detector software [167]. Figure 5.6(a) shows a sample ECG signal that was collected with our prototype with the detected R-peaks marked in dots. The deflation curve values corresponding to the detected R-peaks were then interpolated to form a detrended cuff pressure signal. Figure 5.6(b) illustrates the recorded cuff deflation curve in solid black line. The detrended cuff pressure signal using the ECG-based technique described above is plotted in dashed light gray line (visible in inset). The OMW was found by subtracting the detrended cuff pressure signal from the recorded cuff deflation curve, as shown in Fig. 5.6(c). The peaks, troughs, and maximum slope points of the OMW were detected with the help of ECG R-peaks. The oscillometric peaks and troughs were determined as the maximum and the minimum of the extracted OMW between each two consecutive R-peaks, respectively. The detected peaks and troughs of the OMW are shown with upward and downward triangles in Fig. 5.6(c). The oscillometric maximum slope points were determined as the maximum of the derivative of the extracted OMW between each two consecutive trough and peak. The detected maximum slope points of the OMW are shown with squares in Fig. 5.6(c). Unlike high-pass filtering techniques [17, 19] that can alter the peaks, troughs, and maximum slope points locations depending on the filter parameters, the utilized ECG-based method can find the exact location of the OMW peaks and troughs without any approximation.

Detecting the Zero-Crossings

Although the ECG-based OMW detection method is very accurate in determining the location of the peaks, troughs, and maximum slope points, it cannot completely remove the slow-varying component of the cuff deflation curve, and therefore it introduces some bias to the oscillometric pulses. This, makes it challenging to find the correct location of the OMW zero-crossings. Therefore, in order to detect the zeros of the OMW, we adopt a filtering approach. In this method, we find the detrended cuff pressure waveform by applying a low-pass filter on the recorded cuff deflation curve. The detrended cuff pressure signal is then subtracted from the deflation curve to form the OMW. The detrended cuff pressure signal is plotted in dashdot dark gray line in Fig. 5.6(b) and is visible in the inset. Figure 5.6(d) depicts the OMW obtained by subtracting the detrended signal from the cuff deflation curve. The zeros are marked as squares in the figure.

5.5.2 Pulse Transit Time Detection

$\tau_p(t)$, $\tau_t(t)$, $\tau_z(t)$, and $\tau_{ms}(t)$ were measured as the time interval between the ECG R-peaks and the peaks, troughs, zeros, and maximum slope points of the OMW, respectively. The calculated $\tau_p(t)$, $\tau_t(t)$, $\tau_z(t)$, and $\tau_{ms}(t)$ are plotted in grey lines in Figs. 5.7(a-d), respectively. Since the calculated PTTs are very noisy, several steps were performed before determining their true maximum, as follows:

Outlier Removal

An outlier removal technique was applied to remove the PTT samples that appear to be inconsistent with the remainder of the signal. The adopted outlier removal technique was based on fitting a quadratic polynomial function to the PTT waveforms. An outlier was defined as a value that is more than three standard deviations away from the quadratic polynomial fit [168]. The outliers were then removed and this procedure was repeated

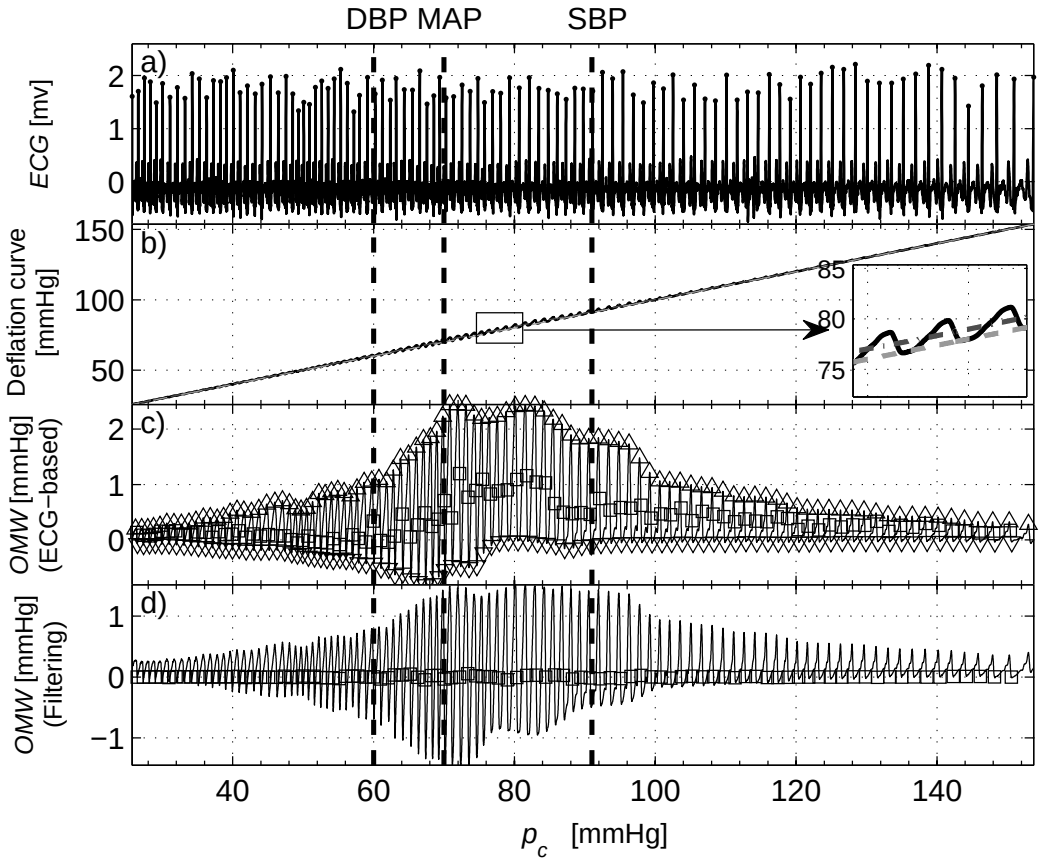

Figure 5.6: Example of oscillometric waveform (OMW) detection. (a) A Real electrocardiogram (ECG) signal. (b) Recorded cuff deflation curve (simultaneous with the ECG). The detrended cuff pressure signals using the ECG-based method and the filtering technique are depicted in dashed and dashdot lines in the same figure, respectively, which can be seen more clearly in the inset. (c) OMW obtained using the ECG-based method. The peaks, troughs, and maximum slope points are shown in upward triangles, downward triangles, and squares, respectively. (d) OMW obtained through filtering. The zeros of the OMW are shown as squares.

until no more outliers were detected.

Smoothing

The PTTs were first smoothed using a moving average filter. Afterwards, a cubic smoothing spline function was fitted to the smoothed signal to remove any remaining artifacts. Since $\tau_t(t)$ exhibited the most fluctuations, a 9-point moving average filter and a spline

function with smoothing parameter 0.01 were used to smooth the signal. On the other hand, $\tau_p(t)$ exhibited the least fluctuations around its peak, and therefore it was smoothed using a 3-point moving average filter and a spline function with smoothing parameter 0.2. $\tau_z(t)$ was smoothed using a 7-point moving average filter and a spline function with smoothing parameter 0.02. The filter parameters used in this study were chosen empirically.

Maximum Detection

The smoothed PTTs were linearly interpolated and resampled at 5 Hz. In order to avoid any remaining noise and artifacts, the search region for maximum was limited. For detection of $\tau_z(t)$ and $\tau_{ms}(t)$ maximums, the search was performed from $p_c(t) = 55$ mmHg to $p_c(t) = 140$ mmHg. For detection of $\tau_p(t)$ maximum, the search was performed from $p_c(t) = (MAP + 12)$ mmHg to $p_c(t) = 150$ mmHg. For detection of $\tau_t(t)$ maximum, the search was performed from $p_c(t) = 50$ mmHg to $p_c(t) = (MAP - 5)$ mmHg. MAP was estimated as the cuff pressure at which OMWE has a maximum. These limits were preliminary choices based on the available data.

The resulting $\tau_p(t)$, $\tau_t(t)$, $\tau_z(t)$, and $\tau_{ms}(t)$ after outlier removal and smoothing are depicted in solid black lines in Figs. 5.7(a-d), respectively. The smoothed PTTs are only plotted in the limited interval where the search for the maximum is performed. Note that the PTTs depicted in Figs. 5.7(a-d) are consistent with those computed theoretically (shown in Figs. 5.3 and 5.5).

5.5.3 Results and Discussion

The performance of our proposed BP estimation method was tested on the whole recorded dataset introduced in Appendix A.2. This dataset comprised 150 oscillometric BP recordings acquired with a prototype designed in our research laboratory [79]. The estimation results were compared with the FDA-approved Omron oscillometric BP monitor (HEM-790IT) as the reference. The performance was analyzed in terms of ME, MAE, and

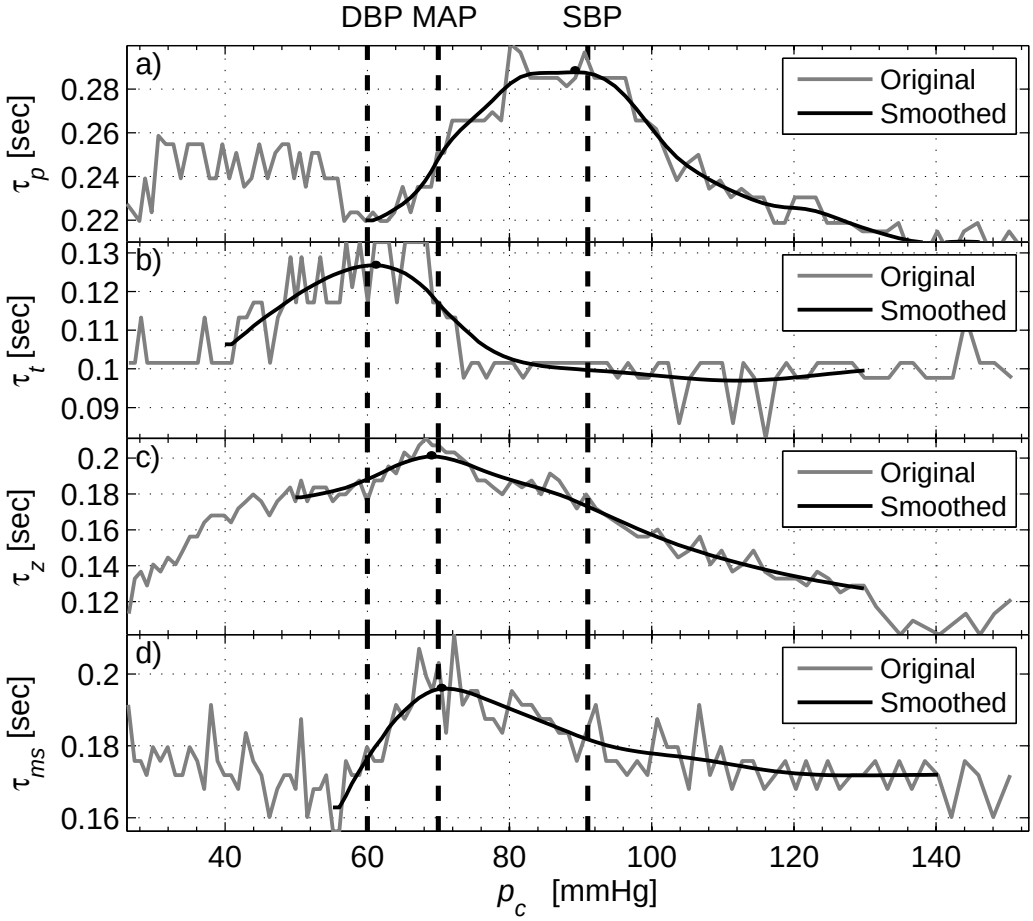

Figure 5.7: Example of detected pulse transit time (PTT). (a-d) PTT computed as the time interval between the ECG R-peaks and the peaks, troughs, zeros, and maximum slope points of the OMW, respectively. All the waveforms are plotted as a function of cuff pressure p_c. The vertical dashed lines from left to right show the points at which cuff pressure is equal to DBP, MAP, and SBP, respectively.

SDE.

Table 5.1 summarizes the values of ME, MAE, and SDE for our proposed coefficient-free BP estimation method obtained on the dataset of 150 recordings. It is observed that the ME of our proposed method in estimating systolic and diastolic pressures is within 3.09 mmHg relative to the Omron device, the SDE of our proposed method in estimating systolic and diastolic pressures is within 5.81 mmHg relative to the Omron device, and the MAE of our proposed method in estimating systolic and diastolic pressures is within

Table 5.1: Mean error (ME), mean absolute error (MAE), and standard deviation of error (SDE) of the coefficient-free BP estimates using pulse transit time analysis on the dataset of 150 recordings. The columns from left to right show the coefficient-free SBP, DBP, MAP (using zero-crossings), and MAP (using maximum slope points) estimation errors using our proposed PTT-based method.

	SBP	DBP	MAP-ZC	MAP-MS
ME [mmHg]	-3.09	-2.39	-5.31	3.27
MAE [mmHg]	5.31	4.51	5.74	4.12
SDE [mmHg]	5.81	5.78	4.30	5.25

5.31 mmHg relative to the Omron device. Comparing the PTT-based method's MAP estimates, it is found that the maximum slope approach achieves improved results in terms of ME (2.04 mmHg improvement) and MAE (1.62 mmHg improvement) relative to the zero-crossing approach. However, the zero-crossing method achieves smaller SDE.

In order to further analyze the agreement between our proposed method and the Omron monitor, we performed Bland-Altman analysis [106, 107]. Figure 5.8 shows the Bland-Altman plots of the SBP, DBP, and MAP estimates for our proposed method versus Omron monitor. The x-axis of the plots show the average of our proposed method and the Omron monitor, while the y-axis shows the difference between the two methods. The bias (ME) and the limits of agreement (ME $\pm$ 1.96 $\times$ SDE) are shown in dashed and dotted lines, respectively. From Fig. 5.8(a), it is observed that our method slightly overestimates the SBP at pressures approximately under 90 mmHg compared to the Omron monitor. From Fig. 5.8(b), it is observed that our method slightly overestimates the DBP at pressures approximately above 70 mmHg and underestimates the DBP at pressures approximately under 60 mmHg compared to the Omron monitor. From Fig. 5.8(c), it is observed that our proposed zero-crossing method underestimates the MAP at pressure under 65 mmHg compared to the Omron monitor. However, in total, the errors are almost evenly distributed over the measured pressure range. That is, the BP estimates made by our proposed methods are in close agreement with those made by the Omron device.

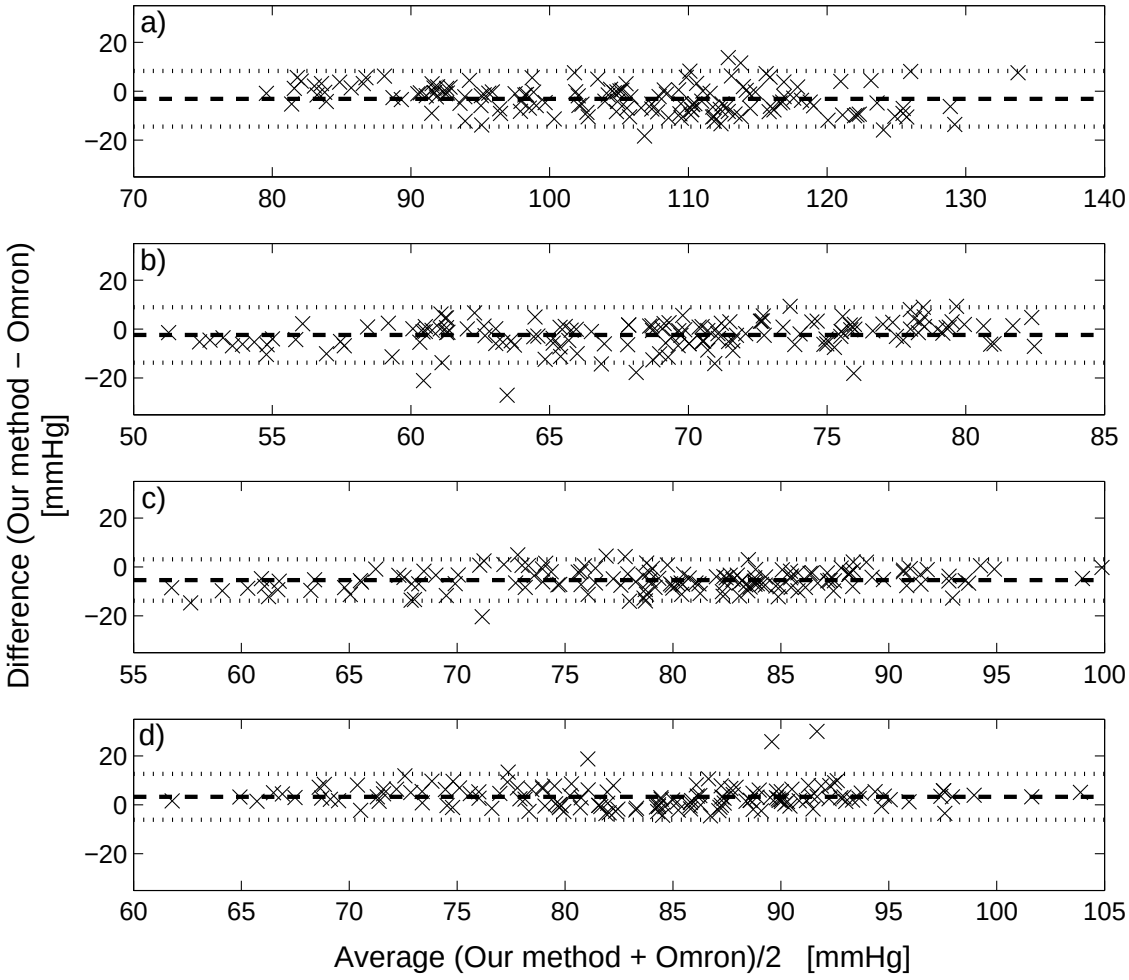

Figure 5.8: Bland-Altman plot of the (a) SBP, (b) DBP, (c) MAP (using the zero-crossings), and (d) MAP (using the maximum slope points) estimates for our proposed method versus Omron monitor. The horizontal dotted lines show the limits of agreement (mean error $\pm$ 1.96 $\times$ standard deviation of error), while the horizontal dashed line shows the bias.

5.6 Conclusion

We presented a comprehensive theory and developed a model for the dependence of PTT on cuff pressure within an oscillometric BP measurement framework. Through this model, we analytically showed that SBP, DBP, and MAP can be accurately esti-

mated from PTT-cuff pressure mappings without using empirical coefficients. Finally, we cross-validated our findings on 150 recordings (oscillometric and ECG) from ten healthy subjects and compared results with the FDA-approved Omron monitor. The theoretical model and the empirical results conformed well to the reference measurements. For comparison with the Omron device, the method achieved an MAE of 5.31 mmHg for SBP, 4.51 mmHg for DBP, and 4.12 mmHg for MAP.

In this study, we assumed that the various parameters inside our model do not change with cuff deflation during a measurement. We understand that for certain patient populations and disease states, such as atrial fibrilation, the PTT model parameters may well change during a measurement which may be as short as 30-45 seconds. Therefore, future work will focus on models that incorporate the time variability of these parameters.

Chapter 6

Discussion [1]

In Chapters 3-5, a comprehensive model of oscillometry was developed and the fundamental relationship between the BP and the oscillometric and electrocardiogram recordings was formulated. Based on the developed models, novel methods were proposed that are capable of estimating the BP without the need for any empirical coefficients. In this chapter, we compare the proposed methods in Chapters 3-5, discuss their particular applications and limitations, and propose a fusion algorithm that combines these methods to obtain more robust and accurate estimate of BP.

6.1 Comparison and Applications

The performance of our proposed oscillometric BP estimation methods was evaluated on the dataset of 150 simultaneous oscillometric BP and ECG recordings acquired with a prototype designed in our research laboratory (See Appendix A.2). These methods include: i) the feature-based NN described in Chapter 3, ii) the OMW modeling method described in Chapter 4, and iii) the PTT-cuff pressure dependence modeling/analysis

[1] Parts of this chapter have been published in:

1. M. Forouzanfar, H. R. Dajani, V. Z. Groza, and M. Bolic, , "Model-based oscillometric blood pressure estimation," *IEEE Int. Symp. Medical Measurements and Applications (MeMeA'14)*, Lisbon, Portugal, May 2014, in press.

Table 6.1: Comparison of different methods in estimation of systolic blood pressure (SBP) on the dataset of 150 recordings.

SBP	Feature-based NN	OMW Modeling	PTT Analysis	Fusion (Mean)	Fusion (Weighted Mean)
ME (mmHg)	0.47	0.04	-3.09	-0.94	-1.20
MAE (mmHg)	6.31	4.60	5.31	4.45	4.40
SDE (mmHg)	7.54	5.84	5.81	5.40	5.30

described in Chapter 5. The estimation results were compared with the FDA-approved Omron oscillometric BP monitor (HEM-790IT) as the reference. The performance was analyzed in terms of ME, MAE, and SDE.

Tables 6.1 and 6.2 summarize the SBP and DBP estimation errors of the three proposed methods in terms of ME, MAE, and SDE. It is found that the OMW modeling and PTT analysis methods achieve close estimation results in terms of MAE and SDE. However, the PTT analysis is slightly biased with ME of -3.09 mmHg in estimation of SBP and -2.39 mmHg in estimation of DBP. On the other hand, the feature-based NN achieves the best DBP estimation results with ME of 0.40 mmHg, MAE of 3.31 mmHg, and SDE of 4.08 mmHg. However, the MAE and SDE of the feature-based NN in estimation of SBP is more than 1 mmHg higher than the other two methods. Table 6.3 summarizes the MAP estimation errors of the two proposed PTT analysis methods in terms of ME, MAE, and SDE. It is found that the PTT analysis using the maximum slope points on the oscillometric pulses achieves 2.04 mmHg improvement in terms of ME and 1.62 mmHg improvement in terms of MAE relative to the PTT analysis using the zero-crossings of the oscillometric pulses. However, PTT analysis using the zero-crossings achieves smaller SDE.

In order to further analyze the performance of the proposed oscillometric methods versus the FDA-approved Omron monitor (HEM-790IT), Bland-Altman analysis was

Table 6.2: Comparison of different methods in estimation of diastolic blood pressure (DBP) on the dataset of 150 recordings.

DBP	Feature-based NN	OMW Modeling	PTT Analysis	Fusion (Mean)	Fusion (Weighted Mean)
ME (mmHg)	0.40	-1.75	-2.39	-1.25	-0.83
MAE (mmHg)	3.31	4.53	4.51	3.09	3.00
SDE (mmHg)	4.08	5.97	5.78	3.84	3.70

performed [106, 107]. Bland-Altman plots of the SBP, DBP, and MAP estimates for our proposed methods versus the Omron monitor are shown in Figs. 6.1-6.3, respectively. The x-axis of the plots shows the average of our proposed methods and the Omron monitor, while the y-axis shows the difference between the two methods. The bias (ME) and the limits of agreement (ME $\pm$ 1.96 $\times$ SDE) are shown in dashed and dotted lines, respectively. Compared to the Omron monitor, it is observed that: for the feature-based NN, there is a slight underestimation of SBP at pressures above 120 mmHg and overestimation of DBP at pressures under 60 mmHg, for the OMW modeling method, there is a slight overestimation of SBP and DBP at pressures under 90 mmHg and 60 mmHg, respectively, and for the PTT analysis, there is a slight overestimation of SBP at pressures under 90 mmHg and underestimation of DBP at pressures under 70 mmHg. It is also observed that the zero-crossing method slightly underestimates the MAP at pressure under 65 mmHg compared to the Omron monitor. The maximum slope method does not show any obvious unevenness over the measured pressure range compared to the Omron monitor. In total, the errors for all the methods are almost evenly distributed over the measured pressure range. These results prove that the BP estimates made by our proposed methods are in close agreement with those made by the Omron device.

The proposed feature-based NN can be used to learn from multiple measurements obtained from the same subject taken over a period of time. Therefore, the feature-based

Table 6.3: Comparison of different methods in estimation of mean arterial pressure (MAP) on the dataset of 150 recordings.

MAP	PTT Analysis (Zero-crossings)	PTT Analysis (Maximum slope points)	Fusion (Mean)	Fusion (Weighted Mean)
ME (mmHg)	-5.31	3.27	-1.04	-1.50
MAE (mmHg)	5.74	4.12	3.05	3.21
SDE (mmHg)	4.30	5.25	3.78	3.76

NN can be customized for any particular patient if enough training data is provided. Even though the featured-based NN estimation results are promising, its usage is limited to particular applications. First, the NN has a black box structure that implicitly models the relationship between the BP and the OMWE. Once the network recognizes a given input pattern (OMWE features), it predicts an output pattern (BP value) corresponding to the given input. However, it is very difficult to explicitly describe the meaning of weights at the nodes of the NN. Therefore, in applications where an explicit relationship between the oscillometric recordings and the BP is required (such as sensitivity analysis of BP estimates to the change in cardiovascular parameters) the use of NN is limited. Second, once the NN has been trained, it is not possible to incorporate additional knowledge such as new data or system settings into the network without repeating the whole training process. Third, NNs require a large training dataset representative of all the target patient populations, since the NN can only perform well in various patient populations if the training dataset contains a uniform distribution of all those populations. However, collecting a large dataset is expensive and time consuming, and finding a sufficient number of volunteers in all the target patient populations is not always trivial.

Our proposed NN approach is based on extracting features from the OMWE and using the extracted features to estimate the BP. Therefore, just as with many other oscillometric algorithms, the useful information contained in the oscillometric pulses was

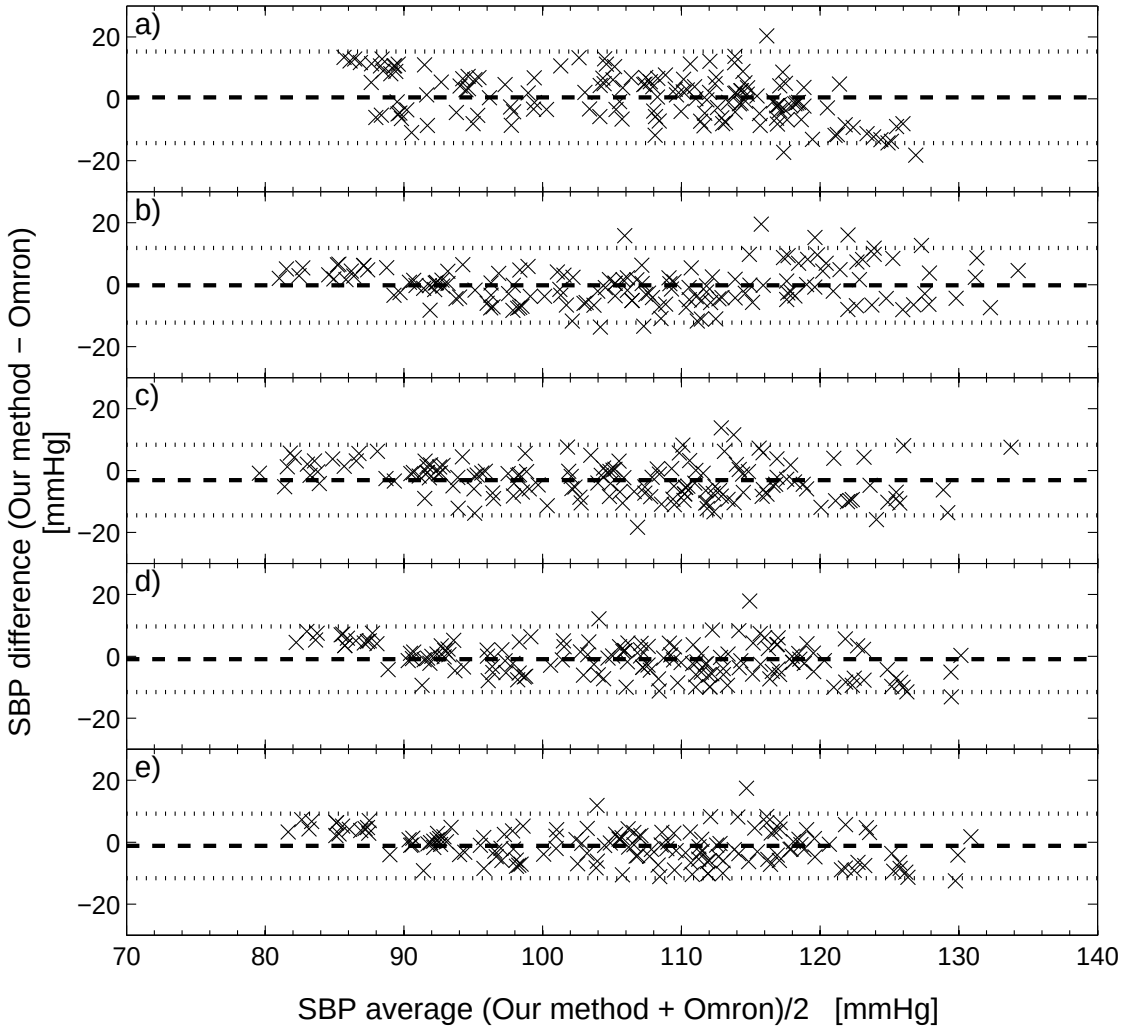

Figure 6.1: Bland-Altman plot of the SBP estimates for our proposed methods versus Omron monitor. (a) Feature-based NN. (b) OMW modeling. (c) PTT analysis. (d) Fusion using unweighted mean. (e) Fusion using weighted mean. The horizontal dotted lines show the limits of agreement, while the horizontal dashed line shows the bias.

not considered. In contrast, the OMW modeling method incorporates existing models of the arterial blood pressure (ABP) pulse waveform and the arterial pressure-area relationship along with the occlusive cuff mechanics to obtain an explicit model between the oscillometric recordings and the BP. The SBP and DBP are estimated by minimizing the

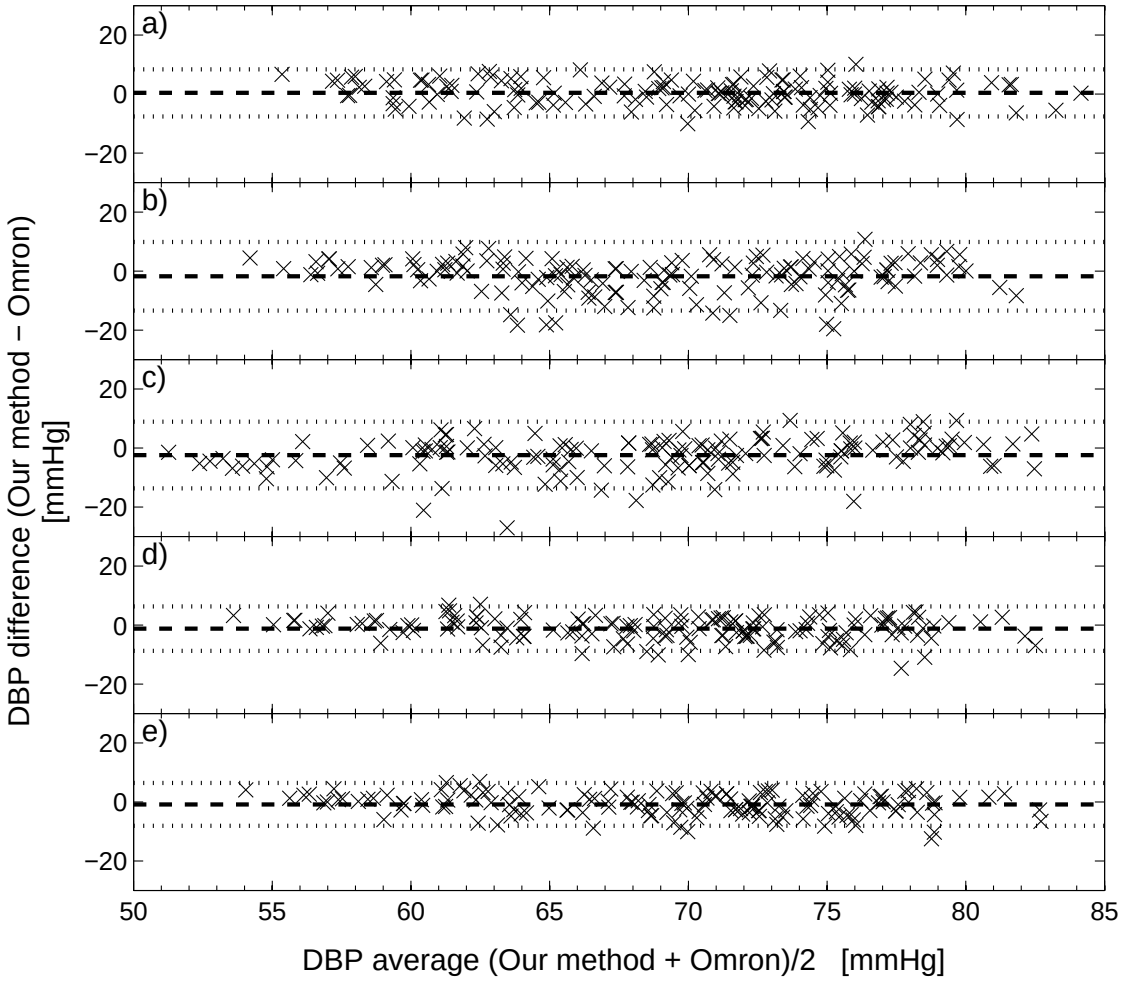

Figure 6.2: Bland-Altman plot of the DBP estimates for our proposed methods versus Omron monitor. (a) Feature-based NN. (b) OMW modeling. (c) PTT analysis. (d) Fusion using unweighted mean. (e) Fusion using weighted mean. The horizontal dotted lines show the limits of agreement, while the horizontal dashed line shows the bias.

sum of the squares of the differences between the extracted OMWE and the developed model. The the OMW modeling method does not require a training dataset and is only based on analysing the oscillometric recordings, therefore it can be used in almost any application. Since the proposed OMW model is a function of the ABP and cuff-arm-artery system parameters, it can be used to study the effects of different cardiovascular

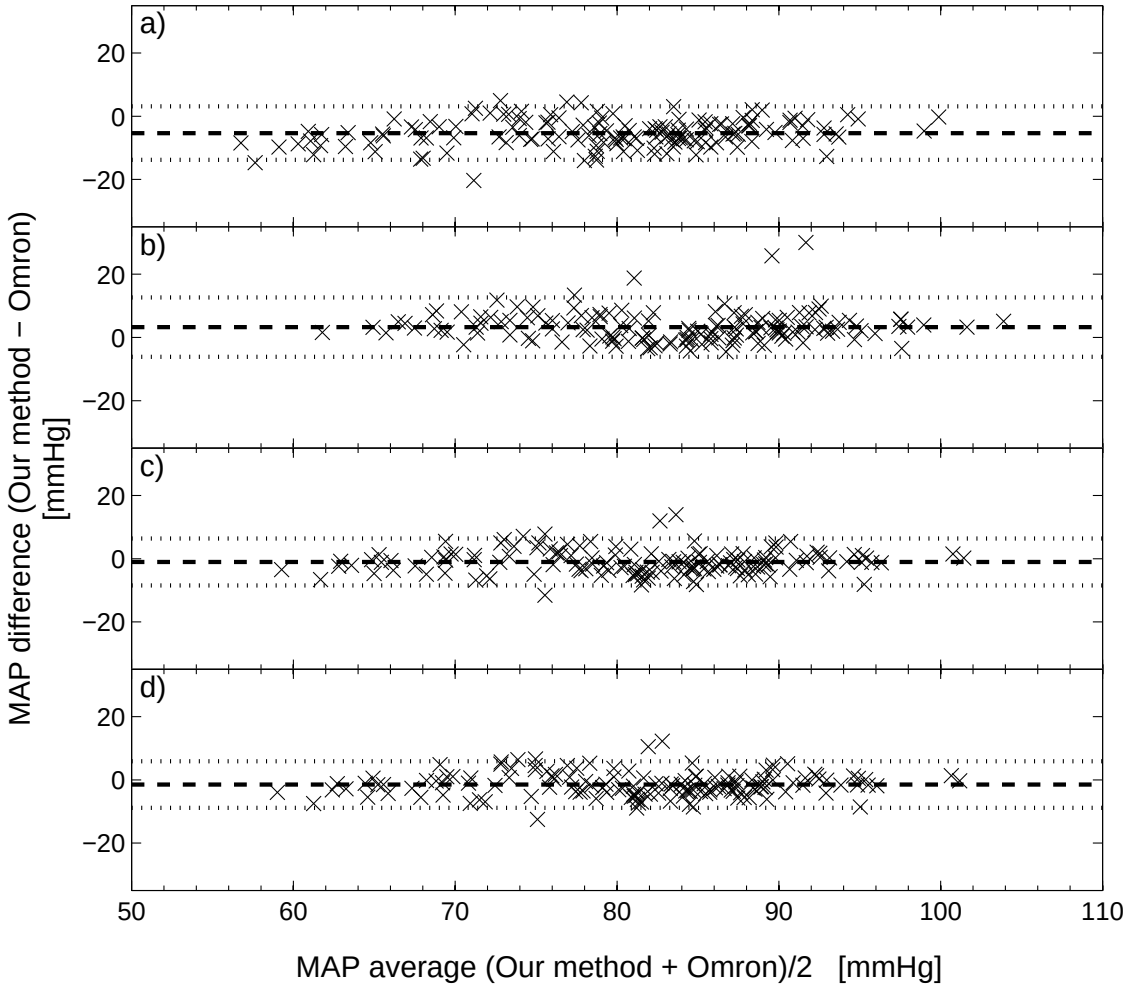

Figure 6.3: Bland-Altman plot of the MAP estimates for our proposed methods versus Omron monitor. (a) PTT analysis using zero-crossings of the oscillometric pulses. (b) PTT analysis using maximum slope points on the oscillometric pulses. (c) Fusion using unweighted mean. (d) Fusion using weighted mean. The horizontal dotted lines show the limits of agreement, while the horizontal dashed line shows the bias.

system parameters on the accuracy of BP estimate. It can be also used to estimate arterial stiffness in oscillometry. Moreover, given the time variability of the cardiovascular parameters, through appropriate modifications to the proposed OMW model, the time varying cardiovascular system parameters including the SBP and DBP can be estimated,

tracked, and predicted and the BP variability over time can be studied. The main drawback of the OMW modeling method is that the optimization problem in equation (4.21) may converge toward local minima due to the number of unknown parameters of our model presented in equation (4.20).

The OMW is the only signal acquired in conventional oscillometry, and therefore it is the only source of information available for estimation of BP. If the recorded oscillometric pulse amplitudes are affected by noise and artifacts (such as due to muscle contractions, movements, etc.), or are weak and erratic (such as due to atrial fibrillation, obesity, atherosclerosis, etc.), the OMW modeling method may fail to provide accurate estimates of BP. The PTT analysis method overcomes this drawback by the use of the higher fidelity ECG signal measured simultaneously along with the OMW. The ECG signal improves the detection of the true oscillometric pulses and enables the measurement of PTT. In the PTT analysis method, the BP is easily estimated as the cuff pressure at which the PTT is maximum, and therefore it does not rely on any optimization approach or a training dataset. Unlike the feature-based NN approach described earlier, the proposed PTT analysis method provides an explicit relationship between the BP and the OMW and ECG signals. This was accomplished by the development of a new mathematical model that describes the behaviour of PTT computed as the time interval between the ECG R-peaks and certain points on the oscillometric pulses. Since the proposed PTT model is a function of the ABP and arterial vessel parameters, it can be used to estimate arterial stiffness. The main problem in estimating the BP from the PTT was that the PTT signals were very noisy. Therefore, it was somehow difficult to find the true maxima of the PTT signals. This problem was addressed by preforming several noise reduction steps before determining the PTT true maximum.

It should be also noted that unlike the conventional model-based oscillometric BP estimation methods [14,15,17–21], our three proposed model-based methods are independent of any empirical coefficients. Moreover, unlike the model-based methods introduced in [16, 24, 25], our proposed methods do not require pre-estimates of BP using an inde-

Table 6.4: Comparison of our proposed model-based oscillometric blood pressure (BP) estimation methods in terms of their requirements, applications, and limitations.

Method	Requirements	Applications	Limitations
Feature-based NN	–Large training dataset representative of all the target patient populations	–Coefficient-free estimation of BP –Learn from multiple measurements from one subject	–Has a black box structure that implicitly models the relationship between the BP and the oscillometric recordings –Not possible to incorporate additional knowledge such as new data or system settings into the network without repeating the whole training process
OMW Modeling	——	–Coefficient-free estimation of BP –Tracking of the cardiovascular system parameters including SBP, DBP, and MAP –Study the BP variabilty –Sensitivity analysis of BP estimates to different cardiovascular parameters –Estimation of vessel elasticity	–Involves an optimization process that may converge towards local minima due to the number of unknown parameters –Sensitive to weak or erratic oscillometric pulse amplitudes
PTT Analysis	–Simultaneously recorded ECG signal	–Coefficient-free estimation of BP –Estimation of vessel elasticity	–PTT-cuff pressure mappings are very noisy that makes it difficult to find their true maximum

pendent approach.

Table 6.4 compares our three proposed oscillometric BP estimation methods in terms of their requirements, applications, and limitations.

6.2 Fusion Algorithm

In order to obtain more robust and accurate estimates of BP, the three proposed model-based oscillometric BP estimation methods are fused. Two simple fusion algorithms are employed in this section to explore the potential of achieving improved estimation results by combining our three proposed methods.

The first fusion algorithm is based on computing the unweighted arithmetic mean of the three proposed methods' estimates, as follows:

$$SBP_{Mean} = \frac{SBP_{NN} + SBP_{OMW} + SBP_{PTT}}{3} \tag{6.1}$$

$$DBP_{Mean} = \frac{DBP_{NN} + DBP_{OMW} + DBP_{PTT}}{3} \tag{6.2}$$

$$MAP_{Mean} = \frac{MAP_{ZC} + MAP_{MS}}{2} \tag{6.3}$$

where SBP, DBP, and MAP represent the systolic, diastolic, and mean arterial pressures, respectively. The subscripts NN, OMW, PTT, and $Mean$ are used to distinguish between the BP estimates obtained by the feature-based NN, OMW modeling, PTT analysis, and fusion (using the arithmetic mean) methods, respectively. The subscripts ZC, MS are used to distinguish between the MAP estimates obtained by the PTT analysis using zero-crossings and maximum slope points on the oscillometric waveform, respectively.

The second fusion algorithm is based on a weighted arithmetic mean of the three proposed methods' estimates. The weight of each method's estimates is set to the method's standard deviation of error (SDE), as follows:

$$SBP_{WMean} = \frac{SBP_{NN}/\sigma^2_{S,NN} + SBP_{OMW}/\sigma^2_{S,OMW} + SBP_{PTT}/\sigma^2_{S,PTT}}{1/\sigma^2_{S,NN} + 1/\sigma^2_{S,OMW} + 1/\sigma^2_{S,PTT}} \tag{6.4}$$

$$DBP_{WMean} = \frac{DBP_{NN}/\sigma^2_{D,NN} + DBP_{OMW}/\sigma^2_{D,OMW} + DBP_{PTT}/\sigma^2_{D,PTT}}{1/\sigma^2_{D,NN} + 1/\sigma^2_{D,OMW} + 1/\sigma^2_{D,PTT}} \tag{6.5}$$

$$MAP_{WMean} = \frac{MAP_{ZC}/\sigma^2_{M,ZC} + MAP_{MS}/\sigma^2_{M,MS}}{1/\sigma^2_{M,ZC} + 1/\sigma^2_{M,MS}} \tag{6.6}$$

where σ represents the SDE, subscript $WMean$ indicates the fusion algorithm using the weighted arithmetic mean, and subscripts S, D, and M are used to distinguish between the SBP, DBP, and MAP SDEs.

In order to test the performance of our proposed fusion algorithm using the weighted arithmetic mean of the estimates, our dataset of 150 recordings was divided into two sets: training and testing. The SDEs of the three proposed model-based oscillometric methods were obtained on the training data. The obtained SDEs were then used as the corresponding weights for the test data to assess the fusion algorithm's performance. The error obtained on the test data was used as a measure to evaluate the fusion algorithm's performance when new data that was not provided during the training was presented. In our study, one subject (with 15 measurements) was selected for the test, which led to the largest possible set of data for training. The rest of the subjects' data was used for the training. This process was then repeated such that each subject in the dataset was used once for the test.

The last two columns of Tables 6.1-6.3 list the SBP, DBP, and MAP estimation errors of the proposed fusion algorithms. It is found that the two fusion algorithms achieve very close results in estimation of SBP, DBP, and MAP. It is also found that the fusion of the proposed SBP estimation methods results in improvements of up to 1.89 mmHg in ME, 1.91 mmHg in MAE, and 2.24 mmHg in SDE, fusion of the proposed DBP estimation methods results in improvements of up to 1.56 mmHg in ME, 1.53 mmHg in MAE, and 2.27 mmHg in SDE, and fusion of the proposed MAP estimation methods results in improvements of up to 4.27 mmHg in ME, 2.69 mmHg in MAE, and 1.49 mmHg in SDE.

From Figs. 6.1(d)-(e), it is observed that our fusion algorithms slightly overestimates

the SBP at pressures under 90 mmHg compared to the Omron monitor. However, unlike the feature-based NN method, the fusion algorithms do not show any underestimation of SBP at high pressures. From Figs. 6.2(d)-(e), it is observed that our fusion algorithms slightly overestimates the DBP at pressures under 60 mmHg compared to the Omron monitor. From Figs. 6.3(c)-(d), it is observed that our fusion algorithms do not show obvious unevenness in estimation of MAP over the measured pressure range compared to the Omron monitor. In total, the errors for the fusion algorithms are more evenly distributed over the measured pressure range and they have smaller biases and narrower limits of agreements compared to their underlying three model-based methods.

These results confirm the possible potential of achieving robust and accurate estimates of BP by fusing the proposed model-based oscillometric BP estimation methods. As the focus of this thesis was on deriving new models between the BP and the oscillometric recordings and developing new coefficient-free BP estimation methods, only two simple fusion algorithms were proposed and assessed. Future work can involve developing advanced statistical approaches for optimal fusion of the proposed BP estimation methods.

6.3 Limitations of Our Study

Our dataset of 150 oscillometric BP and ECG recordings consists of reference readings obtained by the Omron HEM-790IT BP monitor (See Appendix A.2). We understand that the references could have been either based on the noninvasive auscultatory or the invasive intra-arterial methods. However, it should be noted that the FDA-approved Omron HEM-790IT has gone through rigorous clinical validation according to protocols set forth by the European Society of Hypertension (ESH), Association for the Advancement of Medical Instruments (AAMI), and British Hypertension Society (BHS) [32, 33, 169]. Therefore, for this pilot study, the successful validation of our proposed methods against the Omron monitor is sufficient to support their potential significance and efficacy.

In all comparisons and analysis, the reference MAP was calculated using the common formula $MAP = DBP + 1/3 \times (SBP - DBP)$ [2]. However, this formula has been found to be only valid at normal resting heart rates [170]. Therefore, future work can be directed toward invasive measurements of reference MAP.

Our dataset of 150 oscillometric BP and ECG recordings was collected from a modest cohort of 10 healthy subjects and no patients were included. It should be pointed out that although the number of subjects was 10, to increase the validity of the empirical data, we recorded 15 simultaneous ECG and oscillometric BP signals from every participant (five recordings in three days). This resulted in a substantial dataset of 150 recordings for the pilot investigation. Future work will involve undertaking clinical testing on a larger number of healthy subjects as well as patients, whereby the method will be compared against nurse-recorded auscultatory measurements, and if possible, against invasive measurements.

Our dataset of 150 oscillometric BP and ECG recordings consists of oscillometric measurements that were performed as soon as the reference Omron measurement ended (See Appendix A.2). Also, our dataset of 425 oscillometric wrist measurements consisted of reference and oscillometric measurements that were made one minute apart (See Appendix A.1). This lack of simultaneity of the oscillometric and reference measurements contributes to the error in our estimation due to the intrinsic physiological variability over time. It has been demonstrated that the arterial BP can vary by up to 20 mmHg within around 10 seconds, in normal healthy humans [41]. Therefore, future work can look at simultaneously recorded test and reference data.

Our proposed models of the OMW and PTT in Chapters 4 and 5 were derived using existing models of the ABP and the cuff-arm-artery system. Several assumptions have been made in the derivation of the adopted models that can affect the accuracy of our developed models and the proposed BP estimation methods, and these are summarized as follows: (a) The ABP model adopted in this study is based on the approximation of ABP pulse as a sum of harmonically related sinusoids which does not model the relatively sharp

peaks of the ABP pulse [149]. (b) The cuff-arm-artery system model adopted in this study is based on the approximation of the arterial pressure-area relationship by an exponential shape function [17]. (c) The cuff-arm-artery system model adopted in this study is also based on the assumption that the arm tissue is mostly incompressible [17]. However, these assumptions have been found to be valid through experiments on empirical data in several studies [14–17, 146–151].

We modeled the PTT with two main components: the time it takes for the BP pulse wave to arrive from the heart to the brachial artery under the cuff and the time it takes for the BP pulse wave to travel in the brachial artery underneath the cuff. We understand that the arterial elastic properties may change along the arterial branch, and therefore the PTT model parameters could change at different locations of the artery. However, our model parameters were assumed to be constant and equal to their average value over the corresponding arterial segment. Moreover, the proposed BP estimation method based on PTT analysis was shown to be independent of all the model parameters. Future work can involve validating our proposed coefficient-free BP estimation method using a more detailed model of the PTT.

Chapter 7

Conclusions and Future Work

Blood pressure (BP) is an important indicator of cardiovascular health. High BP increases the risk for heart disease and stroke. Moreover, high BP can cause other problems such as heart failure, kidney disease, and eye pathologies. As a consequence, regular BP monitoring is an essential part of health maintenance, especially in patients with cardiovascular disease.

The use of automated BP monitoring is growing as it does not require much expertise and can be performed by patients several times a day at home. Oscillometry is one of the most common measurement methods used in automated electronic BP monitors. A variety of oscillometric BP algorithms exist in the literature. However, most of these algorithms are without physiological and theoretical foundation. Moreover, most of the existing oscillometric algorithms ignore the wealth of information that is contained in the amplitude and time characteristics of the oscillometric pulses. Among the oscillometric algorithms, the maximum amplitude algorithm (MAA) is the most popular one. In the MAA, the mean arterial pressure (MAP) is estimated as the cuff pressure at which the oscillometric pulses attain maximum amplitude. Fixed empirical coefficients are then used on the oscillometric waveform envelope (OMWE) to find the time points at which the cuff pressure equals to the SBP and DBP. However, it has been shown that these coefficients should be changed as the characteristics of the cardiovascular system vary

between different health conditions, age groups, etc.

This thesis aimed to derive a comprehensive model of oscillometry and find the fundamental relationship between the BP and the oscillometric recordings. Based on the developed models, novel methods were proposed that are capable of estimating the BP without the need for any empirical coefficients. The proposed BP estimation methods were physiologically and/or theoretically supported. A block diagram representation of the proposed methods was shown in Fig. 1.1.

In the first phase of this research, a novel feature-based neural network (NN) approach for estimation of BP from oscillometric measurements was proposed. Unlike previous methods that used the raw OMWE as input to the NN, we used features extracted from the envelope. A new feature extraction technique based on approximating the OMWE with a sum of two Gaussian functions was proposed to derive a small set of features that forms an effective representation of the entire OMWE. The parameters of the Gaussian functions that had the best fit to the OMWE were considered as features. A Feed-forward neural network (FFNN) and an adaptive neuro-fuzzy inference system (ANFIS) were trained to find an implicit model between the SBP/DBP and the extracted features. The networks were trained and tested on a dataset of oscillometric recordings collected from 85 subjects in accordance to the ANSI/AAMI/ISO standard. It was found that the proposed approach achieves lower values of mean error (ME), mean absolute error (MAE) and standard deviation of error (SDE) in the estimation of BP compared to the MAA and the existing NN-based methods. In addition, the proposed approach has the following advantages compared to the existing NN-based methods: lower complexity with respect to the design parameters, smaller training dataset, and lower computational load.

In the second phase of this research, a new physiologically-based mathematical model was developed for the oscillometric waveform (OMW). Existing models of the arterial blood pressure (ABP) pulse waveform and the cuff-arm-artery system were incorporated to derive a model for the arterial lumen area (ALA). The ABP pulse waveform was

modeled as a sum of harmonically related sinusoids and the arterial pressure-area relationship was modeled by considering the arterial collapse and distension. It was shown that the ALA is composed of two main components: the slow-varying component due to the deflating cuff pressure and the oscillations due to the ABP. Since the oscillations of the ALA during the cuff deflation period are proportional to the oscillometric pulses, the difference between the ALA model and its slow-varying component was proposed as the model of the OMW. An explicit mathematical model was then derived between the OMWE and the SBP and DBP. Based on the developed model, a novel coefficient-free BP estimation method was proposed. The proposed method was based on minimizing the least squares error between our model and the OMWE using the trust region reflective algorithm. To validate our proposed method, a pilot study was undertaken on a dataset of oscillometric BP recordings collected by our research group. The dataset comprised 150 recordings acquired from 10 subjects. The successful cross-validation with empirical data confirmed the accuracy of the proposed theoretical model and the BP estimation method.

In order to improve the estimation of BP using oscillometry, the ECG signal was recorded simultaneously along with the OMW using a device prototype which has been designed by our research group. This device consists of a brachial cuff with conductive fabric, a wrist band with conductive fabric, and a control unit that consists of a pressure sensor and hardware/software for simultaneous ECG and oscillometric BP acquisition and analysis. The ECG R-peaks were detected and used to: (i) extract the oscillometric pulses from the recorded cuff deflation curve; and (ii) calculate the pulse transit time (PTT). By combining our developed model of oscillomtery with an existing model of the pulse wave velocity given by the Bramwell and Hill equation, a new mathematical model was derived for the PTT during the cuff deflation. It was analytically shown that the PTT measured as the time interval between the ECG R-peaks and certain points on the oscillometric pulses can be used to estimate the BP. In particular, it was proved that: the PTT measured as the time interval between the ECG R-peaks and the peaks

of the oscillometric pulses attains a maximum at a cuff pressure equal to the SBP; the PTT measured as the time interval between the ECG R-peaks and the troughs of the oscillometric pulses attains a maximum at a cuff pressure equal to the DBP; and the PTT measured as the time interval between the ECG R-peaks and the zero-crossing points of the oscillometric pulses attains a maximum at a cuff pressure equal to the MAP. Since determining the zero-crossings of the oscillometric pulses is not always trivial, an alternative method was also proposed for estimating the MAP. It was shown that the PTT measured as the time interval between the ECG R-peaks and the maximum slope points of the oscillometric pulses also attains a maximum at a cuff pressure very close to the MAP. This was the first study in which a mathematical validation was provided for the theory of BP estimation from PTT-cuff pressure dependence. Moreover, it was the first study to propose a coefficient-free PTT-based BP estimation method within an oscillometric measurement framework. The theoretical model for the PTT-cuff pressure analysis was developed based on earlier works which focused solely on oscillometric BP measurement models. To validate our proposed methods, a pilot study was undertaken on a dataset of simultaneous ECG and oscillometric BP recordings collected by our research group. The dataset comprised 150 recordings acquired from 10 subjects with the device prototype we developed. The successful cross-validation with empirical data confirmed the accuracy of the proposed theoretical models and the BP estimation methods.

Finally, the three proposed model-based oscillometric BP estimation methods were fused by computing the weighted arithmetic mean of their estimates. The proposed fusion algorithm was validated with a pilot study undertaken on a dataset of 150 simultaneous ECG and oscillometric BP recordings collected from 10 subjects. By comparing the fusion algorithm's performance with that of the three proposed model-based methods in terms of ME, MAE, and SDE, it was found that the fusion algorithm achieves more robust and accurate estimates of BP.

Conventionally, OMW is the only signal obtained in oscillometry. The envelope of this signal is usually detected and analyzed to find the systolic, diastolic, and mean

arterial pressures. In this research, we recorded the ECG simultaneously with the OMW as an extra source of information. Therefore, the OMW and the ECG were the input signals considered for the further analysis. The proposed feature-based NN and the OMW modeling method use the OMW as the input signal. The proposed PTT analysis method uses the OMW and ECG signals as inputs. In order to find the fundamental relationship between BP and the recorded signals, a comprehensive modeling approach was employed. Accurate modeling of these signals enabled us to develop and test new coefficient-free oscillometric algorithms for BP estimation.

The following are several relevant directions that can be explored in future work:

- Since our datasets consisted of reference and oscillometric measurements that were not simultaneous, an error of zero is not possible even in principle. Therefore, future work can focus on collecting simultaneous reference and oscillometric measurements and testing the proposed methods on the simultaneous data.

- Our datasets consisted of a non-uniform distribution of the reference BP values, in the sense that most of the subjects' BPs were around normal range. Since neural networks can only perform well if the training dataset is uniformly distributed [121], future work can be directed to the collection of a dataset of oscillometric measurements with a uniform distribution of the reference BP values.

- Future work can also be directed toward testing our proposed methods on different patient populations such as patients with obesity, arterial stiffness, atrial fibrilation, etc.

- Future work can also be directed toward designing networks that would utilize multiple measurements from the same subject taken over a period of time.

- In our study, we only incorporated two intelligent networks: the FFNN and the ANFIS. Future work can incorporate other architectures of the NNs. Future work can

also investigate the application of support vector regression [171] to BP estimation from the OMWE.

- One of the main challenges in training the NNs is the overfitting problem. In our work, we used the early-stopping technique to avoid overfitting. Another possible approach to avoid overfitting that could be incorporated in future work is called regularization [172]. In regularization, the performance function that is usually the mean square of errors is modified by adding the sum of squares of the network weights and biases. The resulting network will a have smoother response and is less likely to overfit.

- In our study, the NN was used to extract BP information from the envelope of the oscillometric pulses. NNs can also be incorporated to extract BP information from the oscillometric pulse morphology in future work.

- In Chapter 4, we assumed the the BP parameters (SBP and DBP) and the cuff-arm-artery parameters do not change with cuff deflation during a measurement. Through appropriate modifications to the proposed OMW model, the time variability of these parameters can be incorporated in the model. The OMW model can then be used to estimate the SBP and DBP values that correspond to any heartbeat, in contrast to the conventional oscillometric method that estimates the SBP and DBP at two random instants in time over the deflation period. Moreover, the proposed approach can be used to estimate, track, and predict the BP variability over time.

- In Chapter 5, we assumed that the various parameters inside our PTT model do not change with cuff deflation during a measurement. We understand that for certain patient populations and disease states, such as atrial fibrillation, these parameters may well change during a measurement which may be as short as 30-45 seconds. Future work will focus on models that incorporate the time variability of these

parameters. For example, to simulate atrial fibrillation, amplitudes and pulse-to-pulse intervals of the arterial pressure pulse waveform can be randomized.

- The effect of respiration on our proposed methods' BP estimates was not studied in this thesis. Future work can involve investigation of the effect of respiration on the accuracy of our proposed methods.

- We have observed that along with PTT, which changes with cuff pressure, the morphology of the individual oscillometric pulses also changes [75]. Our future work will analyze changes in oscillometric pulse morphology with respect to cuff pressure. This method promises to provide a coefficient-free estimate of BP and does not rely on an ECG signal for PTT computation.

- Finally, in this thesis simple fusion algorithms were proposed to explore the potential of achieving improved estimation results by combining our three proposed methods. To obtain a more stable and robust estimation of BP, future work can focus on fusing the proposed BP estimation methods using a more advanced statistical approach.

Appendix A

Datasets

The two datasets that were used to evaluate the performance of the proposed methods in this thesis are described in this Appendix.

A.1 Dataset 1

The first oscillometric waveform dataset was provided by Biosign Technologies Inc. This dataset was acquired using an automated wrist BP monitor (UFIT TEN-10) in accord with the recommendations of the ANSI/AMMI/ISO standard [37]. The dataset included 85 subjects, 48 males and 37 females, aged from 12 to 80. Five sets of oscillometric wrist BP measurements were obtained from each subject resulting in a total of 425 measurements. Following each wrist oscillometric measurement, and after a one-minute delay, two independent simultaneous reference readings were also recorded at the arm level by two nurses using the auscultatory method. A double stethoscope was used for this purpose, as shown in Fig. A.1. The average value of these two measurements was used as the reference pressure of each subject for the corresponding trial. The measurement conditions stipulated by the ANSI/AMMI/ISO standard aim to minimize the intrinsic physiological variability of the BP over time, but still the SBP and DBP may change from the moment of the wrist measurement until the reference measurements

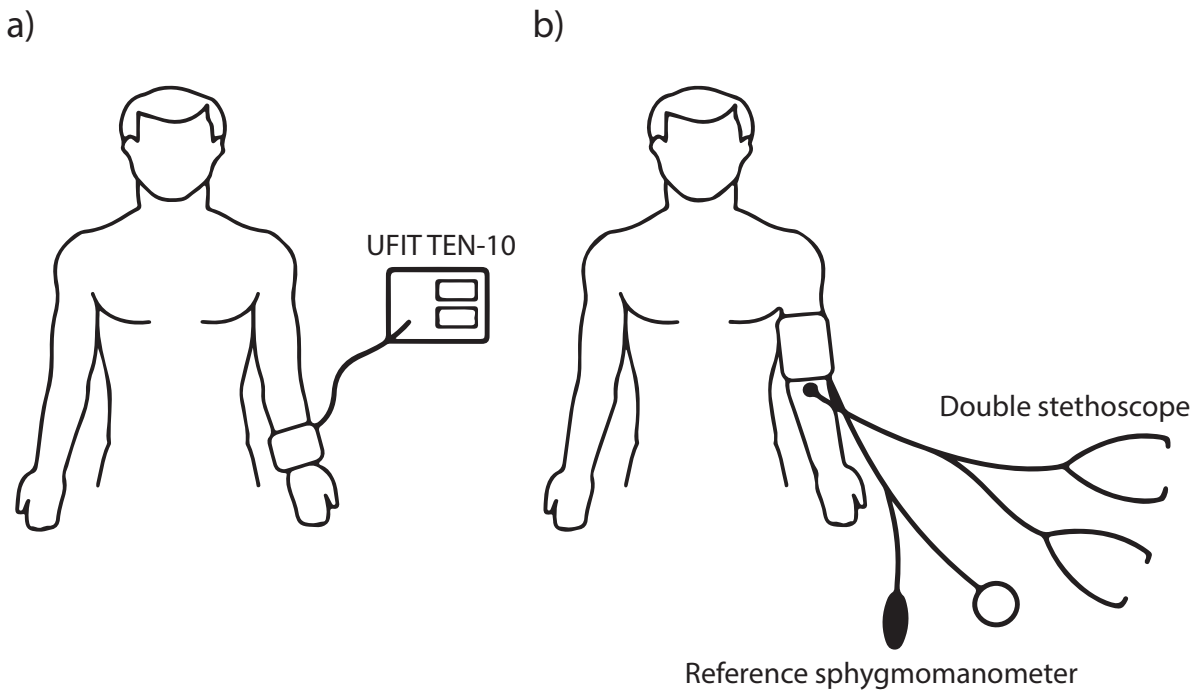

Figure A.1: Illustration of the data recording method used to collect 425 wrist measurements from 85 subjects. (a) UFIT TEN-10 measurement from left wrist. (b) After a one-minute delay, two independent simultaneous reference readings are recorded at the arm level by two nurses using the auscultatory method.

are performed. The ranges of the recorded SBPs and DBPs were 78-147 mmHg and 42-99 mmHg, respectively. The reference MAP was calculated using the common formula $MAP = DBP + 1/3 \times (SBP - DBP)$ [2], for all comparisons and analysis. For more details the reader is referred to [10, 66].

The data collection protocol for each subject can be summarized as follows:

1) Invite the participant to the trial area and inform him/her of the measurement steps.

2) Sit the participant comfortably and apply the arm cuff appropriately to left arm and the UFIT cuff to the left wrist at heart level.

3) Start the UFIT recording from left wrist.

4) Wait one minute.

5) Start the two simultaneous auscultatory readings from the left arm.

6) Wait one minute.

7) Repeat steps 3-6 four times.

8) End session.

Figure A.1 illustrates the data recording method.

A.2 Dataset 2

The second dataset was collected by our research group. This dataset comprised 150 simultaneous oscillometric BP and ECG recordings acquired with a prototype designed in our research laboratory [79]. The data was collected from 10 healthy subjects, six males and four females, aged from 24 to 63 years. This study was approved by the University of Ottawa Research Ethics Board, and written informed consent was obtained from all subjects. To the best of our knowledge, no subject had a history of cardiovascular or respiratory disease. Recordings from each subject were obtained on three separate days with five sets of recordings in each day.

Each set of recordings started with the Food and Drug Administration (FDA)-approved Omron monitor (HEM-790IT) measurement on the right arm. As soon as the Omron measurement ended, our prototype measurement started on the left arm. The subject also wore the wristband of the prototype on the right wrist for simultaneous ECG recording as shown in Fig. A.2. Since the American Heart Association recommends at least a 1 min gap between two consecutive BP measurements [173], the five sets of measurements were performed with three-minute gaps. Although there may be differences in BP measured from right and left arms, studies have shown that such differences are not statistically significant in healthy subjects [174] such as the ones tested in this pilot investigation.

The data collection protocol for each subject can be summarized as follows:

1) Invite the participant to the trial area and inform him/her of the measurement steps.

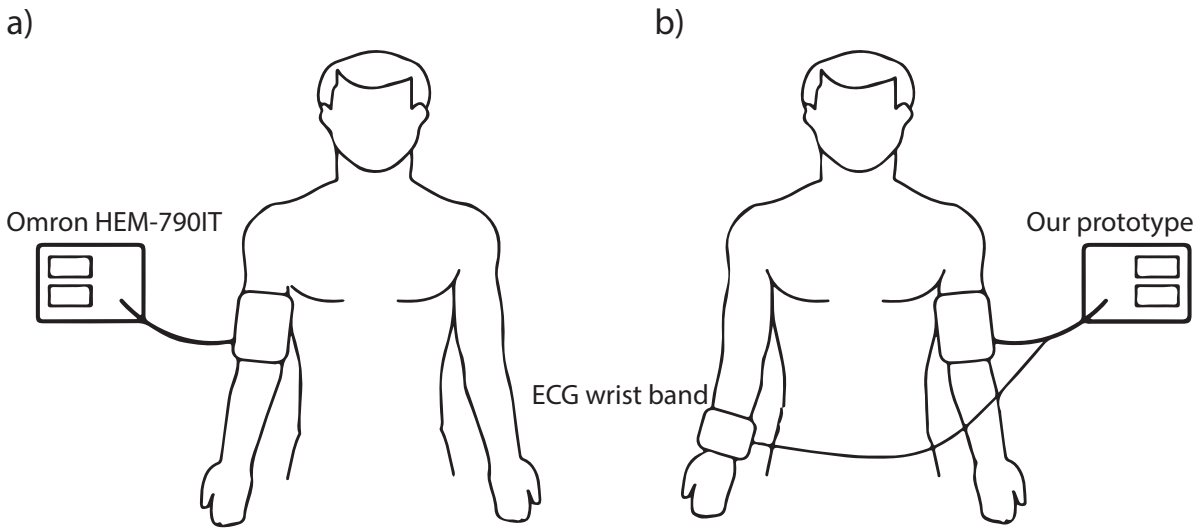

Figure A.2: Illustration of the data recording method used to collect 150 arm measurements from 10 subjects. (a) Omron HEM-790IT measurement from right arm. (b) As soon as the Omron measurement ends, our prototype measurement starts on the left arm. The subject also wears the wristband of the prototype on the right wrist for simultaneous ECG recording.

2) Sit the participant comfortably and apply the prototype arm cuff appropriately to left arm at heart level, the prototype wristband to the right wrist, and the Omron cuff to the right arm at heart level.

3) Start Omron recording from right arm.

4) Start the prototype recording from left arm, as soon as Omron recording ends.

5) Wait three minutes.

6) Repeat steps 3-5 four times.

7) End session.

8) Wait for at least 24 hours.

9) Repeat steps 1-8 two times.

Our prototype recordings comprised inflating the prototype cuff to a pressure of 160 mmHg and then deflating it slowly to a pressure of 20 mmHg. The deflation rate was 1.5-3.5 mmHg/sec. Following the measurement, the oscillometric and ECG signals corresponding to a cuff pressure range of 25-155 mmHg were chosen for further analysis.

The ranges of the reference recorded SBPs and DBPs were 79-136 mmHg and 52-86 mmHg, respectively. Since the Omron device only provides the SBP and DBP values, the reference MAP was calculated using the common formula $MAP = DBP + 1/3 \times (SBP - DBP)$ [2], for all comparisons and analysis.

Figure A.1 illustrates the data recording method. Our measurement prototype is shown in Fig. 5.2 and is described in more detail in Section 5.1. For more details the reader is referred to [79].

Bibliography

[1] C. R. Taylor, C. Lillis, P. LeMone, and P. Lynn, *Fundamentals of Nursing: The Art and Science of Nursing Care*. Baltimore, MD: Lippincott Williams & Wilkins, seventh ed., 2010.

[2] W. W. Nichols, M. F. O'Rourke, and C. Vlachopoulos, *McDonald's Blood Flow in Arteries: Theoretical, Experimental and Clinical Principles*. London, UK: Hodder Arnold Publishers, sixth ed., 2011.

[3] W. A. Littler and B. Komsuoglu, "Which is the most accurate method of measuring blood pressure?," *Am. Heart J.*, vol. 117, pp. 723–728, 1989.

[4] H. F. Stegall, M. B. Kardon, and W. T. Kemmerer, "Indirect measurement of arterial blood pressure by doppler ultrasound sphygmomanometry," *J. Appl. Physiol.*, vol. 25, pp. 793–798, 1968.

[5] M. Ramsey, "Noninvasive automatic determination of mean arterial pressure," *Med. Biol. Eng. Comput.*, vol. 17, pp. 11–18, 1979.

[6] L. A. Geddes, M. Voelz, C. Combs, D. Reiner, and C. F. Babbs, "Characterization of the oscillometric method for measuring indirect blood pressure," *Ann. Biomed. Eng.*, vol. 10, pp. 271–280, 1982.

[7] J. Penaz, "Photoelectric measurement of blood pressure, volume and flow in the finger," in *Int. Conf. Medical and Biological Engineering*, (Dresden, Germany), p. 104, 1973.

[8] G. L. Pressman and P. M. Newgard, "A transducer for the continuous external measurement of arterial blood pressure," *IEEE Trans. Biomed. Eng.*, vol. 10, pp. 73–81, 1963.

[9] K. Yamakoshi, H. Shimazu, and T. Togawa, "Indirect measurement of instantaneous arterial blood pressure in the human finger by the vascular unloading technique," *IEEE Trans. Biomed. Eng.*, vol. 27, pp. 150–155, 1980.

[10] S. Chen, V. Z. Groza, M. Bolic, and H. R. Dajani, "Assessment of algorithms for oscillometric blood pressure measurement," in *IEEE Int. Instrumentation and Measurement Technology Conf. (I2MTC'09)*, (Singapore), pp. 1763–1767, May 2009.

[11] K. Wilkins, N. R. C. Campbell, M. R. Joffres, F. A. McAlister, M. Nichol, S. Quach, H. L. Johansen, and M. S. Tremblay, "Blood pressure in canadian adults," *Statistics Canada, Catalogue no. 82-003-XPE – Health Reports*, vol. 21, pp. 1–10, 2010.

[12] A. V. Chobanian, G. L. Bakris, H. R. Black, W. C. Cushman, L. A. Green, J. L. Izzo, D. W. Jones, B. J. Materson, S. Oparil, and J. T. Wright, "Seventh report of the joint national committee on prevention, detection, evaluation, and treatment of high blood pressure," *Hypertension*, vol. 42, pp. 1206–1252, 2003.

[13] D. W. Jones and J. E. Hall, "Hypertension: Pathways to success," *Hypertension*, vol. 51, pp. 1249–1251, 2008.

[14] G. W. Mauck, C. R. Smith, L. A. Geddes, and J. D. Bourland, "The meaning of the point of maximum oscillations in cuff pressure in the indirect measurement of blood pressure–part ii," *J. Biomech. Eng.*, vol. 102, pp. 28–33, 1980.

[15] F. K. Forster and D. Turney, "Oscillometric determination of diastolic, mean, and systolic blood pressure – A numerical model," *J. Biomech. Eng.*, vol. 108, pp. 359–364, Nov. 1986.

[16] W. T. Link, "Techniques for obtaining information associated with an individual's blood pressure including specifically a stat mode technique." U.S. Patent 4,664,126, Oct. 13, 1987.

[17] G. Drzewiecki, R. Hood, and H. Apple, "Theory of the oscillometric maximum and the systolic and diastolic detection ratios," *Ann. Biomed. Eng.*, vol. 22, pp. 88–96, Jan. 1994.

[18] G. Drzewiecki, "Noninvasive arterial blood pressure and mechanics," in *The Biomedical Engineering HandBook* (J. D. Bronzino, ed.), Boca Raton, FL: CRC Press, third ed., 2006.

[19] M. Ursino and C. Cristalli, "A mathematical study of some biomechanical factors affecting the oscillometric blood pressure measurement," *IEEE Trans. Biomed. Eng.*, vol. 43, pp. 761–778, Aug. 1996.

[20] M. Ursino and C. Cristalli, "Techniques and applications of mathematical modeling for noninvasive blood pressure estimation," in *Biomechanical Systems Techniques and Applications, Volume II: Cardiovascular Techniques* (C. Leondes, ed.), CRC Press, 2000.

[21] M. James, *Simplified Model for the Design of an Oscillometric Blood Pressure Measuring System*. PhD thesis, University of Guelph, 2012.

[22] E. Pinheiro and O. Postolache, "Modelling of oscillometric blood pressure monitor – from white to black box models," in *Recent Advances in Biomedical Engineering* (G. R. Naik, ed.), InTech, 2009.

[23] S. Sun, *A total compliance method for noninvasive arterial blood pressure measurement*. PhD thesis, University of Utah, 1990.

[24] J. S. Clark and S. Sun, "Total compliance method and apparatus for noninvasive arterial blood pressure measurement." U.S. Patent 5,423,322, Jun. 13, 1995.

[25] C. F. Babbs, "Oscillometric measurement of systolic and diastolic blood pressures validated in a physiologic mathematical model," *Biomed. Eng. Online*, vol. 11, pp. 1–22, 2012.

[26] J. Talts, R. Raamat, K. Jagomagi, and J. Kivastik, "An influence of multiple affecting factors on characteristic ratios of oscillometric blood pressure measurement," in *15th Nordic-Baltic Conf. Biomedical Engineering and Medical Physics (NBC'11)*, (Aalborg, Denmark), pp. 73–76, Jun. 2011.

[27] J. Liu, J.-O. Hahn, and R. Mukkamala, "Error mechanisms of the oscillometric fixed-ratio blood pressure measurement method," *Ann. Biomed. Eng.*, vol. 41, pp. 587–597, 2012.

[28] J. Liu, J. O. Hahn, and R. Mukkamala, "Model-based error analysis of the oscillometric fixed-ratio blood pressure measurement method," in *34th Ann. Int. Conf. IEEE Engineering in Medicine and Biology Society (EMBC'12)*, (San Diego, CA), pp. 633–636, Aug.-Sep. 2012.

[29] R. Smith, J. Argod, J. Pepin, and P. Levy, "Pulse transit time: an appraisal of potential clinical applications," *Thorax*, vol. 54, pp. 452–457, May 1999.

[30] G. S. Mattu, "Validation of oscillometric blood pressure measuring devices; a case study of the BpTRU," Master's thesis, University of British Columbia, Vancouver, BC, Canada, Jul. 2003.

[31] L. Beckett and M. Godwin, "The BpTRU automatic blood pressure monitor compared to 24 hour ambulatory blood pressure monitoring in the assessment of blood pressure in patients with hypertension," *BMC Cardiovasc. Disord.*, vol. 5, pp. 1–6, 2005.

[32] R. N. Feghali, J. A. Topouchaian, B. M. Pannier, H. A. El Assaad, and R. G. Asmar, "Validation of the Omron M7 (HEM-780-E) blood pressure measuring device

in a population requiring large cuff use according to the international protocol of the European Society of Hypertension," *Blood Press. Monit.*, vol. 12, pp. 173–178, 2007.

[33] A. Coleman, S. Steel, P. Freeman, A. de Greeff, and A. Shennan, "Validation of the Omron M7 (HEM-780-E) oscillometric blood pressure monitoring device according to the British Hypertension Society protocol," *Blood Press. Monit.*, vol. 13, pp. 49–54, 2008.

[34] M. G. Myers and M. Godwin, "Automated office blood pressure," *Can. J. Cardiol.*, vol. 28, pp. 341–346, 2012.

[35] M. G. Myers and M. Valdivieso, "Evaluation of an automated sphygmomanometer for use in the office setting," *Blood Press. Monit.*, vol. 17, pp. 116–119, 2012.

[36] W. Gerin, A. R. Schwartz, J. E. Schwartz, T. G. Pickering, K. W. Davidson, J. Bress, E. O'Brien, and N. Atkins, "Limitations of current validation protocols for home blood pressure monitors for individual patients," *Blood Press. Monit.*, vol. 6, pp. 313–318, 2002.

[37] *Non-invasive sphygmomanometers – Part 2: Clinical validation of automated measurement type*, ANSI/AAMI/ISO 81060-2 Standard, Arlington, TX, 2009.

[38] S. Lewington, R. Clarke, N. Qizilbash, R. Peto, and R. C. R, "Age-specific relevance of usual blood pressure to vascular mortality: a meta-analysis of individual data for one million adults in 61 prospective studies," *Lancet*, vol. 360, pp. 1903–1913, 2002.

[39] K. Soueidan, S. Chen, H. R. Dajani, M. Bolic, and V. Groza, "Augmented blood pressure measurement through the noninvasive estimation of physiological arterial pressure variability," *Physiol. Meas.*, vol. 33, pp. 881–899, 2012.

[40] K. Soueidan, "Augmented blood pressure measurement through the estimation of physiological blood pressure variability," Master's thesis, School of Electrical Engineering and Computer Science, University of Ottawa, 2010.

[41] K. Soueidan, S. Chen, H. R. Dajani, M. Bolic, and V. Groza, "The effect of blood pressure variability on the estimation of the systolic and diastolic pressures," in *IEEE Int. Workshop Medical Measurements and Applications (MeMeA'10)*, (Ottawa, ON), pp. 14–18, May 2010.

[42] A. M. G. Pierina, D. C. Alavarcea, Josiane, L. Gusmao, A. Halpernb, and D. Mion, "Blood pressure measurement in obese patients: comparison between upper arm and forearm measurements," *Blood Press. Monit.*, vol. 9, pp. 101–105, 2004.

[43] A. M. Thompson, K. Eguchi, M. E. Reznik, S. S. Shah, and T. G. Pickering, "Validation of an oscillometric home blood pressure monitor in an end-stage renal disease population and the effect of arterial stiffness on its accuracy," *Blood Press. Monit.*, vol. 12, pp. 227–232, 2007.

[44] M. J. Stewart, K. Gough, and P. L. Padfield, "The accuracy of automated blood pressure measuring devices in patients with controlled atrial fibrillation," *J. Hypertens.*, vol. 13, pp. 297–300, 1995.

[45] M. Forouzanfar, H. R. Dajani, V. Z. Groza, M. Bolic, and S. Rajan, "Feature-based neural network approach for oscillometric blood pressure estimation," *IEEE Trans. Instrum. Meas.*, vol. 60, pp. 2786–2796, Aug. 2011.

[46] M. Forouzanfar, H. R. Dajani, V. Z. Groza, M. Bolic, and S. Rajan, "Oscillometric blood pressure estimation using principal component analysis and neural networks," in *IEEE Toronto Int. Conf. – Science and Technology for Humanity (TIC-STH'09)*, (Toronto, ON), pp. 981–986, Sep. 2009.

[47] M. Forouzanfar, H. R. Dajani, V. Z. Groza, M. Bolic, and S. Rajan, "Adaptive neuro-fuzzy inference system for oscillometric blood pressure estimation," in *IEEE Int. Workshop Medical Measurements and Applications (MeMeA'10)*, (Ottawa, ON), pp. 125–129, May 2010.

[48] M. Forouzanfar, H. R. Dajani, V. Z. Groza, M. Bolic, and S. Rajan, "Comparison of feed-forward neural network training algorithms for oscillometric blood pressure estimation," in *IEEE 4th Int. Workshop Soft Computing Applications (SOFA'10)*, (Arad, Romania), pp. 119–123, Jul. 2010.

[49] M. Forouzanfar, H. R. Dajani, V. Z. Groza, M. Bolic, S. Rajan, and I. Batkin, "Ratio-independent blood pressure estimation by modeling the oscillometric waveform envelope," *IEEE Trans. Instrum. Meas.,* in press.

[50] B. Balasingam, M. Forouzanfar, M. Bolic, H. R. Dajani, V. Z. Groza, and S. Rajan, "Arterial blood pressure parameter estimation and tracking using particle filters," in *IEEE Int. Workshop Medical Measurements and Applications (MeMeA'11)*, (Bari, Italy), pp. 473–476, May 2011.

[51] M. Forouzanfar, B. Balasingam, H. R. Dajani, V. Groza, M. Bolic, S. Rajan, and E. M. Petriu, "Mathematical modeling and parameter estimation of blood pressure oscillometric waveform," in *IEEE Int. Symp. Medical Measurement and Applications (MeMeA'12)*, (Budapest, Hungary), pp. 208–213, May 2012.

[52] M. Forouzanfar, S. Ahmad, I. Batkin, H. R. Dajani, V. Z. Groza, and M. Bolic, "Coefficient-free blood pressure estimation based on pulse transit time–cuff pressure dependence," *IEEE Trans. Biomed. Eng.*, vol. 60, pp. 1814–1824, 2013.

[53] I. Batkin, S. Ahmad, M. Bolic, V. Z. Groza, H. R. Dajani, and M. Forouzanfar, "Apparatus and method for electrocardiogram-assisted blood pressure measurement." US Patent 20,120,283,583, May 1, 2012.

[54] M. Forouzanfar, H. R. Dajani, V. Groza, and M. Bolic, "Model-based oscillometric blood pressure estimation," in *IEEE Int. Symp. Medical Measurement and Applications (MeMeA'14)*, (Lisbon, Portugal), Jun. 2014, in press.

[55] M. Ward and J. A. Langton, "Blood pressure measurement," *Contin. Educ. Anaesth. Crit. Care Pain*, vol. 7, pp. 122–126, 1997.

[56] D. Sahu and M. Bhaskaran, "Palpatory method of measuring diastolic blood pressure," *J. Anaesthesiol. Clin. Pharmacol.*, vol. 26, pp. 528–530, 2010.

[57] N. D. Markandu, F. Whitcher, A. Arnold, and C. Carney, "The mercury sphygmomanometer should be abandoned before it is proscribed," *J. Hum. Hypertens.*, vol. 14, pp. 31–36, 2000.

[58] E. O'Brien, "Replacing the mercury sphygmomanometer – requires clinicians to demand better automated devices," *Brit. Med. J.*, vol. 320, pp. 815–816, 2000.

[59] A. Reisner, P. A. Shaltis, and D. M. H. H. Asada, "Utility of the photoplethysmogram in circulatory monitoring," *Anesthesiology*, vol. 108, pp. 950–958, 2008.

[60] F. Lamonaca, K. Barbe, Y. Kurylyak, D. Grimaldi, W. Van Moer, A. Furfaro, and V. Spagnuolo, "Application of the artificial neural network for blood pressure evaluation with smartphones," in *IEEE Int. Conf. Intelligent Data Acquisition and Advanced Computing Systems: Technology and Applications (IDAACS'13)*, (Berlin, Germany), pp. 408–412, May 2013.

[61] Y. Kurylyak, F. Lamonaca, and D. Grimaldi, "A neural network-based method for continuous blood pressure estimation from a PPG signal," in *IEEE Int. Instrumentation and Measurement Technology Conf. (I2MTC'13)*, (Minneapolis, MN), pp. 280–283, May 2013.

[62] Y. Kurylyak, K. Barbe, F. Lamonaca, D. Grimaldi, and W. Van Moer, "Photoplethysmogram-based blood pressure evaluation using Kalman filtering and

neural networks," in *IEEE Int. Symp. Medical Measurement and Applications (MeMeA'13)*, (Gatineau, QB, Canada), pp. 170–174, May 2013.

[63] E. J. Ciaccio, G. M. Drzewiecki, and E. Karam, "Algorithm for reduction of mechanical noise in arterial pulse recording with tonometry," in *15th Northeast Bioengineering Conf. (NEBEC'89)*, (Boston, MA), pp. 161–162, Mar. 1989.

[64] L. W. J. Bogert and J. J. van Lieshout, "Non-invasive pulsatile arterial pressure and stroke volume changes from the human finger," *Exp. Physiol.*, vol. 9, pp. 437–446, 2005.

[65] S. Omboni, G. Parati, A. Frattol, E. Mutti, M. D. Rienzo, P. Castiglioni, and G. Mancia, "Spectral and sequence analysis of finger blood pressure variability: comparison with analysis of intra-arterial recordings," *Hypertension*, vol. 22, pp. 26–33, 1993.

[66] S. Chen, "Improving algorithms for oscillometric blood pressure estimation by suppressing breathing effects," Master's thesis, School of Electrical Engineering and Computer Science, University of Ottawa, 2010.

[67] S. Lee, J. H. Chang, S. W. Nam, C. Lim, S. Rajan, H. R. Dajani, and V. Z. Groza, "Oscillometric blood pressure estimation based on maximum amplitude algorithm employing gaussian mixture regression," *IEEE Trans. Instrum. Meas.*, vol. 62, pp. 3387–3389, Dec. 2013.

[68] R. Medero, "Determination of oscillometric blood pressure by linear approximation." US Patent 5,577,508, Nov. 26, 1996.

[69] P. D. Baker, J. A. Orr, D. R. Westenskow, and T. P. Egbert, "Method for determining blood pressure utilizing a neural network." US Patent 5,339,818, Aug. 23, 1994.

[70] S. Narus, T. Egbert, T. Lee, J. Lu, and D. Westenskow, "Noninvasive blood pressure monitoring from the supraorbital artery using an artificial neural network oscillometric algorithm," *J. Clin. Monitor.*, vol. 11, pp. 289–297, 1999.

[71] S. Colak and C. Isik, "Blood pressure estimation using neural networks," in *IEEE Int. Conf. Computational Intelligence for Measurement Systems and Applications*, (Boston, MA), pp. 21–25, Jul. 2004.

[72] M. Mafi, M. Bolic, V. Z. Groza, H. R. Dajani, and M. Rajan, "Oscillometric blood pressure pulse morphology," in *IEEE Int. Workshop Medical Measurements and Applications (MeMeA'11)*, (Ottawa, ON), pp. 413–417, May 2011.

[73] M. Mafi, "Blood pressure estimation using oscillometric pulse morphology," Master's thesis, School of Electrical Engineering and Computer Science, University of Ottawa, 2012.

[74] S. H. Song, D. K. Kim, J. S. Lee, Y. J. Chee, and I. Y. Kim, "Mean arterial pressure estimation method using morphological changes in oscillometric waveform," in *IEEE Conf. Computers in Cardiology*, (Park City, UT), pp. 737–739, Sep. 2009.

[75] M. Mafi, M. Rajan, M. Bolic, V. Z. Groza, and H. R. Dajani, "Blood pressure estimation using oscillometric pulse morphology," in *Ann. Int. Conf. Engineering in Medicine and Biology Society (EMBC'11)*, (Boston, MA), pp. 2492–2496, Aug. 2011.

[76] K. Barbe and W. Van Moer, "An innovative oscillometric blood pressure measurement: getting rid of the traditional envelope," in *IEEE Int. Symp. Medical Measurement and Applications (MeMeA'12)*, (Budapest, Hungary), pp. 1–6, May 2012.

[77] E. R. Nye, "The effect of blood pressure alteration on the pulse wave velocity," *Brit. Heart J.*, vol. 26, pp. 261–265, 1964.

[78] S. S. Najjar, A. Scuteri, V. Shetty, J. G. Wright, D. C. Muller, J. L. Fleg, H. P. Spurgeon, L. Ferrucci, and E. G. Lakatta, "Pulse wave velocity is an independent predictor of the longitudinal increase in systolic blood pressure and of incident hypertension in the baltimore longitudinal study of aging," *J. Amer. Coll. Cardiol.*, vol. 51, pp. 1377–1383, 2008.

[79] S. Ahmad, S. Chen, K. Soueidan, I. Batkin, M. Bolic, H. Dajani, and V. Groza, "Electrocardiogram-assisted blood pressure estimation," *IEEE Trans. Biomed. Eng.*, vol. 59, pp. 608–618, Mar. 2012.

[80] Y. Chen, L. Li, C. Hershler, and R. P. Dill, "Continuous non-invasive blood pressure monitoring method and apparatus." US Patent 6,599,251, Jul. 29, 2003.

[81] K. Meigas, J. Lass, D. Karai, R. Karai, and J. Kaik, "Pulse wave velocity in continuous blood pressure measurements," in *World Congr. Medical Physics and Biomedical Engineering*, (Seoul, Korea), pp. 626–629, Aug.-Sep. 2006.

[82] Y. Kim, "Automatic blood pressure measuring instrument and method thereof." US Patent 7,226,418, Jun. 5, 2007.

[83] Y. Yoon, J. H. Cho, and G. Yoon, "Non-constrained blood pressure monitoring using ECG and PPG for personal healthcare," *J. Med. Syst.*, vol. 33, pp. 261–266, 2009.

[84] K. Ha, Y. Park, and J. Lee, "Apparatus and method for measuring blood pressure." US Patent 20,100,049,059, Feb. 25, 2010.

[85] H. Gesche, D. Grosskurth, G. Kuchler, and A. Patzak, "Continuous blood pressure measurement by using the pulse transit time: comparison to a cuff-based method," *Eur. J. Appl. Physiol.*, vol. 112, pp. 309–315, 2012.

[86] F. S. Cattivelli and H. Garudadri, "Noninvasive cuffless estimation of blood pressure from pulse arrival time and heart rate with adaptive calibration," in *IEEE*

Int. Conf. Body Sensor Networks (BSN'13), (Los Angeles, CA), pp. 114–119, May 2013.

[87] C. Poon, Y. Zhang, and Y. Liu, "Modeling of pulse transit time under the effects of hydrostatic pressure for cuffless blood pressure measurements," in *Int. Summer School and Symp. Medical Devices and Biosensors (ISSS-MDBS'06)*, (Boston, MA), pp. 65–68, Sep. 2006.

[88] T. Ma and Y. T. Zhang, "A correlation study on the variabilities in pulse transit time, blood pressure, and heart rate recorded simultaneously from healthy subjects," in *Ann. Int. Conf. Engineering in Medicine and Biology Society (EMBC'05)*, (Shanghai, China), pp. 996–999, Sep. 2005.

[89] Y. Sawada, "A correlation analysis between pulse transit time and instantaneous blood pressure measured indirectly by the vascular unloading method," *Biol. Psychol.*, vol. 21, pp. 1–9, 1985.

[90] X. He, R. A. Goubran, and X. P. Liu, "Evaluation of the correlation between blood pressure and pulse transit time," in *IEEE Int. Symp. Medical Measurement and Applications (MeMeA'13)*, (Gatineau, QB, Canada), pp. 17–20, May 2013.

[91] J. D. Lane, L. Greenstadt, D. Shapiro, and R. Rubinstein, "Pulse transit time and blood pressure: An intensive analysis," *Psychophysiology*, vol. 20, pp. 45–49, 1983.

[92] Y. Sawada and K. Yamakoshi, "A correlation analysis between pulse transit time and instantaneous blood pressure measured indirectly by the vascular unloading method," *Biol. Psychol.*, vol. 21, pp. 1–9, 1985.

[93] R. A. Payne, C. N. Symeonides, D. J. Webb, and S. R. J. Maxwell, "Pulse transit time measured from the ECG: An unreliable marker of beat-to-beat blood pressure," *J. Appl. Physiol.*, vol. 100, pp. 136–141, 2006.

[94] L. A. Geddes, M. Voelz, S. James, and D. Reiner, "Pulse arrival time as a method of obtaining systolic and diastolic blood pressure indirectly," *Med. Biol. Eng. Comput.*, vol. 19, pp. 671–672, Mar. 1981.

[95] T. Sharir, A. Marmor, C.-T. Ting, J.-W. Chen, C.-P. Liu, M.-S. Chang, F. C. P. Yin, and D. A. Kass, "Validation of a method for noninvasive measurement of central arterial pressure," *Hypertension*, vol. 21, pp. 74–82, 1993.

[96] H. Sorvoja, R. Myllyl, P. Krj-Koskenkari, J. Koskenkari, M. Lilja, and Y. Antero, "Accuracy comparison of oscillometric and electronic palpation blood pressure measuring methods using intra-arterial method as a reference," *Mol. Quant. Acoust.*, vol. 26, pp. 235–260, 2005.

[97] J. Kerola, V. Kontra, and R. Sepponen, "Non-invasive blood pressure data acquisition employing pulse transit time detection," in *18th Annu. Int. Conf. IEEE Engineering in Medicine and Biology Society (EMBS'96)*, (Amsterdam, Netherlands), pp. 1308–1309, Oct.–Nov. 1996.

[98] T. Massey, L. Selavo, D. Crawford, C. Bor-rong, K. Lorincz, V. Shnayder, L. Hauenstein, F. Dabiri, J. Jeng, A. Chanmugam, D. White, M. Sarrafzadeh, and M. Welsh, "The advanced health and disaster aid network: a light-weight wireless medical system for triage," *IEEE Trans. Biomed. Circuits Syst.*, vol. 1, pp. 203–216, Sep. 2007.

[99] R. A. Walloch, "Automatic blood pressure monitor employing artifact rejection method and apparatus." U.S. Patent 5,337,750, 1994.

[100] *American standard for electronic and automated sphygmomanometers*, ANSI/AAMI SP10 Standard, Washington, DC, 1987.

[101] *American standard for electronic and automated sphygmomanometers*, ANSI/AAMI SP10 Standard, Arlington, TX, 1993.

[102] *Manual, Electronic, or Automated Sphygmomanometers*, ANSI/AAMI SP10 Standard, Arlington, TX, 2002.

[103] E. O'Brien, J. Petrie, W. Littler, M. de Swiet, P. L. Padfield, K. O'Malley, M. Jamieson, D. Altman, M. Bland, and N. Atkins, "The British Hypertension Society protocol for the evaluation of automated and semi-automated blood pressure measuring devices with special reference to ambulatory systems," *J. Hypertens.*, vol. 8, pp. 607–619, 1990.

[104] E. O'Brien, J. Petrie, W. Littler, M. de Swiet, P. L. Padfield, D. Altman, M. Bland, A. coats, and N. Atkins, "The British Hypertension Society protocol for the evaluation of blood pressure measuring devices," *J. Hypertens.*, vol. 11, pp. S43–S62, 1993.

[105] E. O'Brien, N. Atkins, G. Stergiou, N. Karpettas, G. Parati, R. Asmar, Y. Imai, J. Wang, T. Mengden, and A. Shennan, "European Society of Hypertension international protocol revision 2010 for the validation of blood pressure measuring devices in adults," *Blood Press. Monit.*, vol. 15, pp. 23–38, 2010.

[106] D. G. Altman and J. M. Bland, "Measurement in medicine: the analysis of method comparison studies," *Statistician*, vol. 32, pp. 307–319, 1983.

[107] J. M. Bland and D. G. Altman, "Statistical methods for assessing agreement between two methods of clinical measurement," *Lancet*, vol. 327, pp. 307–310, 1986.

[108] J. M. Bland and D. G. Altman, "Measuring agreement in method comparison studies," *Stat. Methods Med. Res.*, vol. 8, pp. 135–160, 1999.

[109] J. M. Bland and D. G. Altman, "Comparing methods of measurement: why plotting difference against standard method is misleading," *Lancet*, vol. 346, pp. 1085–1087, 1995.

[110] J.-S. R. Jang, C.-T. Sun, and E. Mizutani, *Neuro-Fuzzy and Soft Computing: A Computational Approach to Learning and Machine Intelligence*. NJ: Prentice-Hall, 1997.

[111] C. M. Bishop, "Neural networks and their applications," *Rev. Sci. Instrum.*, vol. 65, pp. 1803–1832, 1994.

[112] W. S. Sarle, "Neural network FAQ, part 1 of 7: Introduction." periodic posting to the Usenet newsgroup comp.ai.neural-nets, URL: ftp://ftp.sas.com/pub/neural/FAQ.html, 1997.

[113] G. Dorffner and G. Porenta, "On using feedforward neural networks for clinical diagnostic tasks," *Artif. Intell. Med.*, vol. 6, pp. 417–435, 1994.

[114] T. F. Coleman and Y. Li, "An interior trust region approach for nonlinear minimization subject to bounds," *SIAM J. Optimiz.*, vol. 6, pp. 418–445, 1996.

[115] J.-S. R. Jang, "Anfis: adaptive network-based fuzzy inference system," *IEEE Trans. Sys. Man. Cybern.*, vol. 23, pp. 665–685, 1993.

[116] B. Kosko, "Fuzzy systems as universal approximators," *IEEE Trans. Comput.*, vol. 43, pp. 1329–1333, 1994.

[117] B. U. Kohler, C. Hennig, and R. Orglmeister, "QRS detection using zero crossing counts," *Prog. Biomed. Res.*, vol. 8, pp. 138–145, 2003.

[118] L. T. Hersh, B. Friedman, and R. Medero, "Method for oscillometric blood pressure determination employing curve fitting." US Patent 5,704,362, Jan. 6, 1998.

[119] C. T. Lin, S. H. Liu, J. J. Wang, and Z. C. Wen, "Reduction of interference in oscillometric arterial blood pressure measurement using fuzzy logic," *IEEE Trans. Biomed. Eng.*, vol. 50, pp. 432–441, 2003.

[120] H. Chunbao and L. Lingjiao, "Technique research and system design of ambulatory blood pressure monitoring," in *Int. Conf. Electronic Measurement and Instruments (ICEMI'07)*, (Xi'an, China), pp. 669–672, Jul.-Aug. 2007.

[121] K. Yale, "Preparing the right data diet for training neural networks," *IEEE Spectrum*, vol. 34, pp. 64–66, 1997.

[122] G. Cybenko, "Approximation by superpositions of a sigmoidal function," *Math. Control Signals Syst.*, vol. 2, pp. 303–314, 1989.

[123] D. Nguyen and B. Widrow, "Improving the learning speed of 2-layer neural networks by choosing initial values of the adaptive weights," in *Int. Joint Conf. Neural Networks (IJCNN'90)*, (San Diego, CA), pp. 21–26, June 1990.

[124] A. Pavelka and A. Prochazka, "Algorithms for initialization of neural network weights," in *Sbornk prspevku 12th rocnku konference MATLAB*, vol. 2, pp. 453–459, 2004.

[125] M. Riedmiller and H. Braun, "A direct adaptive method for faster backpropagation learning: The RPROP algorithm," in *IEEE Int. Conf. Neural Networks (ICNN'93)*, Mar. 1993.

[126] J. E. Dennis and R. B. Schnabel, *Numerical Methods for Unconstrained Optimization and Nonlinear Equations*. Englewood Cliffs, NJ: Prentice-Hall, 1983.

[127] R. Battiti, "First and second order methods for learning: Between steepest descent and newton's method," *Neural Comput.*, vol. 4, pp. 141–166, 1992.

[128] M. T. Hagan and M. Menhaj, "Training feed-forward networks with the marquardt algorithm," *IEEE Trans. Neural Networ.*, vol. 5, pp. 989–993, 1994.

[129] R. Fletcher and C. M. Reeves, "Function minimization by conjugate gradients," *Comput. J.*, vol. 7, pp. 149–154, 1964.

[130] M. J. D. Powell, "Restart procedures for the conjugate gradient method," *Math. Program.*, vol. 12, pp. 241–254, 1977.

[131] M. F. Moller, "A scaled conjugate gradient algorithm for fast supervised learning," *Neural Networks*, vol. 6, pp. 525–533, 1993.

[132] C. Charalambous, "Conjugate gradient algorithm for efficient training of artificial neural networks," *IEEE Proc.*, vol. 139, pp. 301–310, 1992.

[133] E. H. Mamdani, "Application of fuzzy logic to approximate reasoning using linguistic synthesis," *IEEE Trans. Comp.*, vol. C-26, pp. 1182–1192, 1977.

[134] Y. Tsukamoto, "An approach to fuzzy reasoning method," in *Advances in fuzzy set theory and applications* (M. M. Gupta, R. K. Ragade, and R. Yager, eds.), pp. 137–149, North-Holland, Amsterdam: Elsevier Science Ltd, 1979.

[135] T. Takagi and M. Sugeno, "Fuzzy identification of systems and its application to modeling and control," *IEEE Trans. Syst. Man. Cyb.*, vol. 15, pp. 116–132, 1985.

[136] M. Sugeno and G. T. Kang, "Structure identification of fuzzy model," *Fuzzy Set. Syst.*, vol. 28, pp. 15–33, 1988.

[137] W. S. Sarle, "Stopped training and other remedies for overfitting," in *27th Symp. Interface of Computing Science and Statistics*, June 1995.

[138] A. Blum, *Neural Networks in C++*. NY: John Wiley & Sons, 1992.

[139] K. Swingler, *Applying Neural Networks: A Practical Guide*. London, UK: Academic Press, 1996.

[140] M. J. A. Berry and G. Linoff, *Data Mining Techniques*. NY: John Wiley & Sons, 1997.

[141] Z. Boger and H. Guterman, "Knowledge extraction from artificial neural network models," in *IEEE Systems, Man., and Cybernetics Conf.*, (Orlando, FL), pp. 3030–3035, Oct. 1997.

[142] J. N. Amoore, "A simulation study of the consistency of oscillometric blood pressure measurements with and without artifacts," *Blood Press. Monit.*, vol. 5, pp. 69–79, 2000.

[143] J. N. Amoore and D. H. Scott, "Can simulators evaluate systematic differences between oscillometric non-invasive blood pressure monitors?," *Blood Press. Monit.*, vol. 5, pp. 81–89, 2000.

[144] J. N. Amoore and W. B. Geake, "An evaluation of three oscillometric non-invasive blood pressure simulators," *J. Clin. Eng.*, vol. 22, pp. 93–100, 1997.

[145] A. J. Sims, C. A. Reay, D. R. Bousfield, J. A. Menes, and A. Murray, "Oscillometric blood pressure devices and simulators: measurements of repeatability and differences between models," *J. Med. Eng. Techol.*, vol. 29, pp. 112–118, 2005.

[146] M. Aboy, J. McNames, R. Hornero, T. Thong, D.Cuesta, D. Novak, and B. Goldstein, "A novel statistical model for simulation of arterial and intracranial pressure," in *26th Ann. Int. Conf. IEEE Engineering in Medicine and Biology Society (EMBC'04)*, (San Francisco, CA), pp. 129–132, Sep. 2004.

[147] C. Staats, D. Austin, and M. Aboy, "A statistical model and simulator for cardiovascular pressure signals," *Proc. Inst. Mech. Eng. H*, vol. 222, pp. 991–998, 2008.

[148] J. McNames and M. Aboy, "Cardiovascular signal decomposition and estimation with the extended Kalman smoother," in *28th Ann. Int. Conf. IEEE Engineering in Medicine and Biology Society (EMBC'06)*, (New York City, NY), pp. 3708–3711, Sep. 2006.

[149] J. McNames and M. Aboy, "Statistical modeling of cardiovascular signals and parameter estimation based on the extended Kalman filter," *IEEE Trans. Biomed. Eng.*, vol. 55, pp. 119–129, Jan. 2008.

[150] S. Kim, L. Holmstrom, and J. McNames, "Multiharmonic tracking using marginalized particle filters," in *30th Ann. Int. Conf. IEEE Engineering in Medicine and Biology Society (EMBC'08)*, (Vancouver, BC, Canada), pp. 29–34, Aug. 2008.

[151] J. McNames, S. Kim, and M. Aboy, "Statistical model for cardiovascular signals with independent respiratory modulation for tracking pulse pressure variation," in *33rd Ann. Int. Conf. IEEE Engineering in Medicine and Biology Society (EMBC'11)*, (Boston, MA), pp. 4681–4684, Aug. 2011.

[152] P. J. Parker and B. D. O. Anderson, "Frequency tracking of nonsinusoidal periodic signals in noise," *Signal Process.*, vol. 20, pp. 127–152, 1990.

[153] A. R. Conn, N. I. M. Gould, and P. L. Toint, *Trust Region Methods*. Philadelphia, PA: SIAM, 2000.

[154] Z. M. Anastas, E. Jimerson, and S. Garolis, "Comparison of noninvasive blood pressure measurements in patients with atrial fibrillation," *J. Cardiovasc. Nurs.*, vol. 23, pp. 519–524, 2008.

[155] M. T. Guagnano, V. P. Palitti, R. Murri, L. Marchione, D. Merlitti, and S. Sensi, "Many factors can affect the prevalence of hypertension in obese patients: role of cuff size and type of obesity," *Panminerva Med.*, vol. 40, pp. 22–27, 1998.

[156] G. Beevers, G. Y. H. Lip, and E. O'Brien, "ABC of hypertension: Blood pressure measurement: Part I-sphygmomanometry: factors common to all techniques," *Brit. Med. J.*, vol. 322, pp. 981–985, 2001.

[157] C. Sala, E. Santin, M. Rescaldani, C. Cuspidi, and F. Magrini, "What is the accuracy of clinic blood pressure measurement?," *Am. J. Hypertens.*, vol. 18, pp. 244–248, 2005.

[158] C. A. Lodi, C. Estridge, and C. Ghidini, "In vitro and in vivo evaluation of an oscillometric device for monitoring blood pressure in dialysis patients," *Nephrol. Dial. Transplant.*, vol. 22, pp. 2950–2961, 2007.

[159] L. A. Geddes, M. Voelz, S. James, and D. Reiner, "Pulse arrival time as a method of obtaining systolic and diastolic blood pressure indirectly," *Med. Biol. Eng. Comput.*, vol. 19, pp. 671–672, 1981.

[160] X. F. Teng and Y. T. Zhang, "Theoretical study on the effect of sensor contact force on pulse transit time," *IEEE Trans. Biomed. Eng.*, vol. 54, pp. 1490–1498, Aug. 2007.

[161] D. J. Hughes, C. F. Babbs, L. A. Geddes, and J. D. Bourland, "Measurements of young's modulus of elasticity of the canine aorta with ultrasound," *Ultrason. Imaging*, vol. 1, pp. 356–367, 1979.

[162] H. H. Hardy and R. E. Collins, "On the pressure-volume relationship in circulatory elements," *Med. Biol. Eng. Comput.*, vol. 20, pp. 565–570, 1982.

[163] H. Lan, A. M. AI-Jumaily, and A. Lowe, "An investigation into the upper arm deformation under inflatable cuff," in *Int. Mechanical Engineering Congr. and Expo. (IMECE'08)*, (Boston, MA), pp. 1–4, Oct. 2008.

[164] H. Lan, A. M. AI-Jumaily, W. Hing, and A. Lowe, "Biomechanical basis of oscillometric blood pressure measuring technique," in *Int. Mechanical Engineering Congr. and Expo. (IMECE'09)*, (Lake Buena Vista, Fl), pp. 1–4, Nov. 2009.

[165] H. Lan, A. M. Al-Jumaily, A. Lowe, and W. Hing, "Effect of tissue mechanical properties on cuff-based blood pressure measurements," *Med. Eng. Phys.*, vol. 33, pp. 1287–1292, Dec. 2011.

[166] B. E. Westerhof, I. Guelen, W. J. Stok, K. H. Wesseling, J. A. E. Spaan, N. Westerhof, W. J. Bos, and N. Stergiopulos, "Arterial pressure transfer characteristics: effects of travel time," *Am. J. Physiol. Heart Circ. Physiol.*, vol. 292, pp. H800–H807, Sep 2007.

[167] Harvard-MIT Health Sciences and Technology, "QRS onset detector," Aug. 2010.

[168] D. Ruan, G. Chen, and E. E. Kerre, *Intelligent Data Mining: Techniques And Applications*. New York City, NY: Springer, 2005.

[169] Omron Healthcare Inc., Bannockburn, IL, *Automatic blood pressure monitor with ComFitTM cuff: Model HEM-790IT*, 2006.

[170] D. Moran, Y. Epstein, G. Keren, A. Laor, J. Sherez, and Y. Shapiro, "Calculation of mean arterial pressure during exercise as a function of heart rate," *Appl. Human Sci.*, vol. 14, pp. 293–295, Nov. 1995.

[171] H. Drucker, J. Burges, L. Kaufman, A. Smola, and V. Vapnik, "Support vector regression machines," in *Neural Information Processing Systems Conf. (NIPS'96)*, (Snowmass, CO), pp. 155–161, Dec. 1996.

[172] F. Girosi, M. Jones, and T. Poggio, "Regularization theory and neural network architectures," *Neural Comput.*, vol. 7, pp. 219–269, 1993.

[173] T. G. Pickering, J. E. Hall, L. J. Appel, B. E. Falkner, J. Graves, M. N. Hill, D. W. Jones, T. Kurtz, S. G. Sheps, and E. J. Roccella, "Recommendations for blood pressure measurement in humans and experimental animals–part 1: Blood pressure measurement in humans: A statement for professionals from the subcommittee of

professional and public education of the american heart association council on high blood pressure research," *Hypertension*, vol. 45, pp. 142–161, Dec. 2005.

[174] K. Eguchi, M. Yacoub, J. Jhalani, W. Gerin, J. E. Schwartz, and T. G. Pickering, "Consistency of blood pressure differences between the left and right arms," *Arch. Intern. Med.*, vol. 167, pp. 388–393, 2007.